Plant-Based Structures as an Opportunity to Engineer Optical Functions in Next-Generation Light Management

Joice Jaqueline Kaschuk, Yazan Al Haj, Orlando J. Rojas, Kati Miettunen, Tiffany Abitbol, and Jaana Vapaavuori*

This review addresses the reconstruction of structural plant components (cellulose, lignin, and hemicelluloses) into materials displaying advanced optical properties. The strategies to isolate the main building blocks are discussed, and the effects of fibrillation, fibril alignment, densification, self-assembly, surface-patterning, and compositing are presented considering their role in engineering optical performance. Then, key elements that enable ligno-cellulosic to be translated into materials that present optical functionality, such as transparency, haze, reflectance, UV-blocking, luminescence, and structural colors, are described. Mapping the optical landscape that is accessible from lignocellulosics is shown as an essential step toward their utilization in smart devices. Advanced materials built from sustainable resources, including those obtained from industrial or agricultural side streams, demonstrate enormous promise in optoelectronics due to their potentially lower cost, while meeting or even exceeding current demands in performance. The requirements are summarized for the production and application of plant-based optically functional materials in different smart material applications and the review is concluded with a perspective about this active field of knowledge.

1. Introduction

Plant-based lignocellulosics are an important source of materials, energy, and chemicals.[1] About 181.5 billion tons of lignocellulosic biomass are produced annually in the biosphere, with only 8.2 billion tons used by humans – making lignocellulosics a highly underutilized renewable resource.[2] Constituted of a complex interconnected structure of macromolecules, primarily composed of carbohydrates (cellulose and hemicelluloses) and polyaromatics (lignin and others),[3] plant-based lignocellulosics originate in large part from agricultural crops and forestry (annually consisting of 7 billion tons), but are also available from waste (annually consisting of 1.2 billion tons).[2] As emerging applications of light and energy demand new, advanced materials, lignocellulosics are being utilized in the fabrication of device components, as passive and active substrates, screens, and other applications, increasing the sustainability of related products and displacing conventional glass and oil-derived thermoplastics.

Recently, in response to urgent environmental concerns related to the life cycle of conventional materials, industry is adopting sustainability strategies to improve material production, processing, consumption, and disposal. Considering the traditional materials paradigm, alternatives derived from renewable and sustainable resources are becoming increasingly important across diverse fields, from personal care, packaging, textiles, architecture, to smart devices.[4–6] An assessment of the life cycle impact of lignocellulosics considers aspects such as sowing, growing, harvesting, extraction of isolated components, processing, transport, use, and end of life.[7] Furthermore, there is a pressing societal need to close the loops of material streams to achieve a circular economy.

J. J. Kaschuk, O. J. Rojas
Department of Bioproducts and Biosystems
School of Chemical Engineering
Aalto University
Box 16300, Aalto, Espoo 00076, Finland

Y. Al Haj, J. Vapaavuori
Department of Chemistry and Materials Science
School of Chemical Engineering
Aalto University
Aalto FI-00076, Finland
E-mail: jaana.vapaavuori@aalto.fi

The ORCID identification number(s) for the author(s) of this article can be found under https://doi.org/10.1002/adma.202104473.

O. J. Rojas
Bioproducts Institute
Departments of Chemical Engineering
Department of Biological Engineering
Department of Chemistry
Department of Wood Science
2360 East Mall
The University of British Columbia
Vancouver, BC V6T 1Z3, Canada

K. Miettunen
Department of Mechanical and Materials Engineering
Faculty of Technology
University of Turku
Turku FI-20500, Finland

T. Abitbol
RISE Research Institutes of Sweden
Stockholm SE-114 28, Sweden

**ADVANCED
SCIENCE NEWS**

www.advancedsciencenews.com

**ADVANCED
MATERIALS**

www.advmat.de

The major lignocellulosic component, cellulose, is made up of anhydroglucose units $[(C_6H_{10}O_5)_n]$ linked together by β-1,4 glycosidic bonds.[8] Van der Waals interactions and inter-and intramolecular hydrogen bonds play important roles in the organization and structuring of cellulose elementary fibrils and microfibrils to provide high tensile strength.[9,10] Similar interactions occur between cellulose and hemicelluloses, the latter consisting of heterogeneous polymers comprising of hexoses (glucose, galactose, and mannose), pentoses (xylose, arabinose), glucuronic acid, and galacturonic acid.[11] In this light, hemicelluloses can be viewed as compatibilizers between cellulose and lignin, which is a complex structure composed of a network of aromatic groups (chromophore structures based on p-coumaryl alcohol, coniferyl alcohol, and sinapyl alcohol).[3,12] Chemical crosslinks (α-ether, α-ester, phenyl glycoside linkages) between lignin and hemicelluloses give rise to lignin-carbohydrate complexes, which take part in the transport of water and nutrients in plants and confer chemical and biological resistance.[13,14]

Structurally, lignocellulosics can be categorized into woody and non-woody, which present different chemical compositions and physical properties. The long storage of carbon in wood results in large, dense, and strong fibers of relatively high lignin content.[15] Whereas non-woody fibers are a primary source of chemicals, including ethanol,[16–18] xylitol,[17,19] methane,[20,21] wood fibers represent 60% of the total global supply of lignocellulosic biomass and are the main element of structural materials, such as paper and board.[4,5,15] Related to the abundance of wood fibers, the vast majority of studies that explore the optical properties of lignocellulosic-based materials focus on woody lignocellulosics, as described below.

To understand the opportunities and limitations in designing optical functional components, e.g., for device applications, it is imperative to build a holistic understanding of both the fundamental structures of lignocellulosic materials and their interaction with light. Related phenomena include absorption, reflection, scattering, and, eventually, photo-degradation.[22] The absorption spectrum of wood relates to the optical properties of its components, with 5–20% of UV–vis absorption attributed to carbohydrates and 80–95% to lignin.[23,24] The typical light spectrum of a softwood section shows absorbance from 200 to 500 nm with a defined peak at 280 nm. As cellulose and hemicelluloses do not significantly absorb light, this 280 nm peak is attributed to lignin.[22] Thus, the color variation (light yellow to dark brown) of woody lignocellulosics is largely attributed to lignin, however, structural factors, such as porosity and refractive index also influence their appearance.[25,26]

To fully benefit from wood components in engineered optical materials, the isolation of these components is required. This is achieved by physical and chemical processes that disrupt the interactions and bonds between the polysaccharides and lignin.[27] In these processes, the most arduous step is the separation of lignin, especially if the target is to retain native chemical structure. Wood fibers are usually treated by a chemical bleaching process that yields a high cellulose content pulp and dissolved lignin, in the so-called black liquor, which also includes hemicelluloses and hydrolysis products. The components of the black liquor can be recovered by methods such as precipitation by acidic (lignin) or alcoholic solutions (hemicelluloses).[28,29] The isolation of lignin changes its color from almost colorless[30] or light yellowish[30] to brownish. The mechanism

responsible for the changes in lignin coloration is not fully understood, but they relate to changes in five chromophores, namely, 1) carbon-carbon double bonds conjugated with the aromatic ring; 2) quinone-methines and quinones; 3) chalcone structures; 4) free radicals, and 5) metal complexes with catechol structures.[31,32] Several articles and reviews can be found in the literature discussing the main benefits and drawbacks of a variety of wood processing (pulping) methods in terms of cellulose and lignin extraction yields, structural changes, and component recovery.[33–37] The isolation of pure cellulose, however, can be accomplished without extensive chemical processing if high purity cellulose sources are directly utilized, such as cotton[38] or bacterial cellulose.[39]

Depending on its structure and form, cellulose can interact with light in different ways, to give materials that can be opaque, transparent, hazy, colored, or reflective. Cellulose can be in fiber form (such as in conventional paper), in nano/microscale, or dissolved to give cellulose-backbone polymers with diverse optical properties, depending on functional groups and degree of substitution. Common cellulose-based polymers on the market are cellophane (dissolved alkali-soluble sodium cellulose xanthate regenerated in sulfuric acid and sodium sulfate), cellulose acetate, and carboxymethyl cellulose. These derivatives can be processed into highly transparent films that are commonly used in packaging.[40–42] Cellulose micro- and nanomaterials are undissolved fibers or fiber fragments that may or may not be colloidally stable, depending on their characteristic dimensions and surface compositions. Common plant-based cellulose micro- and nanomaterials include microcrystalline cellulose (MCC), cellulose nanofibrils (CNF), cellulose nanocrystals (CNC), holocellulose nanofibrils (holo-CNF), and lignocellulosic nanofibrils (ligno-CNF).[43] From an optical materials perspective, MCC is already targeted commercially as a biobased opacifier and potential alternative to inorganics such as titania, whereas the size and properties of CNC and CNF lend to potentially diverse optical outcomes, as described in more detail in the next section.

Although nanocellulose isolation routes, characterization approaches, and application areas have been explored in detail in previous reviews,[44–46] it is within the scope of the current review to highlight optically relevant aspects of CNC and CNF. First, CNC is less polydisperse in size, with widths of 5–10 nm and lengths < 500 nm, whereas CNF spans different size scales, with the finest fibrils (3–4 nm in width, hundreds of nm in length) sometimes coexisting with a significant proportion of microscale fibrillar bundles. Second, the most common form of CNC has a surface that is chemically modified with sulfate half-ester groups because of the sulfuric acid hydrolysis used in their isolation. By contrast, CNF has often been obtained in a more native form, although surface modification during processing or post-processing is also common.[47]

The diverse pool of inherent optical properties of cellulosic materials, coupled with the possibility of dialing in new non-native optical features, has led to a significant uptick in the research of these materials, for instance, to obtain green devices from renewable sources.[6,48–53] In the context of this review, by smart devices, we refer to purposefully designed manmade entities that "perform and control functions that attempt to produce useful results".[54] In a broader sense, it is important to note that the definition of smartness is context-dependent,

and from the standpoint of sustainability, a relevant question is, whether any device, whose fabrication does not follow the principles of resource-wise material and energy usage, should be given credit as "smart". Here we provide a broad context of optical features from biobased materials which are required for such devices. We exclude the thermal and mechanical properties of such materials, since a detailed overview of these properties can be found in several reviews.[44,45,48,49,55–57]

Considering that the benchmark requirements for the optical performance of different optoelectronic materials vary significantly, this review presents a critical assessment of lignocellulosics toward optical functionality, which can be engineered only through understanding the complex interplay between the nature of the components, and how they are structured, processed, or combined with other elements, including optically functional molecules or nanoparticles. In other words, here we consider different lignocellulosic starting materials and discuss the effects of fibrillation, fibril alignment, densification, self-assembly, surface-patterning, and compositing on targeted optical properties, such as transparency, haze, luminescence, UV-absorption, and structural colors. Also, to showcase the multiplicity of different optically relevant functionalities available, our scope goes beyond cellulose to include functional materials based on lignin and hemicelluloses, as well as non-lignocellulosic additives bearing an optical function. We compile this information through our tables, correlating the optical properties of lignocellulosic materials with the required optical performance of a given application. Finally, a critical context is provided as to whether the optical performance attainable from these components can meet the demands of modern optoelectronic devices.

2. Lignocellulosic Films for Engineered Light Management

Pinning down an exact definition of opacity, translucency, and transparency is difficult especially considering that these terms are inconsistently used in the literature. Furthermore, translucency co-exists alongside transparency and the visual perception of these properties can be subjective.[58] Moreover, there is no consensus in the literature as to how to best report the optical properties of cellulose-based materials, for instance, light transmittance may be given at a single optical wavelength or as an average value across a wavelength range. In this review, we specify, where possible, quantifiable optical properties and how material thickness/optical pathlength influences these properties. Below, we offer some introductory definitions of opaque, transparent, and translucent materials, as used in this review:

Opaque materials do not transmit incoming light. Instead, they absorb, reflect, or scatter light. For cellulose fiber-based materials, such as paper, which do not significantly absorb light in the visible wavelengths, opacity is achieved by light scattering and reflection at void interfaces, due to refractive index differences between air voids and fibers.[46] The thicker these materials, the more void-fiber interfaces are encountered by light, and the lower the likelihood of light transmission. By definition, these materials have very low transmittance.[59,60]

Translucent materials are also called hazy-transparent materials. Translucency or haze is defined as the percentage of total scattered light transmitted at an angle > 2.5° from the direction of the incident beam.[61] Light is scattered because of inhomogeneities in material composition and structure, including crystallites, voids, additives, and surface roughness or fabrication-induced imperfections, all of which contribute to differences in the refractive index of the material. They have high diffusive transmittance, which means that the incident light is broadly redirected as it is transmitted through the material.[62,63] An important aspect of this property is its dependence on illumination direction, i.e., the degree of haze varies depending on the angle of incidence of the light.[64]

Transparent materials do not absorb or scatter light, i.e., the light goes through the material structure without specific interactions. Transparent materials are compositionally homogeneous, without variations in refractive index.[26,65] For cellulose fiber-based materials, transparency can be obtained through densification, refractive index matching, backfilling strategies, etc., but this feature is compromised with increasing material thickness, which increases the likelihood of the light encountering a material defect, preventing transmission.[46]

As a starting point of this discussion, we introduce the optical properties of paper, alongside cardboard. A standard paper sheet is white and opaque due to the presence of micrometer-sized voids within the fiber network that leads to the scattering of light at the interfaces between the voids and the cellulose fibers (10–50 μm in diameter).[60,66,67] Different approaches have been introduced to increase the transparency of the paper, such as minimizing void space by decreasing the dimensions of the cellulose fibers, from the micrometer-scale down to the nanoscale. As the dimensions of the cellulose fibers are decreased, the size of voids is also reduced, consequently resulting in less light scattering and increased transparency. This has been observed in materials produced from size fractionated CNF suspensions having average fibril diameter fractions of 4.2 ± 2.7, 5.6 ± 3.2, and 19.5 ± 13.2 nm, where the thinner fibrils translated into higher transparency and lower haze (**Figure 1**a–c). The influence of structuration on optical properties was demonstrated by either pressing dewatered CNF networks to reduce porosity and increase density (Figure 1a–c, left side, films) or by solvent exchanging from water to 2-propanol to octane, followed by drying under ambient conditions to give porous membranes (Figure 1a–c, right side, porous membranes). Although the obtained films and membranes had the same thickness (≈10 μm), the films were approximately twice as dense as the porous membranes and as such were more transparent and less hazy.[66]

The solvent used to disperse CNF can influence the optical properties of resultant materials, depending on the colloidal stability and properties of the fibrils in the given solvent.[63] Suspensions of CNF in water can be solvent exchanged to organic solvents such as ethanol, methanol, or acetone, which often leads to colloidal heterogeneity, as the CNF are less compatible with these solvents.[70] Consequently, the films produced by the evaporation of these suspensions contain more voids compared to films cast from aqueous suspensions. This was demonstrated by a comparison of films cast from dispersions of CNF (lateral dimension of 15 nm) in water or water: ethanol
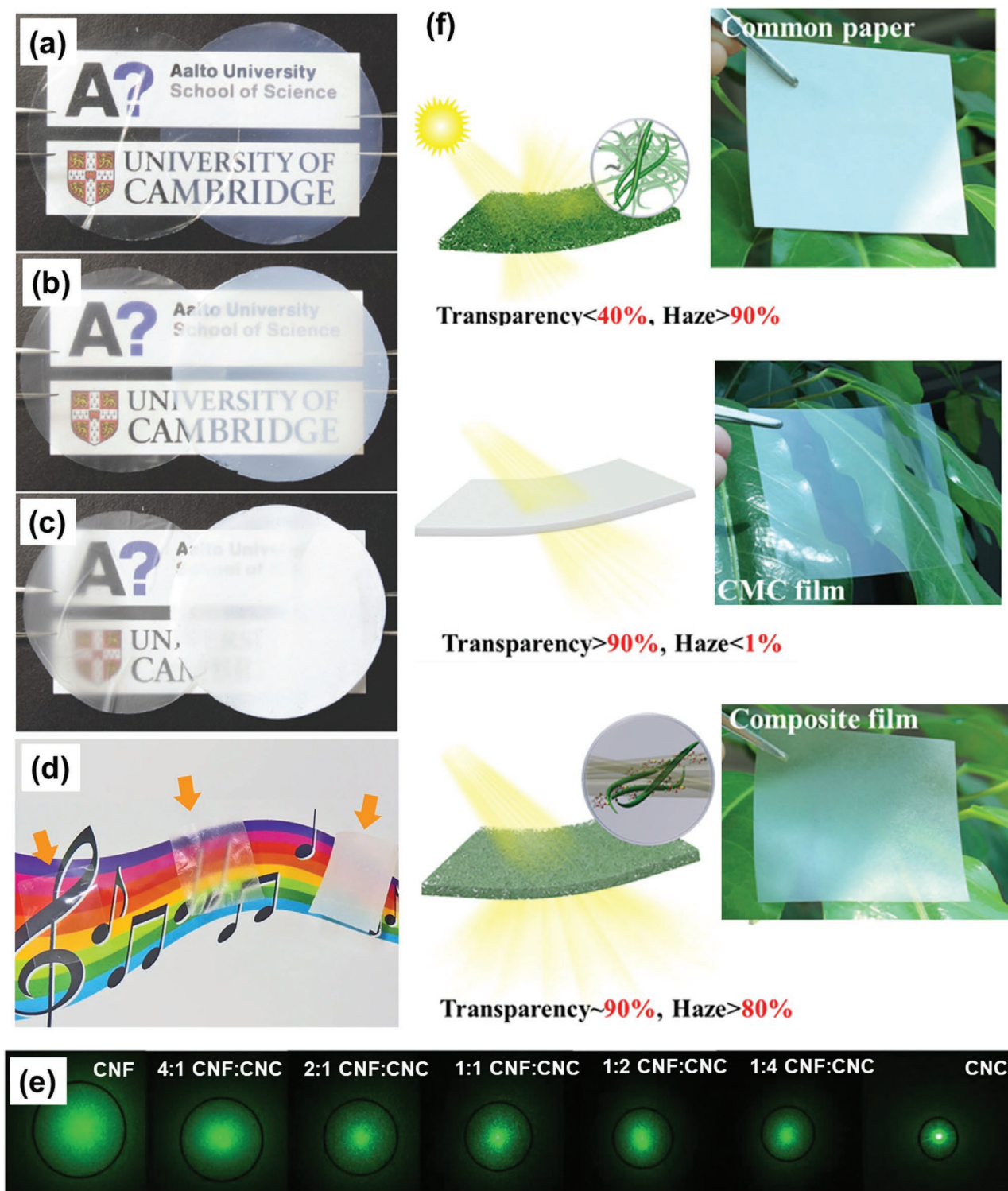
Figure 1. a–c) Nanocellulose films with different optical properties. Effect of fibril size and material porosity of CNF films of 10-µm in thickness. Photographs of pressed (left) and solvent exchanged CNF films (right) produced from (a) finest, (b) medium, and (c) coarsest fibrils; Reproduced with permission.[66] Copyright 2018, Wiley-VCH. d) Effect of colloidal stability. Left: transparent CNF film (density: 1.48 g cm⁻³, Center: translucent CNF film (density: 1.15 g cm⁻³), Right: opaque CNF film (density: 0.81 g cm⁻³); Reproduced with permission.[63] Copyright 2017, Springer Nature. e) Effect of fibril size in CNF/CNC mixed films. Photographs of green laser diffraction through CNF, CNC, and mixed CNF/CNC films; Reproduced with permission.[68] Copyright 2019, Springer Nature. f) Effect of polymer impregnation. Schematics and accompanying photographs of opaque, transparent, and translucent cellulosic films made by impregnation of paper with CMC. Reproduced with permission.[69] Copyright 2018, American Chemical Society.

**ADVANCED
SCIENCE NEWS**

www.advancedsciencenews.com

**ADVANCED
MATERIALS**

www.advmat.de

mixtures (50:50 and 10:90). Both solvents gave 40 μm-thick films with high transparency (≈90% at 550 nm) but drastically different haze values (4.2%, 49.3%, 90% at 550 nm, respectively) depending on the ethanol content of the suspension.[63] With increasing ethanol, films became less dense and hazier due to increased film porosity (Figure 1d). In this case, the reported high transmittance was attributed to scattered light but not to light transmission.[63]

Another way to tailor material transparency and haziness is by combining CNC and CNF, e.g., to produce mixed CNC/CNF films where CNC favors more transparent films due to their smaller size, while CNF tend to produce hazier materials.[47] Li and collaborators[68] produced mixed films from CNF (diameter: 10–80 nm, length: several microns) and four different CNC types [CNC-1 (diameter: 30–129 nm), CNC-2 (diameter: 50–100 nm), CNC-3 (diameter: 26–56 nm), CNC-4 (diameter:12–42 nm)]. Haze was correlated with the diameter of the nanocellulose according to CNF>CNC-1>CNC-2>CNC-3>CNC-4. Additionally, packing voids in CNF films by the addition of CNC-2 resulted in less light scattering, which was visually demonstrated by directing a green laser through these mixed CNC/CNF films (Figure 1e).

High transparency/low haze films can be produced by partial cellulose dissolution followed by regeneration or derivatization.[71] In both cases, the interactions between macroscale cellulosic fibers are disrupted, followed by regeneration in a nonsolvent bath to give homogenous materials with a minimal number of voids.[72] Specific solvents, such as ionic liquids (ILs), NaOH/Urea, N-methyl morpholine-N-oxide (NMMO), N, N-dimethylacetamide/LiCl (DMAc/LiCl), tetrabutylammonium fluoride/dimethyl sulfoxide (DMSO), metal-complex solutions, and molten inorganic salt solutions, can be used to dissolve cellulose.[53] These solvents are also used in homogenous cellulose derivatization, e.g., to produce cellulose polymer derivatives, such as methylcellulose (MC), hydroxypropylmethylcellulose (HPMC), ethyl cellulose (EC), hydroxypropyl cellulose (HPC), and carboxymethyl cellulose (CMC).[50] Leppänen et al.[73] observed lower transmittance for pure regenerated cellulose films in comparison to those from a cellulose polymer derivative, possibly related to larger gaps between the derivatized cellulose chains substituted with methyl, ethyl, or carboxymethyl groups.[73]

Similarly, films of chemically modified CNF are usually more transparent and have different haze characteristics when compared to films from unmodified CNF. Chemically modified CNF is often produced by heterogeneous derivatization of cellulose fibers followed by mechanical fibrillation (e.g., microfluidization, extrusion, grinding), whereas unmodified CNF is produced via direct fibrillation, sometimes coupled with an enzymatic pretreatment. Pulp modification to generate other CNF grades include TEMPO-mediated oxidation, carboxymethylation, cationic modification, and phosphorylation.[74] TEMPO-CNF is widely reported to produce films with transparency >80% and a broad range of haze values (up to 65%),[75] depending on the fibril dimensions, processing approach, film density, and film thickness.[60,76–79]

All-cellulose composite materials are promising for tailoring transparency and haze properties due to the inherent physicochemical compatibilities of their components. Similar to the mixed CNC/CNF films described above,[68] all-cellulose composites are composed of two or more sources of cellulose, where the matrix consists of dissolved and regenerated cellulose and the reinforcing filler is a somewhat more native cellulosic element.[80] Hu,[69] Hou[81] and collaborators produced films with transparency >90% by soaking paper sheets (transmittance: <40%, haze: >90%, thickness: 160 μm) in a solution of carboxymethylcellulose (CMC) to give a 70 μm-thick film or in dissolved cotton cellulose (NaOH/urea solvent) to give a 78.6 μm-thick film. In both cases, the cellulosic solution filled the voids creating a homogenous structure, leading to transparency, with haziness favored by maintaining the cellulosic fibers in the paper sheet intact. The all-cellulose composite film produced by soaking in regenerated cellulose had higher haze (95.2%) in comparison with the film soaked in CMC (haze: >80%, Figure 1f). However, it is unclear whether this difference in haze is related to the dissolution medium, the regeneration process, or differences in film thickness.[69,81]

Composite films produced from CNC- and CNF- stabilized Pickering emulsions can also be used to prepare optically transparent materials.[82–84] For instance, CNF was used as an interface component in the emulsion formation process of polymethyl methacrylate (PMMA), thus, during film formation (melt pressing), PMMA filled the voids and produced the desired transparency.[82] Haze can be tuned in emulsion-based film compositions, for instance, by hot pressing[82] or UV-curing,[83] to change the void size and material density, consequently influencing the scattering of light.

The concept of transparent wood (TW) is a compelling approach to achieve optical effects from common materials.[85] In this case, a thin slice of wood can be chemically modified to remove lignin, yielding a porous structure that appears white and opaque due to light scattering. Next, the voids in the delignified wood are filled with a refractive index-matching polymer to minimize optical heterogeneities and to produce a transparent material that may also exhibit haze (**Figure 2**a). Both transmittance and haze are dependent on the thickness of the wood sample, the degree of matching between the refractive indices, and the uniformity of the polymer filling.[86] Additionally, chemical modifications, such as acetylation[87] or TEMPO oxidation,[88] can increase the transparency of the delignified white wood before the filling step, enabling the production of thicker TW with high transparency and lower haze. Alternatively, TW can be achieved by pressing delignified wood, removing the voids, and thereby creating a transparent film (Figure 2c).[57]

Anisotropic light scattering effects can be achieved in TW samples depending on whether the wood is sectioned longitudinally along the tree trunk, in the direction of the plant cells, or transversely (Figure 2b). Longitudinal wood sections give materials that scatter isotropically, whereas transverse sections scatter anisotropically due to the slow and fast refractive indices of cellulose.[89] The layering of wood sections with perpendicular fiber alignment was found to give a material with high transmittance (≈90%), high haze (≈90%), and isotropic in-plane refractive index.[90,91]

Holo-CNF, consisting of CNF with intact hemicellulose, is a good option for transparent materials since hemicellulose helps to stabilize colloidal suspensions and thus provides
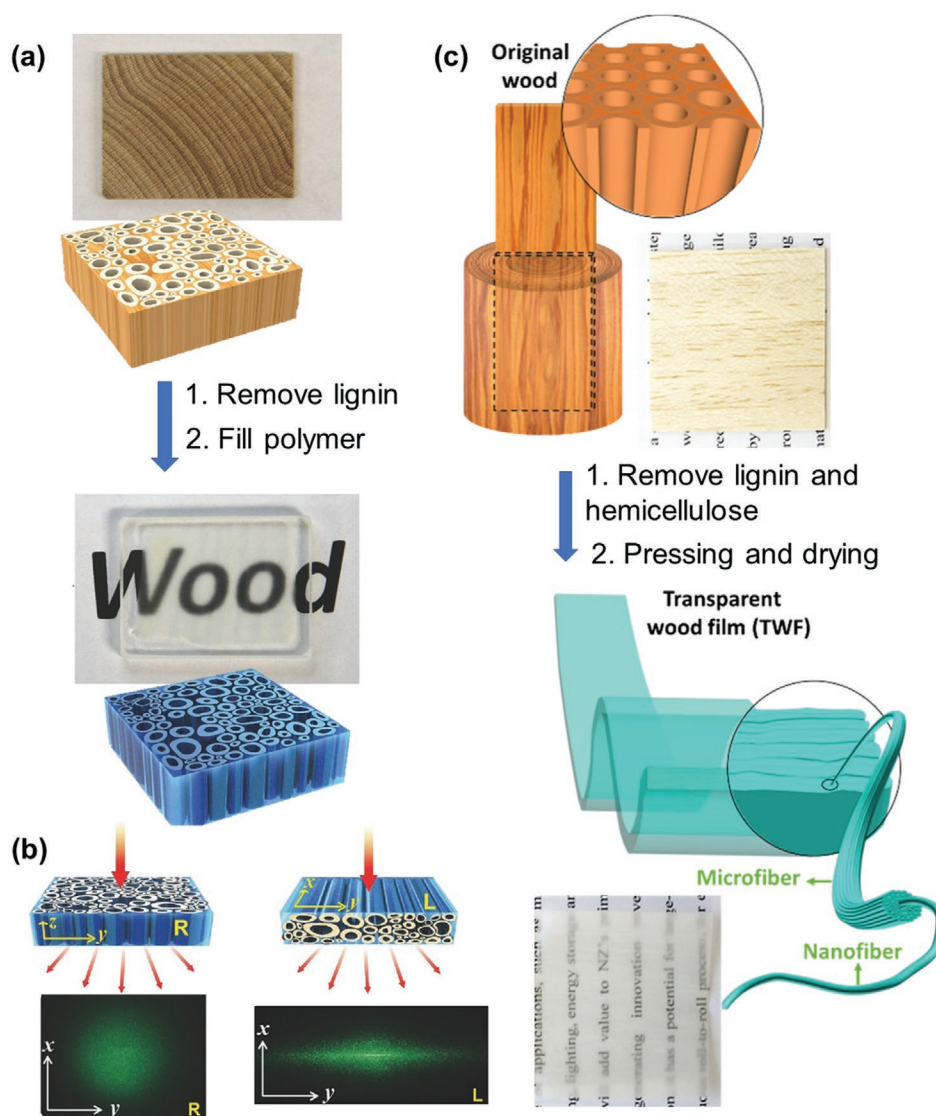
**ADVANCED
SCIENCE NEWS**

www.advancedsciencenews.com

**ADVANCED
MATERIALS**

www.advmat.de

Figure 2. a) Photographs and schematics of a wood structure before removing lignin and after polymer filling. Reproduced with permission.[25] Copyright 2016, Wiley-VCH. b) Different anisotropic structures depending on the sectioning approach and corresponding laser scattering profiles. Reproduced with permission.[25] Copyright 2016, Wiley-VCH; c) Schematics and photographs before and after pressing/drying process, with a transparent film created by pressing delignified wood cell walls together. Reproduced with permission.[57] Copyright 2020, American Chemical Society.

more homogeneous materials.[92] Holo-CNF has been produced by microfluidization[93] and using a kitchen blender,[94] with Holo-CNF films presenting different transparency and haze values, depending on the processing approach. For example, when Holo-CNF were produced by microfluidization, the resultant films (45 µm thickness) had a transparency of 80% (no data for haze),[93] which increased when the Holo-CNF were processed using a blender (35 µm thickness, transmittance of 91%, haze of 26%).[94] Apparently, microfluidization produced a larger fraction of light-scattering nano fibrillar entities; however, the different thicknesses of the films may also account for transparency differences. Finally, isolated hemicellulose can be used as a raw material for transparent films, however, its poor mechanical properties and pale yellow color[95] can be a drawback.[96]

The advantages and disadvantages of preparation conditions and methods are not completely established yet. While it is faster to produce nanocellulose films by filtration, mechanical properties and transparency may be improved by solvent casting. In turn, TW produced by epoxy infiltration have high strength and transparency but are less environmentally friendly and the process is not yet scalable. Hemicellulose films are simple and less energy-intensive to process but have poor mechanical properties. And so on, the particularities of each methodology can generate different properties, and these must be considered for each application, as will be presented in the following sections of this text.

Table 1 summarizes the physical properties that have a direct correlation with the optical performance of lignocellulosic materials. As can be concluded from Table 1, films with

Table 1. Summary of materials with their respective transmittance (T), haze (H), dimension/orientation, thickness, and density values.

Composition	Transmittance (%T) and haze (%H) at 550 nm	Dimensions	Thickness	Density [g cm⁻³]	Ref.
Polyethylene terephthalate (PET)	90	–	–	1.4	[99]
Polyethylene naphthalate (PEN)	87	–	–	1.36	[99]
Polycarbonate (PC)	92	–	–	1.2	[99]
Window glass	99.8[c]	–	–	–	[100]
CNF (never dried birch pulp)	White membranes	Average fibers diameters 19.5 ± 13.2 nm	≈10 μm	0.81 ± 0.16[a]	[66]
	Semi-transparent membranes	Average fibers diameters 5.6 ± 3.2 nm	≈10 μm	0.81 ± 0.16[a]	
	Transparent membranes	Average fibers diameters 4.2 ± 2.7 nm	≈10 μm	0.81 ± 0.16[a]	
CNF (softwood – Japanese cedar/ hardwood – eucalyptus)	T: 90.3–90.7 H: 4.2	15 nm-wide	40 μm	1.48	[63]
	T: 90.3–90.7 H: 49.3			1.15	
	T: 90.3–90.7 H: 90.1			0.81	
CNF (bleached bamboo pulp)	T: 89 H: 77[c]	Diameter: 10–80 nm Length: several microns	38 ± 2 μm	–	[68]
CNC-1 (bleached bamboo pulp)	T: 92 H: 12[c]	Average diameter: 66 nm Diameter distribution: 30–129 nm	22 ± 1 μm		
CNC-3 (bleached bamboo pulp)	T: 95 H: 9[c]	Average Diameter: 37 nm Diameter distribution: 26–56 nm	20 ± 2 μm		
CNC-2 (bleached bamboo pulp)	T: 91 H: 8[c]	Average diameter: 46 nm Diameter distribution: 34–88 nm	24 ± 2 μm		
CNC-4 (bleached bamboo pulp)	T: 90 H: 5[c]	Average diameter: 18 nm Diameter distribution: 12–42 nm	26 ± 1 μm		
4 CNF: 1 CNC-2 (bleached bamboo pulp)	T: 90 H: 60[c]	CNF: Diameter: 10–80 nm Length: several microns CNC: Average diameter: 46 nm Diameter distribution: 34–88 nm	30 ± 1.5 μm		
2 CNF: 1 CNC-2 (bleached bamboo pulp)	T: 91 H: 58		28 ± 2 μm		
1 CNF: 1 CNC-2 (bleached bamboo pulp)	T: 92 H: 50[c]		26 ± 1 μm		
1 CNF: 2 CNC-2 (bleached bamboo pulp)	T: 93 H: 28[c]		24 ± 1 μm		
1 CNF: 4 CNC-2 (bleached bamboo pulp)	T: 94 H: 23[c]		24 ± 2 μm		
Cellulose (bleached softwood pulp)	T: 88[d]	–	30 μm	0.92	[71]
	T: ≈88[d]		–	0.95	
	T: >88[d]		–	1.02	
	T: >88[d]		–	1.09	
CNC (dissolving pulp – Southern Yellow Pine – SYP)	T: 91.3 H: 20.1	Rod-like cellulose crystalline core	40 μm	–	[78]
CNF (dissolving pulp – SYP)	T: 69.7 H: 61.4	Diameter of 3–50 nm and a length of a few micrometers			
TEMPO-CNF (dissolving pulp – SYP)	T: 90.4 H: 49.3	–			
Cellulose (cotton linter pulp)	T: 89.94[d]	–	≈26	0.90469	[76]
CNC (Sugarcane bagasse) / 2,2-Bis[4-(acryloxypolyethoxy) phenyl]propane (resin-in-water Pickering emulsion)	T: ≈90[d,e]	CNC1: 1278 ± 1029 nm long, CNC2: 366 ± 142 nm long CNC3: 341 ± 94 nm long Resin droplets: ≈2 μm	~125–200 μm / T normalized to 100 μm thickness	–	[84]

(Continued)

Table 1. Continued.

Composition	Transmittance (%T) and haze (%H) at 550 nm	Dimensions	Thickness	Density [g cm^{-3}]	Ref.
Cellulose pulp (softwood fibers)	T: 26.4 H: 99.7	2.01 mm of length 28.3 μm of width	152.3 μm	0.48	[81]
Dissolving pulp (cotton linter)	T: ≈90 H: ≈40	–	50.2 μm	1.4	
All-cellulose composite	T: 90.1 H: 95.2	2.01 mm of length 28.3 μm of width	78.6 μm	0.87	
Cellulose pulp (Northern wood)	T: <40 H: >90	3.2 mm of length, 50 μm of diameter	160 μm	–	[69]
Carboxymethyl cellulose (CMC)[b]	T: >90 H: <1	M.W. 700 000 (DS = 0.9)	65 μm		
CMC/cellulose composite[b]	T: ≈90 H: >80	3.2 mm of length, 50 μm of diameter	70 μm		
TEMPO-CNF (wood) / Polymethyl methacrylate (PMMA)	T: 87[c),d]	13 nm of width, 445 nm of average length	≈200 μm	–	[82]
CNF (sugarcane bagasse pulp) / Acrylic resin monomer (2.2 bis[4-(acryloxypolyethoxy) phenyl]propane	T: 48.9[c),d]	10–30 nm of widths and > 2 μm of length	80- 180 μm / T: normalized to 100 μm	–	[83]
	T: 91.5[c),d]				
Acetylated transparent wood (TW) (balsa wood)	T: 86 H: 66.7	longitudinal section	0.24 cm	–	[86]
	T: 82.1[d]		0.32 cm		
	T: 77.1[d]		0.42 cm		
	T: 72.1[d]		0.51 cm		
	T: 66.2[d]		0.65 cm		
TW (balsa wood)	T: 84[d]	longitudinal section	0.11 cm		
	T: 71.5[d]		0.21 cm		
	T: 65.3 H: 78.8		0.25 cm		
	T: 61.6[d]		0.31 cm		
	T: 51.3[d]		0.43 cm		
	T: 44.4[d]		0.46 cm		
TW (balsa wood)	T: 10[d]	longitudinal section	80 mm	18	[88]
	T: 80[d] H:70		1 mm	132	
TW (balsa wood)	T: 92 H: 50	transverse plane	1.5 mm	–	[87]
	T: 89 H: 53		3 mm		
	T: 71 H: 74		7 mm		
	T: 89 H: 50		0.7 mm		
	T: 83 H: 70		1.5 mm		
	T: 60 H: 78		3 mm		
TW (balsa wood)	T: 80 H: 85	longitudinal section	55 μm	1.2	[57]
	T: ≈72[d]		120 μm	–	
	T: 68[d]		140 μm		

Table 1. Continued.

Composition	Transmittance (%T) and haze (%H) at 550 nm	Dimensions	Thickness	Density [g cm^{-3}]	Ref.
	T: ≈60[d]		200 μm		
TW (rotary-cutting poplar veneer)	T: 90 H: 90	two-layer perpendicular (0/90°) to each other	3 mm	–	[90]
Holocellulose nanofibers (Holo-CNF) (Industrial softwood/Spruce chips and Aspen wood chips)	T: 80[d]	–	45 μm	1.48 ± 0.05 (no unit)	[93]
Holo-CNF (Spruce wood)	T: 91 H: 26	–	35 μm	–	[94]
TEMPO-CNF (Spruce sulfite pulp and dissolving sulfite softwood pulp – a mixture of spruce and pine)	T: 92 H: 20				
Enz-CNF (Spruce sulfite pulp and dissolving sulfite softwood pulp – a mixture of spruce and pine)	T: 87 H: 30				

[a]Density values in kg m^{-3}; [b]The only study that presented roughness values; [c]T or H provided at 600 nm; [d]H values not presented; [e]T averaged from 400–800 nm.

transparency exceeding 90% at 550 nm can be fabricated from cellulose polymers, from all nanocellulose forms, including CNF from wood and non-wood sources and CNC, and impregnated wood wafers (transparent wood). The haze values of these films can vary – in a non-trivial manner – from below 10% up to 95%, illustrating that especially for optimized haze, the raw material choice, fabrication route, and use of index-matching filler play a crucial role. Although the interconnectivity of these three parameters is not yet completely understood, the diversity of available optical functions is promising from the point of view of different application requirements – for display covers, high transparency coupled with a low haze is a must, whereas, for the light management layers of photovoltaics, high transparency coupled to high haze can translate into significant improvements in power conversion efficiency.[97]

It must be emphasized that many fundamental factors, such as surface roughness and porosity, and their influence on optical properties, are generally overlooked and therefore not reported. Many studies normalize optical properties with material thickness, which neglects for instance the effects of structural inhomogeneities and those of the surface. Likewise, the comparison between optical properties of materials with different thicknesses makes it difficult to establish any rules to engineer light management in cellulosic materials. Another important point is the lack of data regarding the haze of these materials since many reports only consider transparency but not scattering.

Although many interesting routes exist toward the production of transparent and transparent/hazy materials from cellulose-fiber based materials, there are some potential drawbacks, such as multi-step processing, energy-intensive processing (e.g., fibrillation, dewatering), as well as lab-scale materials and processes that are not necessarily translatable to the industrial scale. In this regard, the interactions of wood-derived materials with water are of prime importance, as has been reviewed recently.[98] Still, transparent/translucent lignocellulosic materials stand out from conventional transparent materials, such as glass and some polymers (e.g., polyethylene terephthalate

– PET), due to their renewability and potential tunability of optical properties, which can provide higher yield performance in electronic devices, such as solar cells or light-emitting diodes (LEDs). Additionally, they can provide a chemically and optically inert (i.e., transparent) matrix within which non-native optical properties can be embedded, either by the addition of functional components or through structural manipulation. In the following sections, we present different ways that lignocellulosics can produce specific optical responses that can be applied in smart materials.

3. UV Protection from Plant-Based Materials or Additives

Ultraviolet light (UV light), comprising UVA (400–315 nm), UVB (315–280 nm), and UVC (200–280 nm), is responsible for the formation of free radicals and photochemical reactions that degrade organic matter, including the oxidation of proteins, lipids, and vitamins, the degradation of antioxidants, dyes, and foods, and can lead to the development of skin and eye diseases.[101] Similarly, UV light can damage electronic devices such as solar cells,[102] especially since polymeric substrates offer minimal UVA protection, but even glass-based solar devices, such as dye solar cells, undergo significant deterioration, making UV protection a must.[103–105] Lignocellulosics can be used to produce biobased UV light blocking materials, which can then be used in devices to shield components from the harmful effects of UV light. In addition to UV-protection from lignocellulosic materials, we consider semiconductor nanoparticles with UV-light absorbing properties included within UV-transparent lignocellulosic matrices.

3.1. Biobased Materials Doped with UV-Absorbers

Semiconductor nanoparticles (NPs) with UV light absorbing properties interact with UV light by absorption, determined
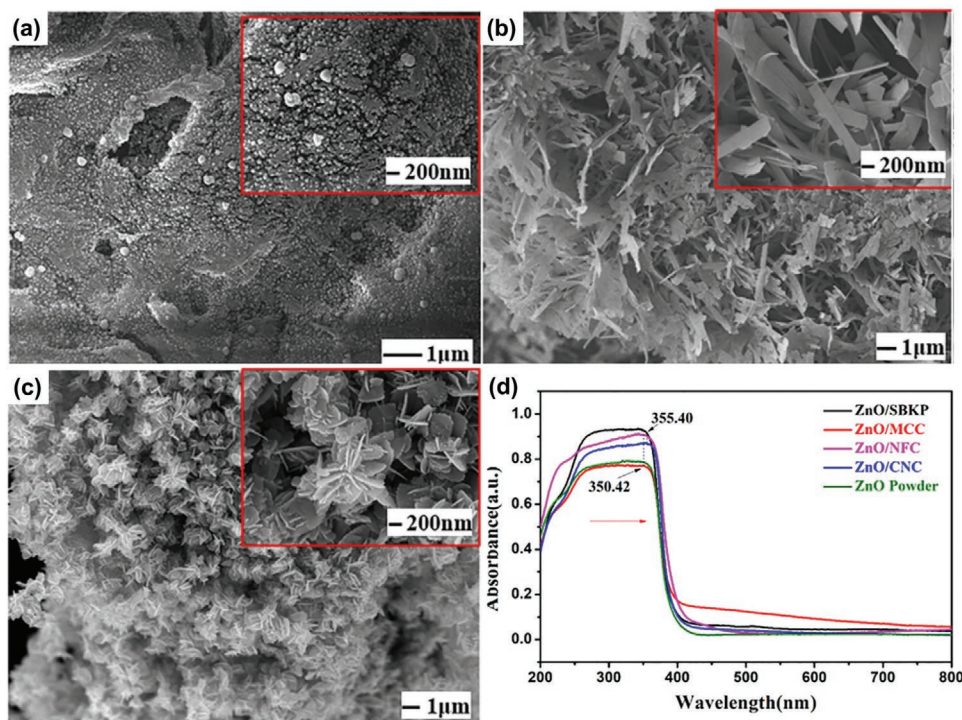
ADVANCED
SCIENCE NEWS
www.advancedsciencenews.com

ADVANCED
MATERIALS
www.advmat.de

Figure 3. Scanning electron microscopy images of ZnO and MCC composites produced in situ with different shapes. a) spherical ZnO, b) sheet-like ZnO, c) flower-like ZnO, and d) UV–vis spectra of ZnO/SBKP (softwood bleached kraft pulp), ZnO/MCC, ZnO/NFC (CNF), and ZnO/CNC. Reproduced with permission.[116] Copyright 2021, Elsevier.

by their bandgap, and scattering. The most common particles used for UV shielding are zinc oxide (ZnO) and titanium dioxide (TiO_2) NPs, which have high transmittance across the visible spectrum as their main advantage for many applications. For instance, ZnO NPs effectively block UVA radiation, whereas TiO_2 NPs block the UVB range. As such, the combination of both, ZnO and TiO_2 NPs provides broadband UV protection.[106,107] Compared to TiO_2, ZnO NPs are considered safer from a nanotoxicological perspective,[108] and for this reason, ZnO NPs are more often included in lignocellulosic materials intended as UV absorbers. Note that CeO_2[109] and flower-like NiO_x structures have been also considered.[110]

The nanoparticles can be synthesized in situ within the material matrix or ex situ and then added to the matrix. The ex situ approach offers tighter control over NP synthesis, polydispersity, stabilization, and loading into the matrix, all of which enable efficient UV blocking optimization.[111–113] The ex situ NP integration into lignocellulosics materials can be achieved in two ways: a) homogeneous dispersion in the material bulk, and b) coating the material surface, which provides higher UV blocking efficiency, once sufficient coverage is reached.[111–113] Stable dispersion within the matrix of the NPs is important for maintaining optical performance, for instance, although agglomerated ZnO NPs in CNC films completely blocked UV light, they simultaneously decreased overall film transmittance, which is a considerable problem for applications such as solar cells.[111] Another example that demonstrates the importance of NP-matrix compatibility is the dispersion of ZnO NPs, which was found to be better in benzoate hemicellulose/poly(vinyl) alcohol (PVA) compared with hemicellulose/PVA films, a

feature that was attributed to the ester groups of the hemicellulose derivative.[112]

NP shape may also be an important feature, for instance changing the shape of ZnO from a belt-like (b-ZnO) to sheet-like (s-ZnO) led to increased absorption of UV light in CNF films.[114] Similarly, when flower-like ZnO nanorods were grown on the surface of electrospun cellulose nanofibers, an increase of ≈50% in UV light blocking was observed compared to electrospun cellulose nanofibers with ZnO seeds on the surface. This increase in UV light blocking was mainly attributed to the increase in UV scattering at the film surfaces due to the presence of the flower-like nanorod structures.[115] However, according to studies by Mun et al.,[113] the photogeneration of electron-hole pairs in the nanorods under UV light may also play a role.[113]

Different NPs morphologies can be obtained using the in situ approach (**Figure 3**).[116] In general, the process consists of dissolution of the salt derivatives, such as zinc salts, in the presence of cellulose, followed by precipitation of NPs on the cellulose surface. For instance, when a cellulose source is immersed in a solution of Zn^{2+}, cellulose hydroxyls interact with the cation and an equilibrium can be achieved.[116] After that, the addition of a polyol (diethylene glycol) mediates the hydrolysis and condensation processes resulting in spherical ZnO NPs adsorbed onto the cellulose.[116,117] To achieve sheet-like ZnO NPs, the mediator can be a urea solution, where the urea is a source of NH_4^+ which helps increase the pH and supports sheet-like growth.[116,118] Lastly, flower-like ZnO can be achieved by dropping a solution of NaOH into a hot mixture of Zn/cellulose.[116] It is possible to obtain the different ZnO shapes

on various cellulose substrates, such CNF or MCC. When the NPs are produced in the presence of CNF, highly porous 3D network structures were easily produced resulting in greater absorption of UV light (Figure 3d).[116]

3.2. Biobased Materials as UV-Absorbers

Although cellulose does not absorb UV light, it can be modified to produce cellulose-based derivatives that exhibit this feature. For instance, poly(cinnamoyloxy ethyl methacrylate)-grafted CNC nanohybrids (PCEM-*g*-CNCs) used as a reinforcement agent in poly(vinyl chloride) (PVC) films (thickness: 90 μm) absorb UV light up to ≈320 nm (UVB and UVC) and also reduced UVA (320–400 nm) absorption.[119] In this case, the UV absorbance was attributed to the conjugated C=C bonds of the grafted polymer.[119] Another example is benzophenone-grafted CNF used as a nanosized UV absorber in polyvinyl alcohol, providing 92% UVB and 52% UVA light absorbance, the extent of which depended on the concentration of the CNF derivative in film (≈25 μm thick).[77] Surprisingly, UV absorption can also be achieved by the heat treatment of TEMPO-CNF films, which creates interfibrillar hemiacetal linkages between hydroxyl groups and C6-aldehydes. The heat treatment is accompanied by yellowing, with the extent of UVA/UVB absorption tunable by the temperature. In addition to the UV blocking feature, heat-treated TEMPO-CNF films (14.5–17.2 μm thick) maintained 72% transparency across the visible spectrum and retained their UV-absorption feature even after long UV irradiation times.[120]

Plant-based components with UV-blocking properties have been explored within plant-based matrices, for instance, a 47% reduction in transmittance at 325 nm was reported for CNF/xylan composite films (20–40 μm thick), which was attributed to the aromatic rings in the xylan structure.[121] There is no consensus regarding the cause of this effect since the pulping process oxidizes several polysaccharides, creating chromophores responsible for UV absorption. Among these chromophores are carboxyl groups (absorption at 200–220 nm), carbonyl groups (absorption at 270–290 nm), heteroaromatics of furan (absorption: 230–250 nm), heteroaromatics of pyran-type (absorption at 290–320 nm) and conjugated heteroaromatics (absorption above 300 nm with peaks at 350–370 and 430–450 nm).[122] Additionally, the presence of pseudo-lignin (lignin re-precipitated during the extraction process) on the surface of these polysaccharides cannot be ruled out.[123,124] In the same way, it is still unclear whether hemicellulose in its native state, bound to cellulose, exhibits the same UV-blocking behavior since the light absorption of holo-CNF films has only been reported across the visible spectral region (400–800 nm).[94]

Lignin has been widely reported for its use as a UV-light absorber, due to its light-active chromophore functional groups, such as carbonyl groups, aromatic rings, and carbon-carbon double bonds.[55] However, the UV-absorbing properties of lignin are highly linked to the extraction process and the characteristics of the resultant lignin, such as molar mass, concentration, size, functional groups, etc., which will be discussed in more detail in the subsequent text.

Different extraction approaches yield lignins with distinct UV absorption properties, mainly because of chemical changes that are induced during the processing related to reagents, temperature, and pressure, e.g., and subsequent precipitation conditions. For example, the organosolv process uses organic solvents or aqueous solutions of organic solvents, and the Kraft process is performed using aqueous solutions containing sodium hydroxide (NaOH) and sodium sulfide (Na_2S) at high temperature and high pressure. Organosolv lignin is purer, contains no sulfur groups, and presents a structure closer to native lignin, whereas Kraft lignin has undergone major depolymerization and changes in chemical structure, including the addition of sulfur groups.[125] Additionally, organosolv lignin has a higher content of $C\alpha=C\beta$ bonds compared to Kraft lignin. This larger number of $C\alpha=C\beta$ bonds is given as the main reason for the higher UV light absorption achieved in chitosan films containing solubilized organosolv lignin, compared with chitosan films containing solubilized Kraft lignin.[126]

UV absorption is also influenced by the concentration of lignin inside of the material. Parit et al.[127] looked at three concentrations of lignin nanoparticles produced in situ in CNC films and found that films containing 1 wt% lignin absorbed mainly UVC, whereas 4 wt% lignin imparted complete UVC and partial UVB absorption and 10 wt% lignin complete broadband UV absorption (UVC, UVB, and UVA).[127] The same relation between lignin concentration and UV absorption was observed when colloidal lignin NPs were dispersed in CNF films.[128]

As usual, compatibility between the matrix and lignin (or other optically functional additive) is important for material optical properties, i.e., UV absorption and transparency. For instance, CNC films containing solubilized Kraft lignin[127] absorbed more UV light and were more transparent in the visible spectrum compared with chitosan films that contained the same lignin.[126] Additionally, lignin that is naturally bound to cellulose also demonstrates UV absorption behavior. Jiang et al.[129] demonstrated that ≈15% residual lignin was needed for 100% UVC, UVB, and UVA absorption in CNF films (thickness: ≈50 μm) produced from unbleached sources, with lower residual lignin (2%) providing incomplete absorbance.[129] UV protection using extracted lignin has also been found in the literature, for instance, Sadeghifar et al.[130] produced highly UV absorbent films (100% UVB protection and more than 90% UVA protection) from microcrystalline cellulose modified with azide functional groups linked to the propargyl groups of lignin by click chemistry.[130] A fair comparison of the UV-blocking potential of different lignin forms (i.e., bound, extracted, solubilized, particulate) is not yet available in the literature.

Lignin NPs can be produced through controlled precipitation by the addition of an antisolvent to a lignin solution, for instance, lignin NPs can be precipitated by adding water to lignin dissolved in tetrahydrofuran.[131] The dispersibility of lignin NPs in the bulk of the material is influenced by NPs size, chemical compatibility between NP and the matrix, and the surface charge of the lignin NPs (**Figure 4**a).[128] The authors studied the optical properties of different CNF films containing colloidal lignin particles (CLP), cationic CLP (c-CLP), Kraft lignin (KL) with different weight ratios as displayed in Figure 4b. In situ lignin NPs prepared by dropping an acetone solution of lignin into aqueous CNF or nano-chitin suspensions had different nucleation behavior depending on the
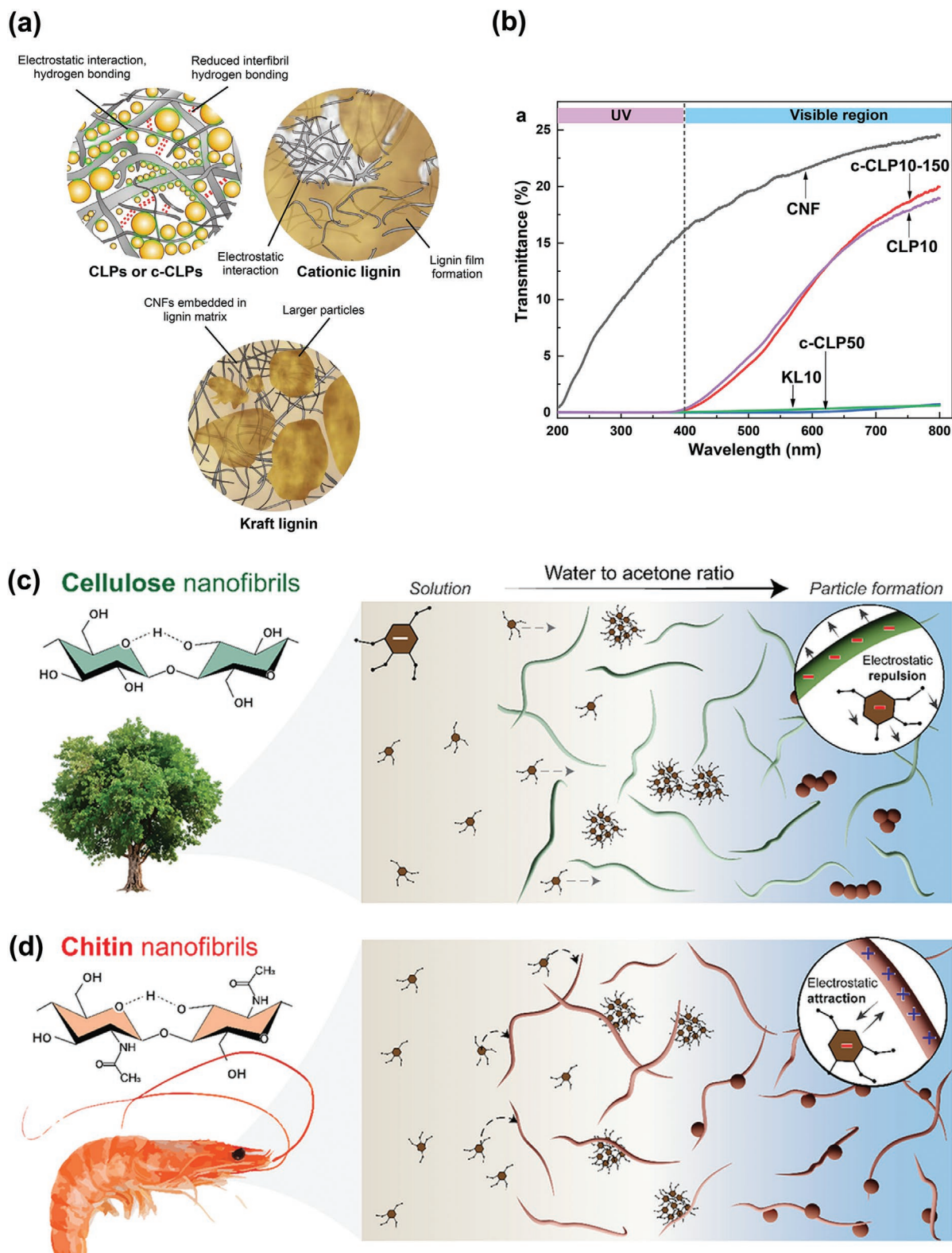
Figure 4. Schematics of interaction between matrixes and lignin. a) Interaction between CNF and different lignin morphologies in films produced by the addition of lignin NPs produced ex situ, b) UV–vis spectra of CNF, Kraft lignin (KL), colloidal lignin particles (CLP), and cationic CLP (c-CLP) films with different weight ratios. Reproduced with permission.[128] Copyright 2018, American Chemical Society. In situ nucleation and growth of lignin nanoparticles in the presence of c) cellulose and d) chitin nanofibers. Reproduced with permission.[132] Copyright 2020, American Chemical Society.

surface charge of the nano-scaffold (Figure 4c,d). In the case of CNF, the anionic lignin NPs were observed in the vicinity of the CNF, but not anchored to the CNF surfaces due to electrostatic repulsion, whereas the lignin NPs adhered to the surface of cationic nano-chitin.[132] Regarding optical properties, improved compatibility between the biobased matrix and NP additive leads to better dispersion of the additive in the matrix, promoting the formation of transparent materials with high UV blocking capacity.[128,132–134]

While lignin can be an effective UV absorber, the color of this material (brown-black color) can be undesirable or even detrimental to device efficiency because it reduces transparency in the visible range. This coloration depends on the number of unsaturated bonds in the lignin[135] and can be manipulated by different methodologies of extraction or modification, e.g., to obtain colorless lignin. For example, depending on the pH of the precipitation medium after extraction or the chemical environment during drying (e.g., presence of O_2), lignin may be oxidized, resulting in darker colored material.[135] Processing also impacts lignin color, for instance, higher shear rates translate into reduced particle size and a consequent decrease in lignin color.[24] This process also leads to a decrease in particle aggregation (which also changes the color of the lignin). Finally, the modification of lignin through processes such as acetylation,[136] sulfonation,[137] and UV irradiation in tetrahydrofuran,[31] or in H_2O_2/ alkaline[138] have been used to obtain lighter-colored materials that retain a UV-absorption capacity.

Another advantage of lignin is its potential association with semiconductor NPs by physically or chemically interacting with the surfaces of NPs such as TiO_2[139] and ZnO.[140] Coating semiconductor NPs with lignin gives rise to an increase in reflectance, and thus, to an increase in UV light blocking. As in the case of semiconductor NPs, the UV-blocking characteristics of semiconductor lignin-coated NPs are influenced by the concentration, shape, and size of the NPs.[141,142]

The applications of lignocellulosic materials as UV absorbers are promising, however, they still present some drawbacks that need to be addressed. For instance, whether and how the UV-absorbing and mechanical properties of lignin-containing materials is altered by long time UV exposure remains to be studied.

4. Light Emission from Lignocellulosic Materials or Additives

Evolution has led to light emitting plants;[143,144] however, direct application of bioluminescence in electronic devices is not yet feasible. An indirect bio-inspired approach can be achieved by the integration of lignocellulosic materials with luminescent particles. In this section, we present an overview of this approach with different dopants, including lanthanides, carbon nanodots (C-dots), and other dopants (perovskite QDs, metal chalcogenides QDs, and organic dyes).

Luminescence is a spontaneous, non-thermal process, in which light is emitted by luminescent materials (or phosphors) in the spectral region of ultraviolet, visible, or infrared.[145] This process may occur due to chemical reactions (chemiluminescence),[146–149] electrical energy (electroluminescence),[150]

mechanical stressors (mechanoluminescence),[151,152] or the absorption of photons (photoluminescence).[153] In this section, we will focus on reviewing the photoluminescence of lignocellulosic materials, because only few studies have been reported on the other types of luminescence in the past five years.

Inorganic luminescent materials, e.g., rare-earth and perovskite phosphors, have been widely applied in household devices such as televisions, mobile phones, and other electronics.[154–157] However, due to high production costs and toxicity concerns associated with the reagents used in the synthesis of inorganic phosphors, the past two decades have seen a significant rise in the development of organic phosphors. However, the performance of pure organic phosphors has some limitations, such as room temperature phosphorescence due to spin-orbit coupling, which is only efficient in heavy-metal atoms.[158] One way to overcome this drawback is to develop organic-inorganic luminescent hybrids, e.g., metal–organic frameworks (MOFs) and perovskite hybrids.[155,159,160] Thanks to their synergetic interactions and interfaces, these hybrids exhibit superior properties, including luminescence that can be generated by both the organic and inorganic moieties.[160]

Nowadays, intensive research on the development of low-cost, biocompatible, and environmentally friendly luminescent hybrid materials is underway.[161] The integration of lignocellulosic materials (e.g., hemicellulose,[162] cellulose,[163–171] lignin[172–175]) with lanthanide complexes, QDs, inorganic NPs, or organic dyes has gained considerable interest due to improvements in photoluminescence (PL) intensity, quantum yield (QY), and crystal lattice homogeneity of luminescent materials, as well as reductions in deleterious quenching interactions.[176,177]

4.1. Lanthanides Integrated into Lignocellulosic Materials

Lanthanide-doped nanomaterials have attracted considerable interest in various fields due to their exceptional properties, including their ladder-like energy level configurations (4f electronic orbitals) and unpaired electrons, which result in high-performance activators for PL.[178–180] Trivalent lanthanide ions (Ln^{3+}) possess outstanding spectroscopic properties, such as sharp emission peaks (pure color emission), high luminescence efficiency, and long lifetimes.[181,182] Xue et al.[163] developed a transparent cellulose nanopaper functionalized with lanthanide complexes (Ytterbium "Yb" and neodymium "Nd") and UV filters (β-diketone) for UV blocking applications.[163] The researchers studied the effect of lanthanide and CNF content on the transmittance, luminescence, and UV blocking properties of the nanopaper. The transmittance of the nanopaper increased from 63% to 83% (at 600 nm) as the concentrations of both lanthanides (from 8 to 2 mg) and CNF (from 800 to 200 mg) was decreased. However, maximum near-infrared (NIR) luminescence and UV blocking (UVA and UVB) were achieved at the highest concentration of Yb^{3+} and Nd^{3+} (8 mg each), reaching 100% at 298 and 345 nm, respectively, mainly attributed to the π–π^* transition of the β-diketone ligands. The researchers also reported an improvement of UVB blocking with increasing thickness of the nanopaper.[163] Wang et al.[183] prepared CNF-based papers functionalized with lanthanum trifluoride-doped europium and terbium (LaF_3:Eu^{3+} and LaF_3:Tb^{3+})

for anti-counterfeiting applications.[183] In addition to the high PL properties of TEMPO-CNF LaF_3:Tb^{3+}/Eu^{3+} papers at excitations of 260 nm/397 nm giving emissions at 545 nm/590 nm, the papers also possessed superhydrophobic and self-healing properties.[183] Zhang et al.[184] doped TEMPO-CNF with Tb^{3+} and/or Eu^{3+} to produce hazy, luminescent nanopapers via the self-assembly of ligand-stabilized lanthanide complexes (ligand: tris(2-benzimidazolymethyl), NTB) and TEMPO-CNF (NTB-Tb^{3+}-tCNF, NTB-Eu^{3+}-tCNF, and NTB-Tb^{3+}/Eu^{3+}-tCNF). The nanopapers had excellent optical properties, such as high fluorescence intensity (at wavelengths of 546, 613, and 618 nm) and lifetimes of 569–575 μs. These results demonstrate the potential of lanthanide-doped nanopapers in optical applications, including solar cells, UV-blocking, and organic LEDs.[184]

As a sustainable and renewable material, wood is an interesting template for impregnation with lanthanide nanomaterials, resulting in luminescent/TW composites. Gan et al.[185] developed a luminescent TW (LTW) composite using lanthanide complexes (γ-Fe_2O_3@YVO_4:Eu^{3+}) with different concentrations of Eu^{3+}.[185] As the concentration of the Eu^{3+} increased (from 0.1 to 0.5 wt%), the transmittance of the LTW decreased from 80.6 to 40.8% in the wavelength range of 350–800 nm due to particle agglomeration within the wood template. However, LTW with a 0.5 wt% Eu^{3+} (LTW-0.5 wt%) concentration showed the highest QY (0.64%) compared to LTW-0.1 wt% (QY = 0.1%), possibly due to improved energy transfer between vanadate groups and Eu^{3+} as the concentration increases.[185]

Upconversion is a nonlinear process that converts low-energy photons (more than one) to higher energy ones, e.g. NIR to UV and/or visible, with Ln^{3+} ions promising as dopants for upconversion due to their significant improvement of luminescence brightness and upconversion nanoparticle (UNCP) performance.[179] The most common Ln^{3+} ions for this purpose include europium (Er), holmium (Ho), thulium (Tm), or Tb ions, which act as activators. In the upconversion process, activators are usually paired with sensitizer ions, mostly Yb^{3+} ions due to their strong light absorption at around 975 nm, which improves the energy transfer process to lanthanide-based activators.[178] The luminescence properties of UCNPs can be tuned by choosing specific activators and sensitizers. Li et al.[186] integrated lanthanide-doped UCNPs, $NaYF_4$:TmYb, with CNCs to fabricate chiral photonic films for upconverting applications.[186] The photonic films exhibited iridescent colors with multiple emission peaks at 450, 474, and 646 nm when excited at 974 nm, and long lifetimes of 192 and 453 μs at 450 and 646 nm, respectively.[186] Recently, Grzyb et al.[187] proposed dual-mode (upconversion and downconversion in the same system) $LaPO_4$ NPs doped with Yb^{3+}/Tm^{3+}/Ln^{3+} (Ln = Eu, Tb) in cellulose fibers as temperature nanosensors.[187] The multifunctional materials emitted both upconversion and downconversion luminescence within a single particle under NIR (at 975 nm) and UV (at 375 nm) excitations, respectively. Excitation at 375 nm resulted in pure red (at 696 nm) and green (at 542 nm) emissions due to the presence of Eu^{3+} and Tb^{3+}, respectively. Whereas the violet-blue emission at 473 nm (under excitation at 975 nm) was attributed to the Tm^{3+} and Yb^{3+} co-dopants. The emission intensities of the upconversion and downconversion processes of the luminescent cellulose fibers depended significantly on the concentration of activators (Eu^{3+} and Tm^{3+}). Lower activator

contents were linked to superior emission intensities, however, the concentration of sensitizer (Yb^{3+}) is usually fixed at a high concentration (around 20%) to ensure high energy transfer efficiency to Tb^{3+} or Eu^{3+} under NIR excitation.[187] Lanthanide complex-doped lignocellulosic materials have promise in many other applications, as shown in **Table 2**.

4.2. Carbon Nanodots Obtained from Lignocellulosic Sources

Carbon nanodots (C-dots), are nanoscale (<10 nm) luminescent materials with characteristics that include low toxicity, high biocompatibility, and straight-forward preparation.[188] The large number of subclasses or classifications of C-dots, e.g., carbon nanodots (C-dots), carbon quantum dots (CQDs), graphene quantum dots (GQDs), and nitrogen-rich quantum dots (N-dots) is problematic and reflective of researchers classifying their materials according to incorrect criteria, reporting them as new materials, with different names. Cayuela et al.[189] proposed that these materials should be classified based on aspects such as the crystallinity of the core structure as well as the presence/absence of quantum confinement, leading to the following simplified nomenclature: CNDs, CQDs, and GQDs. In brief, particles with an amorphous core and the absence of confinement are classified as CNDs, while crystalline particles with quantum confinement can be classified as either CQDs or GQDs, the only difference is the number of graphitic layers, the former, possessing multiple layers compared to a single layer for GQD.[190] In this review, and for simplicity, we designate these materials using the nomenclature by which they were originally reported.

Carbon nanomaterials are usually synthesized from various carbon sources, most commonly citric acid, but also including graphene, carbon nanotubes, or biobased precursors (e.g., urine,[191] watermelon juice,[192] coffee grounds,[193] walnut shells,[194] and crab shells[195]). C-dots can be dispersed in various solvents or matrices, including water, common organic solvents, and cellulosic suspensions (CNC, CNF, or cellulose derivatives) and are easily synthesized by several techniques, including hydrothermal/solvothermal, microwave irradiation, and electrochemical techniques.[188,196–199] For instance, Xu et al.[200] dissolved nitrogen-doped C-dots (N-CD) in CNC suspensions with different concentrations of PVA to produce chiral photonic films by evaporation-induced self-assembly (discussed in detail in Section 6).[200] Both the CNC and PVA acted as the host matrix, with the CDs (2–3 nm) as the luminescent guest. An emission of vivid iridescent fluorescence (at 450–470 nm) was observed at 260 nm excitation, with a QY around 5.2%, although films without PVA showed no obvious afterglow at the same excitation wavelength since the CDs were doped into PVA to increase the restriction of molecular movement, prevent oxygen quenching, and protect the triplet state excitation.[200] Moreover, Guo et al.[165] developed a fluorescent hydrogel based on carboxymethylated CNF (CM-CNF) and N-CDs (from citric acid) with potential applicability in heavy metal absorbance and optical sensing. The multifunctional hydrogel showed intense blue fluorescence at optimal emission and excitation wavelengths of 462 and 382 nm, respectively, with a QY reaching 23.6%.[165]

Table 2. Luminescent materials where the matrix or luminescent particles are obtained from lignocellulosic materials.

Dopant	Dopant matrix (source)	Lignocellulosic material	Excitation [nm]	Emission [nm] [color]	Quantum yield (%)	Application	Ref.
Lanthanides	Yb^{3+} or Nd^{3+} complexes	CNF	269–336	873–1338	0.31–2.06 (Intrinsic QY)	Ultraviolet filter	[163]
	NTB-Tb^3 +NTB-Eu^3 +NTB-Tb^{3+}/Eu^{3+}	TEMPO-CNF	324 346 346	546 [G] 613 [R] 546 & 618	-	-	[184]
	γ-Fe_2O_3@YVO_4:Eu^{3+}	TW	300	619 [R]	74.44 (lanthanide) 0.64 (composite)	-	[185]
	LaF_3:Eu^{3+} LaF_3:Tb^{3+}	TEMPO-CNF	397 260	590 [R] 545 [G]	-	Anticounterfeiting	[183]
	$NaYF_4$:TmYb	CNC	974	450 [B] 620 [R]	-	Upconverting	[186]
	$LaPO_4$:Yb^{3+}/Tm^{3+}/Eu^3 +$LaPO_4$:Yb^{3+}/Tm^{3+}/Tb^{3+}	Cellulose fiber	405 975 375 975	696 [R] 473 [B] 542 [G] 475 [B]	-	Optical thermometer (UC & DC)	[187]
	SrF_2:Yb^{3+} or Er^{3+} NPs	CNF	980	653 [G]	-	Upconverting	[231]
	Eu^{2+}/Dy^{3+} doped $SrAl_2O_4$ particles	CNC hydrogels	203	513 [G]	-	Water absorbent and detection	[164]
Carbon nanodots	N-doped CDs (citric acid)	Carboxymethylated-CNF	382	462	23.6	Heavy metal sensor and adsorber	[165]
	CDs & PVA	CNC	260	460 [G]	5.2	Chiroptical devices	[200]
	N-doped CDs (oxidized cellulose)	Oxidized cellulose	320	410 [B]	30.3	Bioimaging and Detection of Fe^{3+}	[208]
	S-doped CQDs (cellulose fibers)	Cellulose fibers	360	435 [B]	32	Metal ion-sensing	[210]
	N-doped C-dots (CNC)	CNC	380	468 [B]	-	Cell culture	[167]
	CQDs (o-Phenylenediamine)	CNC	365	510	-	Chiroptical devices	[205]
	CQDs	CNC	365	542 [Y]	-	-	[232]
	NH_2-CQDs	TEMPO-CNC	360	488 [G]	16.8	Bioimaging	[233]
	Negatively and positively charged CDs	Cellulose derivative and CMC	239–431	428–605 [G, B, R]	11.3–71.5	LED	[204]
	CDs (carboxymethylated CNC)	CMC	355	381 [B] 460 [B]	-	Detection and removal of F^-	[234]
	N-doped CDs (citric acid) microwave	Microcrystalline cellulose	353	480	17.79	Detection of Hg^{2+} and Cu^{2+}	[235]
	C-dots (o-Phenylenediamine)	CNC	360 450 590	452 [B] 536 [G] 652 [R]	30.22 8.86 7.67	Circularly polarized light	[236]
	N-doped CDs (cellulose)	Cellulose	360	438 [B]	10.9	Detection of Fe^{3+}	[207]
	Lignin reduced CDs via $NaBH_4$	Lignin	440	475 [G]	47.3	Drug carrier and bioimaging	[174]
	N-doped CQDs (lignin and citric acid)	Lignin	377	454 [B]	43	Bioimaging	[175]
	N-doped CQDs (lignin)	Lignin	420	520 [G]	17.6	Detection of Ag^+ and bioimaging	[211]
	CDs (lignin)	Wood	320 440	440 [B] 570 [Y]	-	Detection of formaldehyde gas	[212]
	CDs (wood)	Wood	330	447 [B]	4.69	Detection of Fe^{3+}	[213]
	N-doped CDs (citric acid)	Wood	340 420 470	450 [B] 550 [G] 590 [R]	53.82[a] 36.18[a] 12.73[a]	Light-emitting diode	[201]
	CQDs (lignin)	Wood	580	650 [R] 710 [R]	-	Thermal energy storage	[237]

(Continued)

**ADVANCED
SCIENCE NEWS**

www.advancedsciencenews.com

**ADVANCED
MATERIALS**

www.advmat.de

Table 2. Continued.

Dopant	Dopant matrix (source)	Lignocellulosic material	Excitation [nm]	Emission [nm] [color]	Quantum yield (%)	Application	Ref.
Others	Perovskite QDs (CH₃NH₃PbBr₃)	CNC	UV	518 [G]	63.9	White LED	[216]
	Perovskite QDs (CsPb(Br₀.₄, I₀.₆)₃)	Ethyl cellulose	450	641 [R]	34.2	White light	[238]
	Perovskite QDs (CsPbBr₃)	Ethyl cellulose	450	521 [G]	37.2	LED	[239]
	Metal chalcogenide QDs (CdTe)	TEMPO-CNF	350	520 [G] 555 [Y] 675 [R]	36.9	Anti-counterfeiting	[222]
	Metal chalcogenide QDs (CdS)	TEMPO-CNC	410	660 [R]	-	Anti-counterfeiting	[240]
	Metal chalcogenide QDs (CdSe/ZnS)	Wood	440	550 [G]	22	-	[223]
	Si QDs	Wood	440	870	36	-	[224]
	AIE dye (PhE)	CNC	465	575 [O]	-	Bioimaging and theranostic	[229]
	AIE dyes (BB4FVA, BPP2VA, Fluorescein, RhB)	Sulfate-CNC	375 405 490 555	468 [B] 502 [G] 530 [G] 605 [R]	-	Chiroptical devices	[166]
	Fluorescent dyes	Cellulose acetate dots	400–665	445–680	-	Bio-imaging/targeting	[241]
	Fluorogenic dye (SilaFluo)	Cellulose acetate CNC	478	620	-	Solar concentrator	[242]

a)C-dots only [B] = Blue; [G] = Green; [R] = Red, [O] = Orange.

C-dots can also be uniformly embedded into TW (after delignification) to endow the composite with luminescence properties.[201] Bi et al.[201] fabricated TW (balsa wood) with multiple-color-emission CDs (CDs-TWs) as a white light-emitting diode (LED).[201] The CD suspensions and the CD-TW composites showed various emission colors (blue, green, and red) at the same emission positions (450, 550, and 590 nm, respectively), indicating that the CDs were well-dispersed in the composite without aggregation. The CD-TW composite showed promising optical performance compared to the pristine TW, including high transmittance (85% and 92%, respectively) and large haze (85% and <5%, respectively) for a thickness of 550 μm.[201]

The unique properties of C-dots, such as abundant polar groups on their surfaces and upconversion and room temperature phosphorescence, make them widely applicable in biomedical and light-emitting applications.[202] However, C-dots suffer from intrinsic self-aggregation, which results in the aggregation-induced quenching (ACQ) phenomenon. In other words, at high concentrations or in the solid-state, the nanosized particles tend to aggregate via $\pi - \pi$ stacking, causing a deterioration or even absence of emission that limits their application in many fields.[203] To conquer this challenge, Jin et al. embedded CDs with charged surfaces into oppositely charged cellulose derivatives via electrostatic attractive interactions, as shown in **Figure 5**a.[204] Thin protective shells of either positively (Cel-N⁺) or negatively charged cellulose derivatives (CMC) formed on the negative (NCDs) and positive (FCDs) surfaces, respectively. Both the NCDs@Cel-N⁺ and FCDs@CMC exhibited superior QYs (71.5% and 11.3%, respectively) compared to pristine CDs powders (0.17% and 0.05%, respectively), with bright blue and green fluorescence at the emission wavelengths

of 446 and 530 nm, respectively.[204] On the other hand, Xiong et al.[205] fabricated another type of core/shell nanostructure, by decorating o- and p-phenylenediamines CQDs (o-CQDs and p-CQDs, respectively) around individual CNCs to prevent aggregation and associated quenching effects. CQDs with a size of 1.5 ± 0.5 nm were decorated on a single CNC (lateral size 4.8 ± 0.6 nm) to form CQDs/CNC core/shell nanostructures, with a lateral size of 6.1 ± 0.8 nm, showing yellow (o-CQDs) and blue (p-CQDs) fluorescence under UV irradiation (365 nm). The addition of polyethylene glycol (PEG) into luminescent films was shown to prevent CQDs aggregation as well as improve interfacial interactions between the CQDs and CNCs since the PEG can produce hydrogen bond with both CNC and CQDs surfaces. In contrast to the usual trends for luminescent dopants, the fluorescence intensity (emission at 510 nm) increased with CQD content up to 40 wt%, whereas a significant emission shift (to 523 nm) was observed as the content of CQDs exceeded 40 wt%.[205]

C-dots are non-discriminating as far as the carbon source used for their synthesis since their excited state properties are significantly dictated by defects.[206] Thus, the green production of C-dots from low-cost, abundant, renewable, and environmentally friendly sources can be used to reduce CO_2 and greenhouse gas emissions. Not surprisingly, cellulose, as the most abundant polymer, can be used as a source to synthesize C-dots.[167,207] However, cellulose has limited chemical accessibility, resulting in a low yield and QY for the synthesized C-dots. Liu et al.[208] suggested a new technique to overcome this apparent drawback using an oxidative treatment of softwood pulp that employs both nitric and phosphoric acids, followed by the addition of ammonia (N source) in a
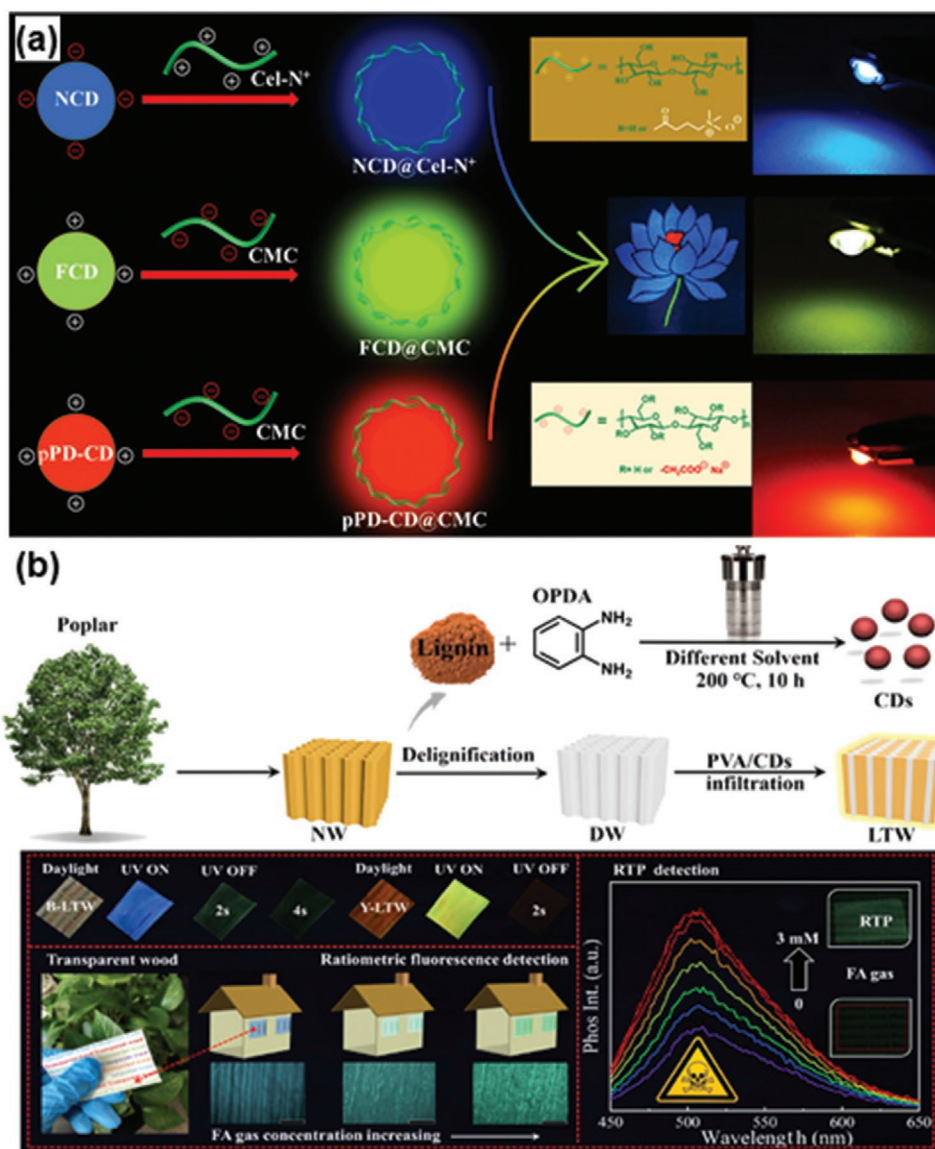
Figure 5. a) Schematic illustration of the electrostatic interactions of charged CDs with oppositely cellulose derivatives to give blue, green, and red fluorescence emissions. Adapted with permission.[204] Copyright 2020, American Chemical Society. b) Schematic diagram for the fabrication of luminescent transparent wood films using lignin CDs. Reproduced with permission.[212] Copyright 2020, American Chemical Society.

hydrothermal reaction to obtain N-CDs.[208] The oxidation treatment significantly improved the yield and QY reaching 16.1% and 30.3%, respectively, compared to non-oxidized CDs (2.9% and 9.7%, respectively), producing blue fluorescence (410 nm) at an excitation wavelength of 320 nm.[208] In addition to N doping, other heteroatomic dopants (e.g., P, B, S) can be used to improve optical and PL properties by increasing C-dot surface defects, effectively expanding their utility in fluorescent bioimaging applications.[209] For instance, Yang et al.[210] fabricated S-doped CQDs (S-CQDs) using cellulose fibers and sulfuric acid as the carbon precursor and dopant, respectively, via hydrothermal treatment.[210] Interestingly, the as-obtained S-CQDs exhibited both bright blue fluorescence (excitation: 360 nm; emission: 435 nm) and upconversion (excitation: 800 nm; emission: 430 nm) PL properties. They were also

found to have pH-dependent properties, showing a maximum PL intensity in acidic media (pH 0) with a QY around 32%, an effect that may be related to the higher net surface charge at low pH values.[210]

Lignin can be also used as a carbon source to synthesize C-dots via molecular aggregation.[172,175] Lignin was converted to C-dots using a simple, one-pot hydrothermal reaction, where it was first dissolved in water, ethylenediamine was added as a nitrogen source, and the solution was transferred to a Teflon-lined autoclave for hydrothermal processing (180 °C for 12 h).[211] The lignin-derived CQDs were 1.5–3.5 nm in size and showed bright green fluorescence (emission at 520 nm) at an excitation of 420 nm with a QY of around 17.6% and a lifetime of 3.11 ns. The fluorescence color of the CQDs changed from green to blue (at excitation 365 nm) as the acidity was

**ADVANCED
SCIENCE NEWS**
www.advancedsciencenews.com

**ADVANCED
MATERIALS**
www.advmat.de

increased, a feature that was attributed to the aggregation of -OH groups on the surface of the CQDs.[211] Microwave irradiation is another fast and straightforward technique to synthesize lignin-based CQDs with promising PL properties. Rai et al.[174] fabricated S-doped CDs (FCDs) from lignosulfonate lignin by microwave irradiation (600 W for 10 min) for drug delivery and bioimaging applications.[174] The obtained FCDs were further reduced using sodium borohydride (NaBH₄) to lignin-based CDs (r-FCD). The PL properties of r-FCD showed more intense green fluorescence and higher QY compared to pristine FCDs (47.3% and 37.4%, respectively) at an excitation of 360 nm, which was mainly related to the reduction of the functional groups on the surfaces of FCDs.[174] This work demonstrated promising PL properties, although choosing a cheaper, safer, and greener reducing agent is recommended for follow-up studies.

Liu et al.[212] reported the fabrication of LTW using lignin-based CDs.[212] After delignification, the extracted lignin was transformed into luminescent CDs via a hydrothermal process using different solvents, and then impregnated within the TW to get LTW. The obtained LTW showed outstanding optical properties, such as high optical transmittance (85%) at 550 nm, tunable room-temperature phosphorescence, and ratiometric fluorescence. The use of ethanol or formamide as a solvent for the synthesis of lignin-based CDs resulted in yellow (at 570 nm) or blue (at 440 nm) emitting LTW, respectively, as shown in Figure 5b.[212] Wood is another lignocellulose resource for the green production of C-dots via hydrothermal techniques, as reported by Zhao et al.,[213] who produced pine wood-based CQDs, with an average diameter of 3.6 nm, that showed high PL intensity and stability that was maintained over 60 days. Investigation of the fluorescence stability under different pH conditions found that intensity increased when the pH was decreased from 4 to 2, whereas negligible changes were observed when the pH was increased from 4 to 12. These results demonstrated the high stability of pine wood-based CQDs under alkaline, neutral, and weakly acidic media, having a high PL intensity and a QY of 4.69%.[213] The design of C-dots with pre-defined chemical and photophysical properties is still lacking, but the field is developing rapidly and represents a significant pathway to produce luminescent composites directly from biobased material sources.

4.3. Other Luminescent Dopants

Other than lanthanides and C-dots, perovskite quantum dots (PQDs), specifically hybrid halide perovskites (ABX₃; where A = CH₃NH₃⁺ (MA); B = Pb, Sn; X = Cl⁻, Br⁻, or I⁻), are promising luminescent dopants that have been widely used in display technologies. This is due to their outstanding properties, including high PL, narrow emission peaks (<25 nm), high QYs (> 95%), and tunable emission colors.[157,214] However, they suffer from low thermal resistance and poor stability under the high energy of UV radiation, resulting in photodegradation and quenching.[215] To overcome such drawbacks, Kang et al.[216] fabricated a flexible luminescent paper based on $CH_3NH_3PbBr_3$ PQDs integrated into CNCs for white LED applications.[216] The PQD paper was prepared by vacuum filtration and exhibited

excellent stability under UV excitation, attributed to the highly crystalline CNC behaving as a ligand and stabilizing the structure of PQDs in the paper formation. The fabricated PQD paper also showed outstanding optical properties, including intense green fluorescence (emission at 518 nm) under UV irradiation, high optical absorption (91%), and a QY of 63.9%.[216] In another study,[217] the photo and thermal stabilities of the same PQD ($CH_3NH_3PbBr_3$) paper were investigated. The prepared PQD paper exhibited <10% and <30% PL decay under continuous UV irradiation (16 W for 60 days) and high temperature (100°C for 20 days), respectively. These excellent properties were also attributed to the integration between polar cations in the PQD and anionic CNC.[217]

Although the high toxicity and poor biocompatibility of metal chalcogenide (e.g., S⁻, Se⁻, and Te⁻) QDs hinders their application in biomedical fields,[218] they have been widely studied due to their simple fabrication that gives tunable compositions, morphologies, and surface properties.[219,220] They are easily tuned to cover a broad range of the spectrum, which makes them promising candidates in the field of solar energy, photonics, and other optoelectronics fields.[221] Li et al.[222] developed a transparent luminescent film based on CdTe QDs bound covalently to TEMPO-CNF (TEMPO-CNF/CdTe QDs) for anti-counterfeiting applications.[222] The QDs were synthesized using different reflux times (1, 4, and 10 h), leading to different emission fluorescence (green, yellow, and red, respectively). The films showed high optical and mechanical properties, including high optical transmittance (86%) in the visible range, high QY (36.9%), fluorescence intensity (emission at 555 nm) when excited at 350 nm, as well as high tensile strengths (110 MPa). The authors also investigated the stability of the film under continuous exposure to UV light (95% PL intensity retention after 6 h) and the effect of pH (PL intensity decreased in acidic or alkaline conditions).[222]

Fu et al.[223] demonstrated luminescent transparent plywood (TPW), in which the pores were filled with pre-polymerized methyl methacrylate (MMA), which was enriched with metal chalcogenide (cadmium selenide/zinc sulfide, CdSe/ZnS) QDs, followed by lamination and polymerization.[223] The lamination in five layers was done at two different cellulose orientation angles, first, cross-orientation (cp-TPW), where each layer was perpendicular to the previous one (0/90/0/90/0), and second, quasi-isotropic (qi-TPW), described according to 0/45/90/-45/0, as shown in **Figure 6**. Both qi-TPW and cp-TPW displayed excellent optical properties including optical haze (80% each), optical transmittance (83% and 75%, respectively), uniform green fluorescence (emission at 550 nm) when excited at 440 nm, and QYs of 22%. Conversely, the single layer TPW had an optical haze of 50–60%, an optical transmittance of 90–95%, and non-uniform fluorescence.[223]

Optical properties are also dependent on the light direction in correspondence to the fiber direction as reported by Li et al.,[224] who prepared luminescent TW from balsa wood, with MMA used as the pore-filler and Si QDs as the luminescent material (emission at 870 nm; QY = 36%).[224] The authors reported that PL intensity and scattering losses were larger (10 dB cm⁻¹) when the direction of propagation of light was perpendicular to the direction of cellulose fibers, in comparison to
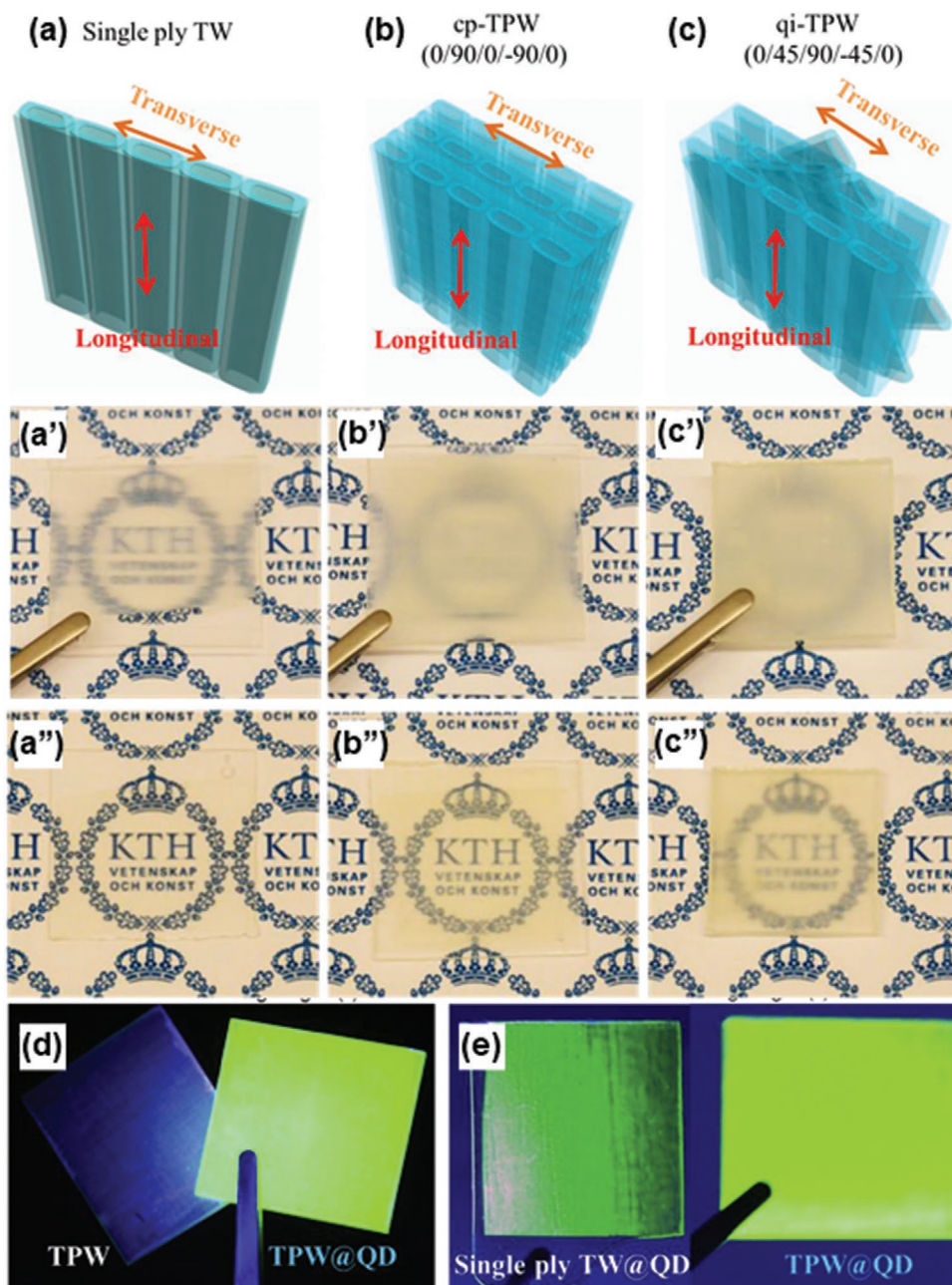
ADVANCED
SCIENCE NEWS
www.advancedsciencenews.com

ADVANCED
MATERIALS
www.advmat.de

Figure 6. Schematic illustration of the lamination designs of TPW. a) Single-layer TW; b) cp-TPW with lamination angles of 0/90/0/−90/0 degrees; c) qi-TPW with lamination angles of 0/45/90/−45/0 degrees; Demonstration of TPW with high haze (a'–c') when placed directly on the logo, and (a"–c") when placed 5 mm above the logo; d) pristine TPW and TPW@QD under UV light, and e) Single ply TW and TPW@QD under UV light (400 nm). Adapted with permission.[223] Copyright 2018, Elsevier B.V.

when the propagation was parallel to the fiber direction (3 dB cm^{-1}), due to fewer scattering centers encountered at the wood interfaces in the latter.[224]

Organic dyes have gained huge interest in the field of optoelectronics due to their promising photophysical properties including broad bandwidths and very high optical gain.[225] However, significant fluorescence quenching or photobleaching is induced when the organic dyes are at a quenching state, called the ACQ effect, due to strong $\pi - \pi$ interactions.[226] The ACQ effect hinders the use of organic dyes and their composites

(in solid-state or aggregate form) in many applications. In 2001, Tang et al.[227] identified a phenomenon that solved the aforementioned drawback of ACQ in organic dyes: aggregation-induced emission (AIE).[227] Briefly, AIE dyes demonstrate weak fluorescence in solution form but strong and bright fluorescence in solid-state and/or aggregate form. It is worth mentioning that few studies have been published in the field of luminescent lignocellulose materials based on organic dyes in the past decade, which is generally related to their poor optical properties including narrow absorption (narrow excitation

**ADVANCED
SCIENCE NEWS**

www.advancedsciencenews.com

**ADVANCED
MATERIALS**

www.advmat.de

range), broad asymmetric emission, low emission brightness, and poor fluorescence lifetimes compared to their counterparts (lanthanides, C-dots or QDs).[228] Cui et al.[229] functionalized CNC with AIE dye (PhE) via surface-initiated redox polymerization.[229] To improve biocompatibility and solubility in water, polyethylene glycol methyl ether methacrylate (PEGMA) was added to the AIE-modified CNC to give CNC-PhE-PEGMA. The optical properties of this material are promising for bioimaging applications – bright orange fluorescence (emission = 575 nm) when excited at 465 nm, as well as excellent resistance to photobleaching (90% intensity retention) after 4 h of continuous irradiation.[229] Organic dyes can also be integrated into TW as was reported by Vaileva et al.[230] In this case, the wood template was impregnated with Rhodamine 6G (Rh6G) molecules and prepolymerized MMA to fill voids, leading to a drop in transmittance (around 420–555 nm) due to Rh6G absorption.[230]

To conclude this section, the integration of luminescent materials, specifically the ones obtained from biobased sources, into lignocellulosic networks is a promising approach for modern applications (e.g., LEDs, sensors, and solar energy). These materials are derived from renewable resources and generally involve simple, low-cost synthesis protocols. However, in the case of C-dots, synthesis can be challenging since the relationship between synthesis parameters (reaction temperature, time of reaction, solvent, pH, purification steps, and storage conditions) and products are not yet well established, and can influence dimensions, structure, distribution (individual/agglomerated), and photoluminescence performance. Table 2 summarizes the recent literature on different luminescent materials obtained from lignocellulosic materials and also the lignocellulosics used as a matrix for luminescent particles.

5. Surface Patterning for Added Optical Functionality

Considering the optical properties of films made from lignocellulosics, their surface roughness is a parameter that is often overlooked. No surface of a biobased material is atomically flat, and its surface roughness will directly impact its interactions with light.[243] As an example, for nanocellulose films cast by vacuum filtration or solvent evaporation, the surface in contact with air is usually rougher, and large-scale buckling effects due to shrinkage upon drying can be observed even though the small-scale roughness is often < 10 nm.

In addition to the inherent surface roughness of lignocellulosic films, surface patterning can be employed to create light-guiding structures, wherein nanoscale and microscale structures are produced to regulate diffraction, scattering, or light outcoupling.[84] Successful surface patterning requires the production of high precision structures in a pre-defined format. All lithographic techniques involve similar steps, differing in the processing and curing details. First, the material to be modified is homogeneously distributed over a surface, the mask or mold is then applied, and finally, after chemical and/or physical processing, the modified surface is obtained.[244,245] **Figure 7** shows schematically how modified surfaces can be obtained by photolithography, soft lithography, and nanoimprint lithography (NIL).

In general, light management from surface topography depends on feature size, possible anisotropy (changing the light path), and structure periodicity (Figure 7d,e). Different structural sizes (Λ) interact differently with incident light of a given wavelength λ. In this way, when $\lambda \gg \Lambda$, a small part of the light is reflected and the vast majority is transmitted to the
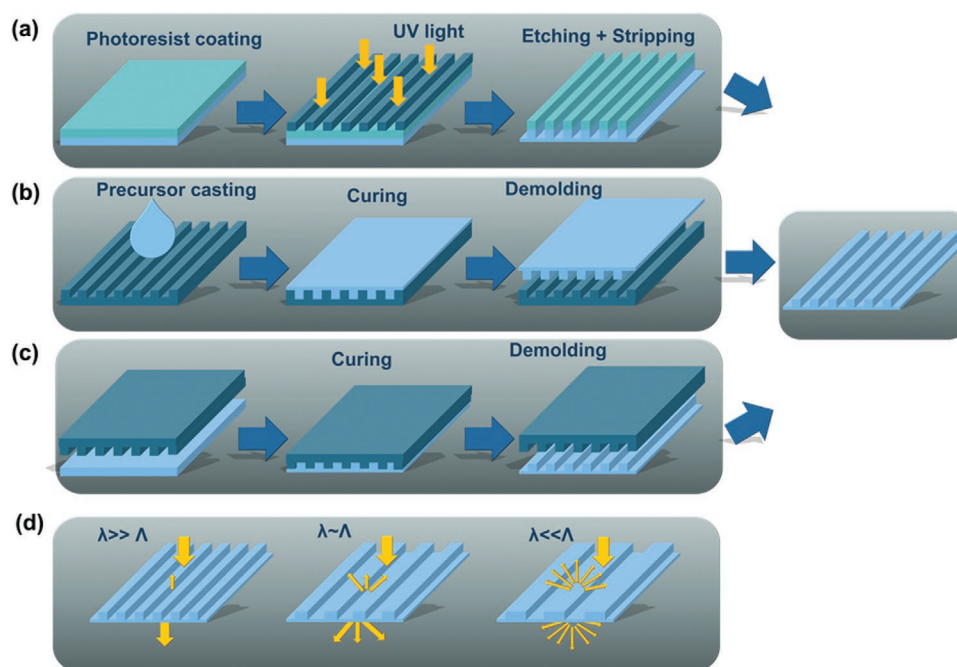

Figure 7. Schematic of a) photolithography, b) soft lithography, and c) NIL processes, and d) light behavior according to the pattering size. Figure based on the following refs. [246–249].

**ADVANCED
SCIENCE NEWS**

www.advancedsciencenews.com

**ADVANCED
MATERIALS**

www.advmat.de

other side of the material, both without changing the direction of the light (no scattering). When the structure size is similar to the wavelength ($\lambda \sim \Lambda$), a change in the direction (scattering) of the reflected and transmitted light occurs, however, the transmission of light to the other side of the material remains dominant. Finally, when the structure size is much bigger than the light wavelength ($\lambda \ll \Lambda$), similar proportions of light are reflected and transmitted at different intensities and directions (higher scattering).[247]

Surface patterning and coupling of the light management properties of the thin film to the light guiding surface topography in lignocellulosic materials remain largely unexplored and are thus very attractive topics for future developments. Here, we discuss few studies that use lithographic approaches with biobased materials; however, we note that these studies do not focus on optical properties and instead address specific aspects, such as the production of cellulose-based molds,[250] the detection of thyroid-stimulating hormones,[251] and micro-supercapacitors,[252,253] among others.

5.1. Photolithography

To adapt biobased materials for photolithography, the main components must be modified with photoactive functional groups. For instance, soluble trimethylsilyl cellulose[254] or cinnamate cellulose[255] were converted into insoluble cellulose and crosslinked cellulose, respectively, after exposure to UV-light, to fabricate well-defined cellulose patterns. In both cases, the resulting materials were applied in organic thin-film transistors and optical properties were not evaluated.

5.2. Electron-Beam Lithography

Electron-beam lithography differs from photolithography by employing electrons (e-beams) to modify the surface of the material. When this technique was applied to cellulose acetate, the radiation of the e-beam decomposed the cellulose chains into shorter ones that were then removed via solubilization.[256] This methodology produces high contrast structures and has potential optics applications, such as LEDs.[256,257]

5.3. Soft Nanoimprinting Lithography

This methodology can be used to produce structurally colored films with periodic submicrometric structures on their surface. Espinha et al., produced photonic and plasmonic structures using hydroxypropyl cellulose (HPC) by patterning submicrometric periodic lattices into its surface.[258] In this case, the structures were obtained by pressing a soft PDMS mold into HPC or by casting HPC onto the mold surface. Different colors were obtained depending on the imprinted structure and topology. These films were able to increase the photoluminescence of the organic dye Rhodamine B (RhB) doped into its surface, due to the improvement of the out-coupling of light, enhancing the PL signal by tenfold due to the surface pattering. Additionally, coating the structures with silver by thermal evaporation (silver

layer thickness: 100 nm) generated plasmonic crystals with properties suitable for use as disposable substrates for Raman spectroscopy.[258] Note that in Espinha's work, the colors arose from light diffraction from the patterned surface topography. However, soft nanoimprinting lithography can also be used to increase the helical pitch (described in Section 6 – from 195, 365, 475 nm, to 1.38 µm) in cholesteric CNC liquid crystals, as shown by Chu et al.[259,260] So, films with tunable (from blue to green and red), vivid structural colors, and photonic bandgaps varying from UV to visible and near-infrared (NIR) regions can be obtained.[259,260]

5.4. Thermal Imprinting (Hot Embossing)

Another option for surface patterning is thermal imprinting,[261] whose application in biobased materials may seem unfeasible (cellulose, hemicellulose, and lignin do not melt). However, these biobased materials can be sources of biodegradable thermoplastics, such as "liquid wood".[262] Thermoplastic biopolymer produced from lignin and cellulose fibers show a melting temperature between 147 and 159°C. The thermal imprinting of "liquid wood" was used to form nano and micrometric structures that interacted with light to give blue and green iridescent structural colors. These materials can be applied to microfluidic components like CE-chips for lab-on-chip applications or cell containers for tissue engineering.[263]

Thermal imprinting was also used to prepare cellulose acetate substrates for LEDs, such as OLED and light-emitting electrochemical cells (LEC). Hexagonal microlens arrays were produced in two sizes (3.6 and 37.1 µm) and were compared with flat films of cellulose acetate. The substrates with the larger hexagonal microlens provided greater light diffusion, and larger pixels, leading to greater light output. When the structures were smaller, the light emission was more homogeneous with a slight blur on the edges of the pixels. Finally, the efficiency of the LEDs was improved when using these structures and, after optimization, the substrates could be used in optoelectronic applications, such as organic solar cells or photodiodes.[264]

5.5. Roll-To-Roll Nanoimprinting Lithography

Industrially, thermal imprinting has been performed using roll-to-roll processing, which can also be applied to thermal nanoimprinting lithography. Mäkelä et al. used a laboratory-scale roll-to-roll imprinting system to produce cellulose acetate films, and CNF and TEMPO-CNF films with imprinted pillar structures, using a Ni-mold.[265–268] Structure formation was highly dependent on the temperature, speed, and pressure applied in the process. The surfaces of these films showed different roughness values, which translated into films of different transparency. When white light propagated through the microstructures, blue, red, and green diffraction colors were observed, demonstrating the potential for optics and electronics applications.[265–268]

Considering the production and application costs of lithography, high throughput techniques such as soft-lithography and roll-to-roll lithography are the less expensive, whereas

**ADVANCED
SCIENCE NEWS**

www.advancedsciencenews.com

**ADVANCED
MATERIALS**

www.advmat.de

photo- and e-beam lithography tend to be more costly due to more difficult scalability.[269] In turn, a concern is that different surface patterning methods impose different limitations for the feature size of the fabricated surface structures.

6. CNC Liquid Crystalline Properties for Structural Colors and Light Manipulation

Since the 1990s, when Gray et al. first reported the spontaneous assembly of a left-handed chiral nematic phase in CNC suspensions and the preservation of this periodic structure in solid films upon drying,[270,271] the pace of discovery has accelerated toward the bottom-up design of new CNC-based self-assembled films with long-range order as an alternative to traditional top-down nanolithographic structuring approaches. Chiral nematic CNC films exhibit 1D photonic bandgap behavior and have exciting potential for light management in photovoltaic devices, where they can be used to selectively reflect and transmit defined wavelengths that may be resonant with the response of another optically active component for an augmented effect.

CNC-based photonic films are similar to self-assembled natural composite structures that rely on the organization of biobased nanoscale elements to deliver distinct optical effects and exceptional mechanical performance.[45] The bottom-up self-assembly of ordered hierarchical composite structures is a natural strategy used to achieve evolutionarily directed material properties. Prototypical examples of this phenomenon are nacre (mother of pearl), which is tough, strong, and iridescent due to a layered arrangement of aragonite crystallites with dimensions on the scale of visible light embedded within a biopolymer matrix, butterfly wings, which present different optics depending on nano-topology and structuration, and the hierarchical structure of wood. Interesting trends that have emerged in the recent literature on CNC self-assembly are related to i) self-assembly control to achieve defect-free homogeneous films; ii) chiral templating for mesoporosity and other diverse functionalities – covered in detail in recent reviews;[45,48,272–277] and iii) creating defined architectures for further control of optics. These chiral nematic structured films have been proposed for different applications, including catalysis,[278] sensors,[279] anticounterfeiting systems,[280] broadband reflectors,[281] solar gain regulators,[282] and lasing.[283,284]

Above a threshold concentration (c*), an aqueous suspension of CNC undergoes self-assembly from an isotropic state into an ordered chiral nematic liquid crystal.[270] The chiral nematic phase is described by the left-handed helical rotation of the average local orientation of the CNC about the chiral nematic axis. This local orientation is defined by a vector called the director. The structure is defined by a periodic length, called the half-pitch (P/2), which is the vertical distance along the chiral nematic axis that is traversed in a 180° rotation of the director (**Figure 8**a). The liquid crystal phase formation in CNC has been described as a competition between two concentration-driven phenomena, equilibrium self-assembly in suspension into a chiral nematic phase and non-equilibrium glass formation caused by the kinetic jamming of CNC brought into proximity.[283] For CNC that undergo phase separation, depending on CNC properties and chemical environment, the transition from disordered to ordered suspensions at concentrations above c* is on the timescale of hours to days, which can limit dynamic applications of the liquid crystalline transition. As mentioned, the liquid crystalline structural organization can be locked into solid films by a process referred to as "evaporation induced self-assembly" (EISA). A distinguishing optical feature of these films is the selective reflection of left-handed circularly polarized light (L-CPL) due to Bragg reflection and the transmission of right-handed CPL (R-CPL). The wavelength of this reflection (λ) is related to P according to $\lambda = nP\cos\theta$, where, n is the average refractive index and θ is the angle between the incident light and the chiral nematic axis.[281] Films that have a pitch at the length scale of visible light appear colorful due to the chiral nematic axes being generally perpendicular to the film surface and are iridescent due to the angular dependence of the reflected light.

The wavelength of light reflected from CNC films can be tuned across the visible spectrum into the NIR by controlling pitch and chiral nematic axis orientation. Chiral nematic liquid crystalline materials, including CNC liquid crystals,[283] can be described as partial 1D photonic bandgap materials because they control light propagation through the selective reflection of wavelengths that coincide with P.[287,288] The ability to modulate the bandgap and design novel architectures that can reflect
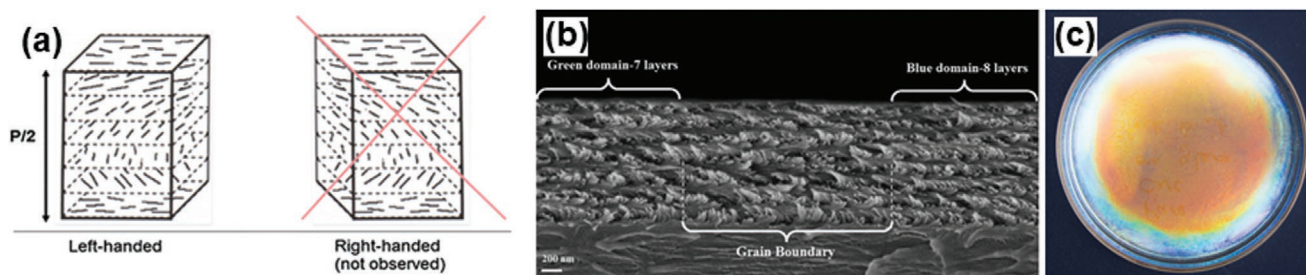

Figure 8. a) Schematic illustration of the chiral nematic arrangement of CNC that is described by the left-handed helical rotation of the director along the chiral nematic axis, where P/2 gives the vertical distance traveled in a 180° rotation of the director about this axis. Reproduced with permission[285] Copyright 2012, Springer Nature. b) SEM cross-section of CNC EISA film showing blue and green domains characterized by different P values and separated by a grain boundary, with CNC self-segregating according to aspect ratio into the different domains. Reproduced with permission[286] Copyright 2014, American Chemical Society c) Photograph of an EISA CNC film (8.5 cm diameter) placed on a black background to better visualize predominately red reflection (permission for the photo is obtained from Elissa Brunato, unpublished as part of "Bio Iridescent Sequin" project, 2020).

both R-CPL and L-CPL can be exploited to manipulate light in optoelectronic devices. Generally, in chiral nematic CNC films, the photonic bandgap corresponds to the wavelengths of L-CPL that are blocked due to the underlying left-handed chirality of the structure and can be tuned through the different variables that influence P, such as CNC aspect ratio,[286] suspension processing,[289] surface charge,[290] ionic strength,[291] initial concentration,[292] and additives,[293,294] among others. For example, the influence of CNC aspect ratio and size polydispersity on P is demonstrated in the film cross-sections shown in Figure 8b, where smaller CNCs self-sort into tighter, smaller P helices that reflect bluer wavelengths.[286] Strategies to control chiral nematic axis orientation can also be used to tailor the photonic bandgap. Whereas the application of shear,[295] electric,[296] and magnetic fields[297] has been used to produce aligned CNC films, alignment of the chiral nematic axis has thus far only been demonstrated using magnetic fields due to negative diamagnetic anisotropic property of CNCs that causes them to align perpendicularly to a magnetic field,[297–299] with the chiral nematic axis aligned parallel to the field.[300] Using this approach, the alignment of chiral nematic domains was recently achieved in EISA CNC films that were dried in the proximity of 0.5–1.2 T commercial magnets.[301]

In the following paragraphs, materials based on left-handed chiral nematic CNC films with optical properties that go beyond the left-handed reflection of a narrow wavelength range are described, with an emphasis on works that were not covered in a recent review of CNC photonic materials.[277] Broadband L-CPL reflectors were reported through a single-step EISA strategy based on the intercalation of chiral nematic domains with micelles that distorted the usual long-range order to produce a jumble of domains of varying P and chiral nematic axis orientation.[281] Similarly, as described in **Figure 9**a–d, micro gap impregnation with a nematic liquid crystal produced films with nematic order intercalated within the chiral nematic domains.[302] These films reflect both L-CPL and R-CPL, increasing optical output from the 50% that is possible from films that selectively reflect only one hand of CPL.[302] Nematic to isotropic transitions triggered by temperature or the application of an electric field produced reversible changes in the birefringence of the nematic layer and the overall optical response of the composite.[302]

The reflection of L- and R-CPL achieved by layering nematic and left-handed chiral nematic structures exist in nature, for example in the *Plusiotis resplendent* beetle cuticle, which comprises a nematic half-wave plate sandwiched between two left-handed chiral nematic layers.[303] Although CNC liquid crystals naturally form a left-handed structure, handedness control has also been achieved in CNC-based photonic films, expanding the potential utility of these films in devices.[280,282,284,304,305] A sophisticated 3-layered structure that reflected both L-and R-CPL was similarly constructed using a combination of strategies to enable control of P, chiral nematic axis orientation, and light retardation magnitude.[282] CNC (37–49 wt%), organosilica (21–33 wt%), and PEG-400 (30 wt%) were dried in the presence of a magnetic field to give flexible composite films with tunable reflection bands across the visible spectrum and into the near-IR (Figure 9e) and uniform chiral nematic structures (Figure 9f).[282] Next, cellulose-based retarders were constructed

by successive shear deposition and rapid evaporation to lock CNCs into alignment along the shear direction. The number of deposition cycles was varied to control film thickness (d) and half-wave retardation (L) according to $L = \Delta nd$, where Δn is the net birefringence.[282] By controlling the thickness of the nematic layer, the half-wave retardation needed to convert R-LCP to L-LCP for polarization-insensitive reflection can be appropriately matched depending on the photonic bandgap of the chiral nematic films, as shown in Figure 9g for near-IR photonic bandgap films.[282]

A recent study demonstrated that both simultaneous L-and R-handed CPL reflection was possible within a single CNC film, with R-CPL more pronounced from films evaporated at higher concentrations and temperatures.[280] This feature was attributed to kinetically arrested micrometer-scale domains of nematic-like organization interspersed within an overall chiral nematic structure.[306] A bi-layer EISA film characterized by nematic-like order near the top surface and chiral nematic-like order at the bottom showed optical properties dependent on which side of the film faced the incident light.[306] These observations are consistent with the work of Hiratani et al. who demonstrated a depolarization effect from nematic-like CNC films dried from high concentration (10 wt%).[279] The addition of photoluminescent polymer dots gave films that emitted both L- and R-CPL, with the R-CPL emission possible due to the nematic-like domains intercalated within the structure that allowed propagation through the film of otherwise forbidden L-CPL.[306] The degree of overlap between the PL wavelength and the L- and R-CPL bands dictates the intensity of the reflections, with R-CPL becoming more pronounced when the PL better overlaps with the L-CPL photonic bandgap.[306] As a proof of concept, QR codes for anticounterfeit were constructed from these films.[306]

Overall, the potential to tune the reflection wavelength and angular dependence of chiral nematic CNC films is highly attractive for the development of high-performance CNC or CNC-templated films for optical applications. As discussed, P and chiral nematic axis orientation can be controlled, and additionally, color inhomogeneity due to the coffee-ring effect[307,308] can be minimized to give films with uniform reflection.[309] Taking a cue from nature, the L-CPL chiral nematic structure can be assembled into nanoarchitectures that reflect light independently of polarization at levels nearing 100%.[282] Furthermore, depending on the photonic bandgap, this feature can be harnessed in different ways, for instance in the light guiding and spectral management for photovoltaic devices for improved efficiency by regulating heat transfer in the case of IR-reflecting structures, by the reflection of harmful UV rays, or through combination with active materials that have an optical response coincident with the photonic bandgap of the chiral nematic films.

7. Light Responsive and Color-Stimuli-Responsive Cellulosic Materials

Stimuli-responsive displays undergo a property change (e.g., shape, wettability, adhesion, optical, electrical, thermal, and mechanical properties) under external stimuli.[310] They have
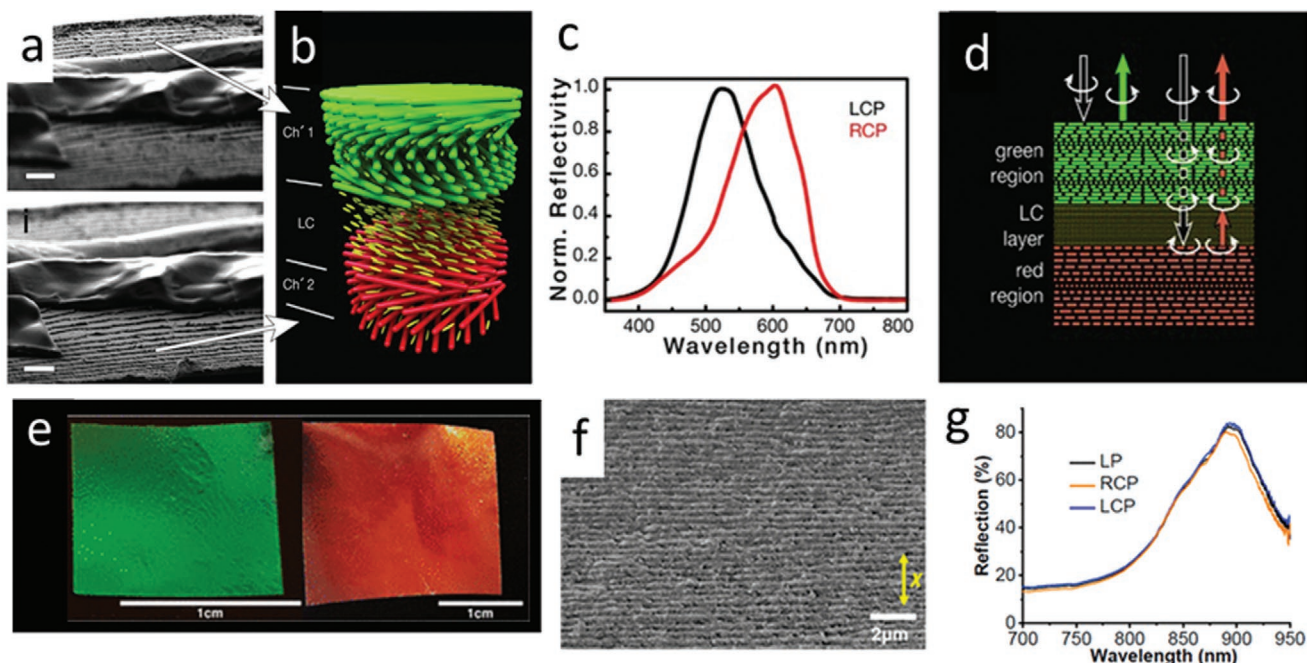
**ADVANCED
SCIENCE NEWS**

www.advancedsciencenews.com

**ADVANCED
MATERIALS**

www.advmat.de

Figure 9. a,b) SEM cross-sections and schematic of composite film showing chiral nematic CNC domains with micro gaps filled by nematic liquid crystal. c) The reflectance spectra show left- and right-handed reflection from the composite film and light propagation through the composite with the transmission of right-handed CPL and reflection of left-handed CPL at the green domain. d) Also, shown is the conversion of right-handed CPL to left-handed CPL at a nematic domain, the reflection of left-handed CPL at the red chiral nematic domain, re-conversion of left-handed CPL to right-handed CPL as the light passes through the nematic domain a second time, and finally transmission of right-handed CPL through the green chiral nematic domain. Examples of films with tunable L-CPL reflection based on the e) pitch, f) cross-section with 660 nm pitch and chiral nematic axis perpendicular to plane of film, and near-IR reflection of L/ R-CPL and linearly polarized (LP) light from the sandwich structure, with high transparency (>85%) outside reflection bands. (a–d) Adapted with permission.[288] Copyright 2016, Elsevier B.V., (e–g) Reproduced with permission.[282] Copyright 2018, American Chemical Society.

excellent potential in various applications, such as on-demand drug delivery, tissue generation/repair, biosensing, smart coatings, artificial muscle drug delivery, diagnostics, biosensors, and textiles.[311,312] In area of stimuli-responsive materials, interest in biocompatible and biodegradable materials based on lignin,[313] hemicelluloses,[314] and cellulose[315–317] is increasing. However, regarding light stimulation or photo-responsive applications, cellulose has been the most investigated until now. Here in this section, we focus on materials that respond to light (Section 7.1) with a color change that is observable by naked eye (Section 7.2).
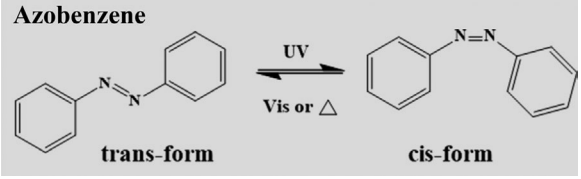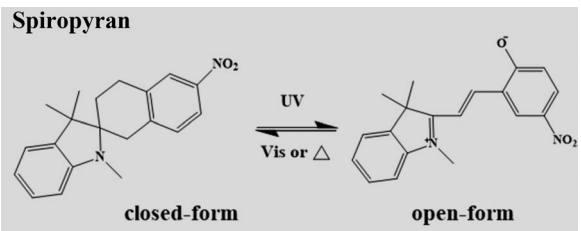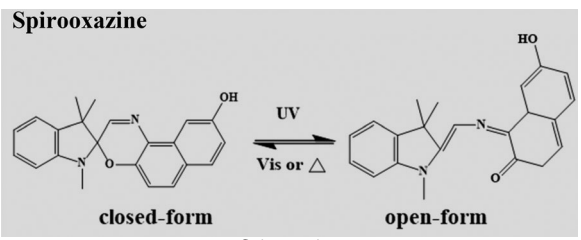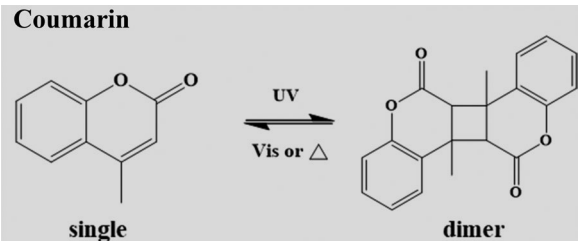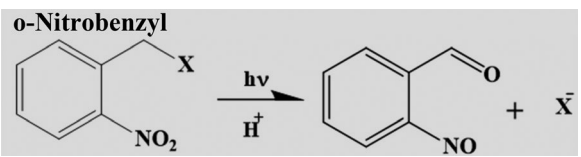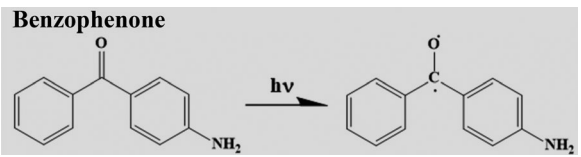
7.1. Light-Responsive Cellulosic Materials by Chemical Modification

Considering the minimal light absorption of cellulose at visible wavelengths, cellulose-based light-responsive materials can be produced by functionalizing cellulose with a light-responsive molecule or by incorporating light-responsive polymers, for instance, taking advantage of supramolecular interactions. Light-responsive cellulosic materials have been produced by derivatization or by graft copolymerization of a chromophore (such as spiropyran or coumarin) onto the cellulose (or cellulose derivative) backbone.[318] These light-responsive cellulosic materials present optically active centers that can be applied in photo recording devices, liquid crystal displays, and other light-sensitive applications.[319]

Table 3 shows some of the chromophore-cellulosic pairing encountered in the recent literature, focusing on polymeric cellulose derivatives and nanocellulose. Three different photoresponsive processes may occur, depending on the applied chromophore: photo-isomerization, photo-dimerization, and photocleavage. Photoisomerization is a process whereby the chromophore switches between two isomers upon exposure to a specific triggering wavelength of light. Azobenzene, spiropyran, and spirooxazine are the main examples of chromophores used in light-responsive cellulosic materials based on photoisomerization.[320] Photo-dimerization is the process by which a photo-excited molecule reacts with a molecule that is not excited. Coumarin is one of the successful examples of a chromophore used in this process with cellulosic materials.[320] These two processes are reversible and accompanied by changes in the color of the material. The last process, photocleavage, is irreversible since it breaks down the excited molecule, creating radicals that react with other molecules and can carry out subsequent reactions, such as crosslinking.[320]

By modifying cellulose and cellulose derivatives, it is possible to produce dynamic optical or phototunable materials that undergo color changes when exposed to a specific light wavelength. Tian et al.[326] developed multicolor inks using CA grafted with spiropyran (SP), fluorescein (FITC), and pyrene (Pyr) groups. These derivatives appeared red (CA-SP), green (CA-FITC), and blue (CA-Pyr) after exposure to 365 nm. With these three colors, a complete color palette

**ADVANCED
SCIENCE NEWS**

www.advancedsciencenews.com

**ADVANCED
MATERIALS**

www.advmat.de

Table 3. Chromophores commonly used in the synthesis of photoresponsive cellulosic materials.

Cellulosic material	Chromophore	Ref.
Reversible photo-responsive groups		
CNC, CNF, microcrystalline cellulose (MCC), carboxymethyl cellulose (CMC), HPC	Azobenzene	[318,321–323]
Cotton, filter paper, MCC, cellulose acetate (CA)	Spiropyran	[324–326]
Nitrocellulose, MMC derivative	Spirooxazine	[327,328]
CNC, CNF	Coumarin	[329]
Irreversible photo-responsive groups		
Cellulose sulfate	o-Nitrobenzyl	[330]
TEMPO-CNF	Benzophenone	[331]

was obtained (**Figure 10**a), in which all colors showed a reversible response to UV-light exposure. This methodology is compelling for encryption or anti-counterfeiting applications (Figure 10b).[326]

Optical materials that respond to multiple wavelengths can be achieved via electrostatic interactions between light-responsive cellulosic materials and CDs.[328] By combining photoresponsive cellulose and CDs, photo-triggering, reversible
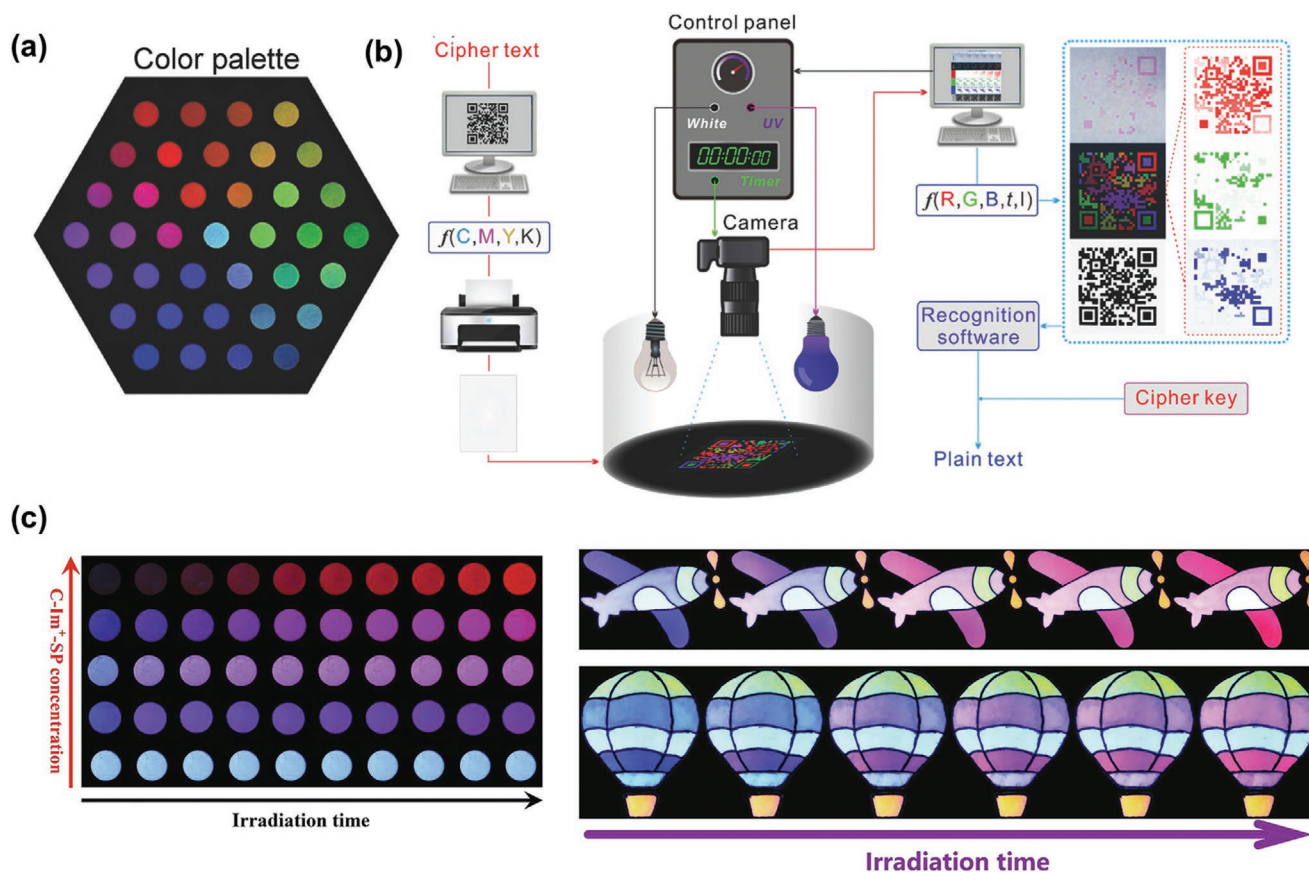
**ADVANCED
SCIENCE NEWS**

www.advancedsciencenews.com

**ADVANCED
MATERIALS**

www.advmat.de

Figure 10. a) Color palette obtained from cellulose-based trichromatic fluorescent materials. Reproduced with permission.[326] Copyright 2018, Wiley-VCH. b) Design of dynamic full-color fluorescent encryption and authentication process using the cellulose-based trichromatic materials. Reproduced with permission.[326] Copyright 2018, Wiley-VCH, c) Fluorescent images of CDs@C-Im$^+$-SP with different C-Im$^+$-SP concentrations and different irradiation times (λ_{ex} = 365 nm) and multi-color dynamic fluorescence patterns. Reproduced with permission.[328] Copyright 2021, Elsevier B.V.

chromic materials were produced that responded to both UV and visible light. Light-responsive cellulosic materials containing imidazole salt (Im$^+$) groups and SP groups were immobilized on the surfaces of negatively charged CDs. In this system, the CDs absorbed UV (365 nm) and emitted blue fluorescence, transferring excess energy to the photoisomerization reaction of SP, making SP emit red fluorescence. With increasing UV irradiation time, the intensity at 460 nm (blue fluorescence) decreased and the intensity at 658 nm (red fluorescence) increased. The material eventually became fully red as a result of this photoinduced fluorochromic phenomenon. Finally, by changing the concentration of CDs in the ink, different colors and shades were obtained, imparting high versatility to these materials (Figure 10c).[328]

7.2. Cellulosic Materials that Change Color upon External Stimulus

The color of chiral nematic CNC films can be manipulated so that the perceived color is easily tuned under the influence of small molecules, solvents, or polymeric materials, for example, for humidity, chemical vapor, and strain sensors.[56,332,333] In this sub-section, we provide a few examples of sensors based on chiral nematic CNCs films. These chiral nematic CNC sensors can be produced by CNC without further modification,[334] with modification,[335] or in the presence of different stabilizing molecules. The reader is referred to excellent recent reviews on the production of chiral nematic CNC films and their main applications.[56,332]

Layer-by-layer CNC films were used to produce an optical spectrometer for H$_2$O, ammonium (NH$_3$·H$_2$O), hydrochloric acid (HCl), and acid acetic (HAc) vapors exhibiting an optical response (red-shift) upon exposure.[334] This redshift occurs due to the expansion of the chiral nematic pitch as the vapor swells the film. The time needed for the color change (response time) was 8 ± 1, 18 ± 2, 38 ± 2, and 68 ± 3 min for HCl > H$_2$O > NH$_3$·H$_2$O > HAc, respectively. The sensors recovered their initial color after exposure to high temperatures, except for HCl, which irreversibly modified the film structure. The reversibility of the color change shows promise for re-useable sensors for H$_2$O, NH$_3$·H$_2$O, and HAc.[334]

Although successful, such sensors have long response times. To improve response time, a different approach was developed based on the treatment of structurally colored CNC films with solvents such as N-methyl morpholine-N-oxide (NMMO).[335] It was possible to tune the color and hygroscopicity of the NMMO-treated films to give a faster response time (<2 min).

Also, with increasing NMMO contents and relative humidity, the response time and H_2O adsorption capacity improved such that the system could be applied as a humidity indicator label (**Figure 11**a).[335]

Another approach involved functionalizing CNC film surfaces with 3-aminopropyltriethoxysilane (APTES) to detect formaldehyde or propanol vapors.[339] CNC structural colors remained intact after film immersion in a solution of APTES dissolved in toluene (60°C, 1 h) and drying (1 h, 120°C). By the naked eye, a detectable color change was observed at gas concentrations of 100 ppm for both gases, which was further lowered to the sub-ppm level (0.5 ppm) using a USB digital microscope camera as the detector (note: response time was not indicated). Unmodified films did not exhibit a significant color change even at higher concentrations of gases. The CNC films modified with APTES have amine-functionalized groups that allowed identification of the gas to which the material was exposed.[339]

The introduction of additives into chiral nematic CNC films can provide another dimension of functionality, i.e., with the introduction of such molecules, different colors can be obtained.[45] For instance, by varying the concentration of glucose, different colors were obtained, as shown in Figure 11b,c, where JLU was written with different colors (J: blue, L: green, and U: orange), achieved by changing the amount of glucose. The letters then changed color (J: green, L: red, and U: colorless) upon exposure to 86%RH.[336] At RH >91%, the films rapidly swelled to give a red-shifted color. In this way, the combination of CNC and glucose at higher humidity (91–100% RH) was effective to induce a fast color change from blue (UV–vis) to colorless (Infrared). At lower RH (10–91%), the color change was slower and the response depended on the thickness of the films.[336] NaCl enabled nearly instantaneous and reversible color changes in chiral nematic CNC films (<1 s, Figure 11d).[337]

In the previous examples, the color change was based on shifts in the pitch of chiral nematic CNC films, however, CNC sensors for humidity,[340–342] heat,[342] and for distinguishing organic solvents[343] can be obtained from nanocomposite films with polymers such as polyvinylpyrrolidone, poly(ethylene glycol), polyacrylamide, among others. Similarly, a crosslinked waterborne polyurethane (WPU) latex and CNC composite was used to produce multifunctional rewritable photonic papers.[338] This rewritable photonic paper was water-resistant and hydrophobic, presenting fast and reversible color changes, within seconds. Figure 11e shows three aqueous inks: 1) water, 2) water with a high concentration of NaCl (0.1 M), and 3) water with a low concentration of NaCl (0.025 M). As shown, the colors shifted from blue to orange for the three inks, and the original blue color of the paper was recovered after drying. The only exception was for the high salt concentration, where the pattern remained visible even after the color shift due to the penetration of the salt into the helical CNC structure. However, washing with the water removed this feature. Additionally, the material responded to exhalation onto the paper by changing color from blue to yellowish green, and the presence of NaCl in the structure facilitated the observation of this color change (Figure 11e). The properties of this photonic paper are highly promising for applications in sensors, photonic circuits, and display systems.[338]

8. Fabricating Devices Out of Plant-Based Materials

Through eons, woody plants evolved for optimization of functionalities, such as mass transport, sensing, temperature regulation, light-harvesting, light-blocking, structural integrity, among others.[344] Recreating these features in engineered materials, considering the level of sophistication of natural materials, is not an easy task. Through the deconstruction and reconstruction of cellulose, lignin, and hemicellulose, environmentally sustainable materials with versatile desirable optical functions can be engineered to meet the contemporary demands of smart devices.

Due to several features, such as high specific mechanical strength and ease of modification,[345] cellulose has emerged as a material with promises to produce electronic devices (**Table 4**).[346] The key optical property that is accessed from cellulose, considering several applications, such as flexible cover layers for displays and LED substrates, is transparency. As we have shown in Section 2, there is a wide variety of lignocellulosic material options that can reach high levels of transparency across the critical visible wavelengths – thus a display or LED designer can choose from different nanocellulose based thin films, all-cellulose composite films, and transparent wood substrates.

Interestingly, many applications in optoelectronics, such as solar cell substrates, can benefit from optimizing the complex interplay between direct and diffusive transmittances (i.e., haze).[347] Ongoing efforts have demonstrated that these properties can help to guide the light path along with an increased distance in the photoactive material of the solar cell, thus increasing the total power conversion efficiency.[85,97,184,348] Taken into account the modularity of the lignocellulosic thin films, these properties could be combined into an optimized surface topology providing, for instance, self-cleaning and antireflection properties. On the other hand, some of the main hurdles, such as brittleness, poor barrier properties for water and water vapor, and swelling under humid conditions still need to be resolved.[349] Lignocellulosic films have typically a water-vapor transmission rate (WVTR) higher than that of plastics (such as PEN or PET), at a level that is not sufficient for many device applications.[350] One way to protect devices from water would be the application of superhydrophobic coatings[351] or surface patterning, for instance using lithography with potential for multifunctional pattern structures that also give optical functions (see Section 5).[268] The more challenging aspect, however, is addressing the water vapor and oxygen penetration, which becomes increasingly problematic for cellulosic substrates as a function of relative humidity. Surface coatings offering sufficient barrier properties have been reached with atomic layer deposition (ALD) which blocks even the smallest cavities, or by coating with a polymeric water barrier layer.[352] Another strategy is to modify the bulk material, e.g., by adding clays that increase the effective path length for water vapor diffusion, reducing the WVTR, however thus far this strategy still generally falls short.[353]

As Table 4 indicates, different types of devices take advantage of the optical functionality of the lignocellulosic films. However, efforts to understand the material design factors that govern optical properties are still ongoing; hence, these
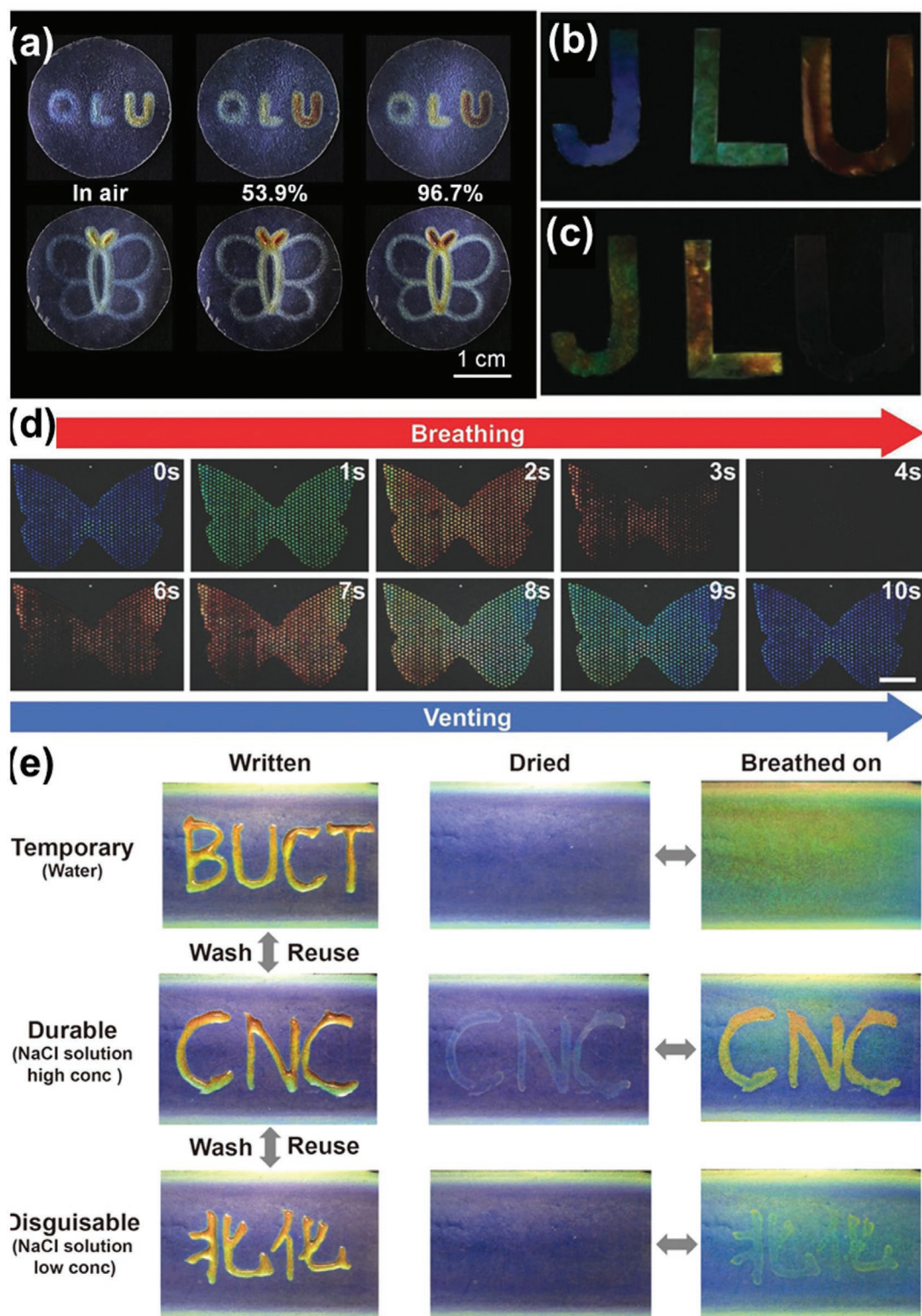
ADVANCED
SCIENCE NEWS

www.advancedsciencenews.com

ADVANCED
MATERIALS

www.advmat.de

Figure 11. a) Color variation of photonic patterns depending on ambient humidity. Reproduced with permission.[335] Copyright 2020, Elsevier B.V.; b) Photograph of "JLU", made of different concentrations of CNC/glucose under natural light on a black background. Reproduced with permission.[336] Copyright 2019, Wiley-VCH c) Photograph of "JLU" after exposure to 86% RH under natural light on a black background. Reproduced with permission.[336] Copyright 2019, Wiley-VCH; d) Blue "butterfly" dot matrix image rapidly and reversibly changes color in response to the moisture in an exhaled breath (scale bars: 5 mm). Reproduced with permission.[337] Copyright 2019, Wiley-VCH; e) A CNC film piece containing 20% waterborne polyurethane as a photonic paper that responds to inks composed of water (top images), high-concentration 0.1 M NaCl solution (middle images), and low-concentration 0.025 M NaCl solution (bottom images). Reproduced with permission.[338] Copyright 2018, American Chemical Society.

**ADVANCED
SCIENCE NEWS**

www.advancedsciencenews.com

**ADVANCED
MATERIALS**

www.advmat.de

Table 4. Optical functionalities produced by wood-derived materials as a replacement for conventional materials for uses in optical devices.

Device	Optical Functionalities	Conventional material	Plant-based materials	Ref.
Solar cell	transparency, anti-reflection, light trapping, patterning, translucency, luminescence, UV-blocking,	glass, polyethylene terephthalate (PET), polyethylene naphthalate (PEN)	TW, CNF films	[85,97]
Printed circuit boards	opaque, transparency	glass, polyimide (PI), PET, PEN, polycarbonate (PC),	α-cellulose	[353]
Light-emitting diodes (LED)	transparency, translucency	glass, PET, PI, PEN, PC, polydimethylsiloxane (PDMS)	Paper, Cellophane, CNC, TEMPO-CNF, TW, cellulose acetate butyrate	[57,216,354–356]
Organic Light-Emitting Diodes (OLED)	transparency, translucency, fluorescence, patterning	glass, PET, PI, PEN, PC,	Tempo-CNF; CNC, Cellulose acetate	[264,348,357–359]
Light-emitting electrochemical cells (LEC)	transparency, patterning	glass	Cellulose acetate	[264,360]
Flexible microwave amplifiers	transparency	–	CNF	[361]
Sensors	opacity, transparency, translucency, luminescence, patterning	–	Hemicellulose, Lignin, CNF, CNC, Cellulose Acetate, carboxymethyl cellulose, TW, TEMPO-CNF	[313,362–373]
Transistors	transparency, low translucency, structural color	glass, polyimide	TEMPO-CNF, CNF, CNC	[374–376]
Triboelectric nanogenerator	opacity, transparency	metal, plastic, organic film	Cellulose	[377–379]

demonstrations are likely not based on the most optimized cellulosic materials. Moreover, many inherent features of these materials, such as the highly anisotropic optical properties of transparent wood, are rarely utilized in demonstrations. Thus, parallel developments in both the fundamental studies (ideally combining computational and experimental approaches) of optical properties of different material combinations, as well as application-driven research are needed.

9. Outlook and Perspectives

In this review, we have highlighted recent developments related to the use of bio-derived lignocellulosic materials for optical functionalization. We have discussed some of the properties relating to the management of light, in the form of films that are transparent across the visible wavelengths, to highly engineered structural colors, and devices with optimized light-guiding surface topologies. Advancing this research requires a fundamental understanding of the link between the properties of the source material and desirable optical outcomes, combined with an understanding of material performance in the context of target device specifications. Once the optical properties can be customized and we solve the known setbacks of lignocellulosics, such as moisture sensitivity, the availability, and the facile tunability of these materials will open business opportunities in the smart device sector.

One key asset that lignocellulosic materials possess is that they hold promise for sustainable fabrication of smart devices, as compared to conventional glass-based substrates and fossil carbon-derived thermoplastics. Further data are called for to solidify the actual environmental impacts of different derivatization processes used with (nano)cellulose and wood (transparent wood, for instance). One example of a sustainability issue related to the recycling of smart devices is the re-collection of rare and expensive metals (Au, Ag, and Pt) that are difficult to replace with alternative materials and, therefore, are important to recycle from degraded devices. Unlike glass, wood-derived materials are compatible with pyroprocessing (acting as a fuel for the process) and the end-product after burning has around two orders of magnitude higher concentration of metals compared to typical glass-based devices, which is a major advantage in terms of recycling and associated commercial prospects.

Another consideration is the integration of circular economy efforts into this field of research. Most of the examples cited in this review focused on wood-derived materials, with major relevance to the forest products industry. However, there is an increasing interest in upcycling agri-food losses and wastes,[380] with some examples including fruit pomace, seaweed, and straw, as a source of biobased lignocellulosic materials. Since the key focus of this research area is still in developing efficient processes for the better valorization of waste biomass, we expect in the near future an increase in the availability of more sustainable raw material sources, also for device applications. Moreover, we anticipate that new research inspired by circular economy considerations will unveil new routes in recycling and reusing processes, beyond pyroprocessing, to support sustainability through the material lifespan and beyond.

Scientific challenges that need to be overcome before these materials can be implemented in broad scale advanced optical applications include efficient and scalable isolation and processing strategies, material uniformity, considering both raw material inputs and engineered products, insufficient material properties, such as brittleness and thermal processing limitations, interfacial compatibility in hybrid compositions, and issues related to hydrophilicity that include slow and inefficient drainage and humidity sensitivity. The use of tools provided by supra-particle and supramolecular chemistry, around biobased streams, is receiving accelerated attention[381] and one can expect discoveries in the facile deconstruction and reassembly of such structures,

and new approaches to tackle the aforementioned hurdles in the path toward the adoption of plant-based material alternatives.

To sum up, we expect the versatility and the simple tunability of the materials that we have presented to inspire the research community to push the limits for the integration of bio-derived materials into smart devices and the potential realization of more sustainable technological platforms and interfaces in the areas of light and energy harvesting and storage. We note that many of the properties that are either inherent to these materials or can be integrated into these materials are also not exclusive but can be used for the creation of multifunctional materials, combining both optical and other important characteristics.

Acknowledgements

Conflict of Interest

The authors declare no conflict of interest.

Keywords

[1] A. M. Abdel-Hamid, J. O. Solbiati, I. K. O. Cann, in *Advances in Applied Microbiology* (Ed: G. M. G. Sima Sariaslani), Academic Press, Cambridge **2013**, pp. 1–28.

[2] N. Dahmen, I. Lewandowski, S. Zibek, A. Weidtmann, *GCB Bioenergy* **2019**, *11*, 107.

[3] K. S. Baig, *Bioresour. Bioprocess.* **2020**, *7*, 21.

[4] L. A. Berglund, I. Burgert, *Adv. Mater.* **2018**, *30*, 1704285.

[5] H. Zhu, W. Luo, P. N. Ciesielski, Z. Fang, J. Y. Zhu, G. Henriksson, M. E. Himmel, L. Hu, *Chem. Rev.* **2016**, *116*, 9305.

[6] Z. Fang, H. Zhang, S. Qiu, Y. Kuang, J. Zhou, Y. Lan, C. Sun, G. Li, S. Gong, Z. Ma, *Adv. Mater. Technol.* **2021**, *6*, 2000928.

[7] F. B. Kadumudi, J. Trifol, M. Jahanshahi, T.-G. Zsurzsan, M. Mehrali, E. Zeqiraj, H. Shaki, M. Alehosseini, C. Gundlach, Q. Li, M. Dong, M. Akbari, A. Knott, K. Almdal, A. Dolatshahi-Pirouz, *ACS Appl. Mater. Interfaces* **2020**, *12*, 48027.

[8] C. Brigham, in *Green Chemistry*, Elsevier, New York **2018**, pp. 753–770.

[9] L. Petridis, J. C. Smith, *Nat. Rev. Chem.* **2018**, *2*, 382.

[10] J. Wang, D. Zhang, F. Chu, *Adv. Mater.* **2021**, *33*, 2001135.

[11] D. Selvi Gökkaya, M. Sert, M. Sağlam, M. Yüksel, L. Ballice, *J. Supercrit. Fluids* **2020**, *162*, 104846.

[12] M. Balakshin, E. A. Capanema, X. Zhu, I. Sulaeva, A. Potthast, T. Rosenau, O. J. Rojas, *Green Chem.* **2020**, *22*, 3985.

[13] H. Nishimura, A. Kamiya, T. Nagata, M. Katahira, T. Watanabe, *Sci. Rep.* **2018**, *8*, 6538.

[14] J. J. Liao, N. H. A. Latif, D. Trache, N. Brosse, M. H. Hussin, *Int. J. Biol. Macromol.* **2020**, *162*, 985.

[15] Y. Y. Tye, K. T. Lee, W. N. Wan Abdullah, C. P. Leh, *Renewable Sustainable Energy Rev.* **2016**, *60*, 155.

[16] F. Wirawan, C.-L. Cheng, Y.-C. Lo, C.-Y. Chen, J.-S. Chang, S.-Y. Leu, D.-J. Lee, *Appl. Energy* **2020**, *266*, 114871.

[17] K. Raj, C. Krishnan, *Renewable Energy* **2020**, *153*, 392.

[18] M. P. Sudhakar, K. Arunkumar, K. Perumal, *Renewable Energy* **2020**, *153*, 456.

[19] E. J. C. de Moraes, D. D. V. Silva, K. J. Dussán, L. Z. Tesche, J. B. A. de Silva, M. Rai, M. G. de A. das Felipe, *Waste Biomass Valorization* **2020**, *11*, 1837.

[20] Rena, K. M. B. Z. , S. Yadav, N. P. Machhirake, S.-H. Kim, B.-D. Lee, H. Jeong, L. Singh, S. Kumar, R. Kumar, *Bioresour. Technol.* **2020**, *309*, 123297.

[21] P. Gautam, Neha, S. N. U. , S. K. Dubey, *Fuel* **2020**, *273*, 117783.

[22] D. N.-S. Hon, N. Shiraishi, *Wood and CellulosicChemistry, Revised, and Expanded*, CRC Press, New York and Basel **2000**.

[23] N. Ayadi, F. Lejeune, F. Charrier, B. Charrier, A. Merlin, *Holz als Roh- und Werkst* **2003**, *61*, 221.

[24] H. Zhang, F. Chen, X. Liu, S. Fu, *ACS Sustainable Chem. Eng.* **2018**, *6*, 12532.

[25] M. Zhu, J. Song, T. Li, A. Gong, Y. Wang, J. Dai, Y. Yao, W. Luo, D. Henderson, L. Hu, *Adv. Mater.* **2016**, *28*, 5181.

[26] Y. Li, E. Vasileva, I. Sychugov, S. Popov, L. Berglund, *Adv. Opt. Mater.* **2018**, *6*, 1800059.

[27] H. Xu, J. Peng, Y. Kong, Y. Liu, Z. Su, B. Li, X. Song, S. Liu, W. Tian, *Bioresour. Technol.* **2020**, *310*, 123416.

[28] N. H. N. Do, H. H. Pham, T. M. Le, J. Lauwaert, L. Diels, A. Verberckmoes, N. H. N. Do, V. T. Tran, P. K. Le, *Sci. Rep.* **2020**, *10*, 21263.

[29] H. Li, Q. Dai, J. Ren, L. Jian, F. Peng, R. Sun, G. Liu, *Carbohydr. Polym.* **2016**, *136*, 203.

[30] S. C. Lee, T. M. T. Tran, J. W. Choi, K. Won, *Int. J. Biol. Macromol.* **2019**, *122*, 549.

[31] J. Wang, Y. Deng, Y. Qian, X. Qiu, Y. Ren, D. Yang, *Green Chem.* **2016**, *18*, 695.

[32] S. C. Lee, S. H. Lee, K. Won, *Biotechnol. Bioprocess Eng.* **2019**, *24*, 258.

[33] A. T. W. M. Hendriks, G. Zeeman, *Bioresour. Technol.* **2009**, *100*, 10.

[34] J. Zakzeski, P. C. A. Bruijnincx, A. L. Jongerius, B. M. Weckhuysen, *Chem. Rev.* **2010**, *110*, 3552.

[35] L. da Costa Sousa, S. P. Chundawat, V. Balan, B. E. Dale, *Curr. Opin. Biotechnol.* **2009**, *20*, 339.

[36] A. J. Ragauskas, G. T. Beckham, M. J. Biddy, R. Chandra, F. Chen, M. F. Davis, B. H. Davison, R. A. Dixon, P. Gilna, M. Keller, P. Langan, A. K. Naskar, J. N. Saddler, T. J. Tschaplinski, G. A. Tuskan, C. E. Wyman, *Science* **2014**, *344*, 1246843.

[37] J. Rajesh Banu, S. Kavitha, R. Yukesh Kannah, T. Poornima Devi, M. Gunasekaran, S.-H. Kim, G. Kumar, *Bioresour. Technol.* **2019**, *290*, 121790.

[38] T. Theivasanthi, F. L. Anne Christma, A. J. Toyin, S. C. B. Gopinath, R. Ravichandran, *Int. J. Biol. Macromol.* **2018**, *109*, 832.

[39] S. Jeremic, L. Djokic, V. Ajdačić, N. Božinović, V. Pavlovic, D. D. Manojlović, R. Babu, R. Senthamaraikannan, O. Rojas, I. Opsenica, J. Nikodinovic-Runic, *Int. J. Biol. Macromol.* **2019**, *129*, 351.

[40] K. Hatamoto, H. Shimada, M. Kondo, S. Nobukawa, M. Yamaguchi, *Cellulose* **2018**, *25*, 4453.

[41] I. Moussa, R. Khiari, A. Moussa, M. N. Belgacem, M. F. Mhenni, *Fibers Polym.* **2019**, *20*, 933.

**ADVANCED
SCIENCE NEWS**

www.advancedsciencenews.com

**ADVANCED
MATERIALS**

www.advmat.de

[42] S. Paunonen, *BioResources* **2013**, *8*, 3098.

[43] X. He, W. Lu, C. Sun, H. Khalesi, A. Mata, R. Andaleeb, Y. Fang, *Carbohydr. Polym.* **2021**, *255*, 117334.

[44] E. Kontturi, P. Laaksonen, M. B. Linder, Nonappa, A. H. Gröschel, O. J. Rojas, O. Ikkala, *Adv. Mater.* **2018**, *30*, 1703779.

[45] A. Tran, C. E. Boott, M. J. MacLachlan, *Adv. Mater.* **2020**, *32*, 1905876.

[46] G. Jacucci, L. Schertel, Y. Zhang, H. Yang, S. Vignolini, *Adv. Mater.* **2020**, *33*, 2001215.

[47] L. Wang, C. Chen, J. Wang, D. J. Gardner, M. Tajvidi, *Food Packag. Shelf Life* **2020**, *23*, 100464.

[48] R. Xiong, J. Luan, S. Kang, C. Ye, S. Singamaneni, V. V. Tsukruk, *Chem. Soc. Rev.* **2020**, *49*, 983.

[49] D. Zhao, Y. Zhu, W. Cheng, W. Chen, Y. Wu, H. Yu, *Adv. Mater.* **2021**, *33*, 2000619.

[50] A. T. Vicente, A. Araújo, M. J. Mendes, D. Nunes, M. J. Oliveira, O. Sanchez-Sobrado, M. P. Ferreira, H. Águas, E. Fortunato, R. Martins, *J. Mater. Chem. C* **2018**, *6*, 3143.

[51] Y. Zhang, L. Zhang, K. Cui, S. Ge, X. Cheng, M. Yan, J. Yu, H. Liu, *Adv. Mater.* **2018**, *30*, 1801588.

[52] O. A. T. Dias, S. Konar, A. L. Leão, W. Yang, J. Tjong, M. Sain, *Front. Chem.* **2020**, *8*, 420.

[53] X. Liu, W. Xiao, X. Ma, L. Huang, Y. Ni, L. Chen, X. Ouyang, J. Li, *Carbohydr. Polym.* **2020**, *250*, 116969.

[54] S. Alter, *Inf. Syst. Front.* **2020**, *22*, 381.

[55] H. Sadeghifar, A. Ragauskas, *Polymers (Basel)* **2020**, *12*, 1134.

[56] K. Ganguly, D. K. Patel, S. D. Dutta, W.-C. Shin, K.-T. Lim, *Int. J. Biol. Macromol.* **2020**, *155*, 456.

[57] Q. Fu, Y. Chen, M. Sorieul, *ACS Nano* **2020**, *14*, 3528.

[58] D. Gigilashvili, J.-B. Thomas, J. Y. Hardeberg, M. Pedersen, in *Work. Mater. Appear. Model.* (Eds: R. Klein, H. Rushmeier), The Eurographics Association, Vienna, Austria **2020**.

[59] Z. Li, W. Liu, F. Guan, G. Li, Z. Song, D. Yu, H. Wang, H. Liu, *Carbohydr. Polym.* **2019**, *214*, 26.

[60] D. Ha, Z. Fang, N. B. Zhitenev, *Adv. Electron. Mater.* **2018**, *4*, 1700593.

[61] B. Geometries, S. Abrasion, *ASTM Int.* **2012**, *1*, 1.

[62] S. Busato, A. Perevedentsev, *Polym. Eng. Sci.* **2018**, *58*, 345.

[63] M.-C. Hsieh, H. Koga, K. Suganuma, M. Nogi, *Sci. Rep.* **2017**, *7*, 41590.

[64] B. Xiao, B. Walter, I. Gkioulekas, T. Zickler, E. Adelson, K. Bala, *J. Vis.* **2014**, *14*, 17.

[65] M. Motamedi, M. E. Warkiani, R. A. Taylor, *Adv. Opt. Mater.* **2018**, *6*, 1800091.

[66] M. S. Toivonen, O. D. Onelli, G. Jacucci, V. Lovikka, O. J. Rojas, O. Ikkala, S. Vignolini, *Adv. Mater.* **2018**, *30*, 1704050.

[67] B. Frka-Petesic, S. Vignolini, *Nat. Photonics* **2019**, *13*, 365.

[68] X. Li, N. Wang, X. Zhang, H. Chang, Y. Wang, Z. Zhang, *Cellulose* **2020**, *27*, 1315.

[69] W. Hu, G. Chen, Y. Liu, Y. Liu, B. Li, Z. Fang, *ACS Sustainable Chem. Eng.* **2018**, *6*, 6974.

[70] Y. Chu, Y. Sun, W. Wu, H. Xiao, *Carbohydr. Polym.* **2020**, *250*, 116892.

[71] X. Niu, Y. Liu, A. W. T. King, S. Hietala, H. Pan, O. J. Rojas, *Biomacromolecules* **2019**, *20*, 2105.

[72] O. A. El Seoud, M. Kostag, K. Jedvert, N. I. Malek, *Macromol. Mater. Eng.* **2020**, *305*, 1900832.

[73] I. Leppänen, M. Vikman, A. Harlin, H. Orelma, *J. Polym. Environ.* **2020**, *28*, 458.

[74] V. López Durán, J. Hellwig, P. T. Larsson, L. Wågberg, P. A. Larsson, *ACS Appl. Nano Mater.* **2018**, *1*, 1959.

[75] F. Rol, M. N. Belgacem, A. Gandini, J. Bras, *Prog. Polym. Sci.* **2019**, *88*, 241.

[76] Y. Wang, L. Yuan, H. Tian, L. Zhang, A. Lu, *J. Membr. Sci.* **2019**, *585*, 99.

[77] X. Niu, Y. Liu, G. Fang, C. Huang, O. J. Rojas, H. Pan, *Biomacromolecules* **2018**, *19*, 4565.

[78] S. Chen, Y. Song, F. Xu, *ACS Sustainable Chem. Eng.* **2018**, *6*, 5173.

[79] C.-N. Wu, K.-C. Cheng, *Cellulose* **2017**, *24*, 269.

[80] K. Labidi, O. Korhonen, M. Zrida, A. H. Hamzaoui, T. Budtova, *Ind. Crops Prod.* **2019**, *127*, 135.

[81] G. Hou, Y. Liu, D. Zhang, G. Li, H. Xie, Z. Fang, *ACS Appl. Mater. Interfaces* **2020**, *12*, 31998.

[82] D. W. Kim, J. Shin, S. Q. Choi, *Carbohydr. Polym.* **2020**, *247*, 116762.

[83] S. Tanpichai, S. K. Biswas, S. Witayakran, H. Yano, *Composites, Part A* **2020**, *132*, 105811.

[84] S. K. Biswas, S. Tanpichai, S. Witayakran, X. Yang, M. I. Shams, H. Yano, *ACS Nano* **2019**, *13*, 2015.

[85] Y. Li, M. Cheng, E. Jungstedt, B. Xu, L. Sun, L. Berglund, *ACS Sustainable Chem. Eng.* **2019**, *7*, 6061.

[86] H. Chen, A. Baitenov, Y. Li, E. Vasileva, S. Popov, I. Sychugov, M. Yan, L. Berglund, *ACS Appl. Mater. Interfaces* **2019**, *11*, 35451.

[87] Y. Li, X. Yang, Q. Fu, R. Rojas, M. Yan, L. Berglund, *J. Mater. Chem. A* **2018**, *6*, 1094.

[88] K. Li, S. Wang, H. Chen, X. Yang, L. A. Berglund, Q. Zhou, *Adv. Mater.* **2020**, *32*, 2003653.

[89] E. Vasileva, H. Chen, Y. Li, I. Sychugov, M. Yan, L. Berglund, S. Popov, *Adv. Opt. Mater.* **2018**, *6*, 1800999.

[90] W. Zou, Z. Wang, D. Sun, X. Ji, P. Zhang, Z. Zhu, *Sci. Rep.* **2020**, *10*, 1947.

[91] J. Qin, X. Li, Y. Shao, K. Shi, X. Zhao, T. Feng, Y. Hu, *Vacuum* **2018**, *158*, 158.

[92] S. Iwamoto, K. Abe, H. Yano, *Biomacromolecules* **2008**, *9*, 1022.

[93] S. Galland, F. Berthold, K. Prakobna, L. A. Berglund, *Biomacromolecules* **2015**, *16*, 2427.

[94] X. Yang, M. S. Reid, P. Olsén, L. A. Berglund, *ACS Nano* **2020**, *14*, 724.

[95] W. Farhat, R. A. Venditti, M. Hubbe, M. Taha, F. Becquart, A. Ayoub, *ChemSusChem* **2017**, *10*, 305.

[96] W. Geng, R. A. Venditti, J. J. Pawlak, H. Chang, L. Pal, E. Ford, *Cellulose* **2020**, *27*, 3359.

[97] M. Zhu, T. Li, C. S. Davis, Y. Yao, J. Dai, Y. Wang, F. AlQatari, J. W. Gilman, L. Hu, *Nano Energy* **2016**, *26*, 332.

[98] R. Ajdary, B. L. Tardy, B. D. Mattos, L. Bai, O. J. Rojas, *Adv. Mater.* **2021**, *33*, 2001085.

[99] J. Liu, H. Ni, Z. Wang, S. Yang, W. Zhou, in *Optoelectronic – Materials Devices*, InTech, London **2015**.

[100] A. C. Liapis, A. Rahman, C. T. Black, *Appl. Phys. Lett.* **2017**, *111*, 183901.

[101] P. Cazón, G. Velazquez, M. Vázquez, *Food Hydrocolloids* **2020**, *99*, 105323.

[102] L. Zheng, Y. Xuan, *Sol. Energy* **2018**, *173*, 1216.

[103] E. Yousif, R. Haddad, *SpringerPlus* **2013**, *2*, 398.

[104] D. Ehrt, *C. R. Chim* **2002**, *5*, 679.

[105] A. Poskela, K. Miettunen, A. Tiihonen, P. D. Lund, *Energy Sci. Eng.* **2021**, *9*, 19.

[106] T. Smijs, Pavel, *Nanotechnol., Sci. Appl.* **2011**, *4*, 95.

[107] S. L. Schneider, H. W. Lim, *Photodermatol., Photoimmunol. Photomed.* **2019**, *35*, 442.

[108] J. Theerthagiri, S. Salla, R. A. Senthil, P. Nithyadharseni, A. Madankumar, P. Arunachalam, T. Maiyalagan, H.-S. Kim, *Nanotechnology* **2019**, *30*, 392001.

[109] T. Abitbol, A. Ahniyaz, R. Álvarez-Asencio, A. Fall, A. Swerin, *ACS Appl. Bio Mater.* **2020**, *3*, 2245.

[110] D. K. Subbiah, K. J. Babu, A. Das, J. B. B. Rayappan, *ACS Appl. Mater. Interfaces* **2019**, *11*, 20045.

[111] E. Lizundia, A. Urruchi, J. L. Vilas, L. M. León, *Carbohydr. Polym.* **2016**, *136*, 250.

[112] X. Zhang, W. Luo, N. Xiao, M. Chen, C. Liu, *Cellulose* **2020**, *27*, 1341.

2104473 (31 of 37)

**ADVANCED
SCIENCE NEWS**

www.advancedsciencenews.com

**ADVANCED
MATERIALS**

www.advmat.de

[113] S. Mun, H. C. Kim, H.-U. Ko, L. Zhai, J. W. Kim, J. Kim, *Sci. Technol. Adv. Mater.* **2017**, *18*, 437.

[114] Y. Jiang, Y. Song, M. Miao, S. Cao, X. Feng, J. Fang, L. Shi, *J. Mater. Chem. C* **2015**, *3*, 6717.

[115] C. Li, Y. Xie, Q. Liu, Y. Zheng, X. Zhang, W. Dong, *Fibers Polym.* **2014**, *15*, 281.

[116] X. Li, L. Zhang, Z. Wang, S. Wu, J. Ma, *Carbohydr. Polym.* **2021**, *259*, 117752.

[117] S. Chen, B. Zhou, W. Hu, W. Zhang, N. Yin, H. Wang, *Carbohydr. Polym.* **2013**, *92*, 1953.

[118] Y.-C. Liang, C.-S. Hung, W.-C. Zhao, *Nanomaterials* **2020**, *10*, 1352.

[119] Z. Zhang, G. Sèbe, X. Wang, K. C. Tam, *ACS Appl. Nano Mater.* **2018**, *1*, 632.

[120] W. Yang, Y. Gao, C. Zuo, Y. Deng, H. Dai, *Carbohydr. Polym.* **2019**, *223*, 115050.

[121] J. Yu, Y. Zhu, H. Ma, L. Liu, Y. Hu, J. Xu, Z. Wang, Y. Fan, *Cellulose* **2019**, *26*, 6023.

[122] T. Bikova, *Carbohydr. Polym.* **2004**, *55*, 315.

[123] H. Zhang, X. Wang, J. Wang, Q. Chen, H. Huang, L. Huang, S. Cao, X. Ma, *Wood Sci. Technol.* **2020**, *54*, 837.

[124] M. Y. Balakshin, E. A. Capanema, I. Sulaeva, P. Schlee, Z. Huang, M. Feng, M. Borghei, O. J. Rojas, A. Potthast, T. Rosenau, *ChemSusChem* **2021**, *14*, 1016.

[125] J. Fernández-Rodríguez, X. Erdocia, F. Hernández-Ramos, M. G. Alriols, J. Labidi, in *Separation of Functional Molecules in Food by Membrane Technology*, Elsevier, New York **2019**, pp. 229–265.

[126] N. Izaguirre, O. Gordobil, E. Robles, J. Labidi, *Int. J. Biol. Macromol.* **2020**, *155*, 447.

[127] M. Parit, P. Saha, V. A. Davis, Z. Jiang, *ACS Omega* **2018**, *3*, 10679.

[128] M. Farooq, T. Zou, G. Riviere, M. H. Sipponen, M. Österberg, *Biomacromolecules* **2019**, *20*, 693.

[129] Y. Jiang, X. Liu, Q. Yang, X. Song, C. Qin, S. Wang, K. Li, *Cellulose* **2019**, *26*, 1577.

[130] H. Sadeghifar, R. Venditti, J. Jur, R. E. Gorga, J. J. Pawlak, *ACS Sustainable Chem. Eng.* **2017**, *5*, 625.

[131] M. Lievonen, J. J. Valle-Delgado, M.-L. Mattinen, E.-L. Hult, K. Lintinen, M. A. Kostiainen, A. Paananen, G. R. Szilvay, H. Setälä, M. Österberg, *Green Chem.* **2016**, *18*, 1416.

[132] E. Pasquier, B. D. Mattos, N. Belgacem, J. Bras, O. J. Rojas, *Biomacromolecules* **2021**, *22*, 880.

[133] L. Wang, L. Tan, L. Hu, X. Wang, R. Koppolu, T. Tirri, B. van Bochove, P. Ihalainen, L. S. Seleenmary Sobhanadhas, J. V. Seppälä, S. Willför, M. Toivakka, C. Xu, *ACS Sustainable Chem. Eng.* **2021**, *9*, 8770.

[134] J. Yang, X. An, L. Liu, F. T. Seta, H. Zhang, S. Nie, S. Yao, H. Cao, Q. Xu, H. Liu, Y. Ni, *Cellulose* **2020**, *27*, 5071.

[135] H. Zhang, S. Fu, Y. Chen, *Int. J. Biol. Macromol.* **2020**, *147*, 607.

[136] B. Wang, D. Sun, H.-M. Wang, T.-Q. Yuan, R.-C. Sun, *ACS Sustainable Chem. Eng.* **2019**, *7*, 2658.

[137] W. Gao, J. P. W. Inwood, P. Fatehi, *J. Wood Chem. Technol.* **2019**, *39*, 225.

[138] Q. Xia, C. Chen, Y. Yao, S. He, X. Wang, J. Li, J. Gao, W. Gan, B. Jiang, M. Cui, L. Hu, *Adv. Mater.* **2021**, *33*, 2001588.

[139] J. Yu, L. Li, Y. Qian, H. Lou, D. Yang, X. Qiu, *Ind. Eng. Chem. Res.* **2018**, *57*, 15740.

[140] R. Kaur, N. S. Thakur, S. Chandna, J. Bhaumik, *J. Mater. Chem. B* **2020**, *8*, 260.

[141] Y. Li, D. Yang, S. Lu, X. Qiu, Y. Qian, P. Li, *ACS Sustainable Chem. Eng.* **2019**, *7*, 6234.

[142] H. Wang, W. Lin, X. Qiu, F. Fu, R. Zhong, W. Liu, D. Yang, *ACS Sustainable Chem. Eng.* **2018**, *6*, 3696.

[143] T. Mitiouchkina, A. S. Mishin, L. G. Somermeyer, N. M. Markina, T. V. Chepurnyh, E. B. Guglya, T. A. Karataeva, K. A. Palkina, E. S. Shakhova, L. I. Fakhranurova, S. V. Chekova, A. S. Tsarkova, Y. V. Golubev, V. V. Negrebetsky, S. A. Dolgushin, P. V. Shalaev,

D. Shlykov, O. A. Melnik, V. O. Shipunova, S. M. Deyev, A. I. Bubyrev, A. S. Pushin, V. V. Choob, S. V. Dolgov, F. A. Kondrashov, I. V. Yampolsky, K. S. Sarkisyan, *Nat. Biotechnol.* **2020**, *38*, 944.

[144] O. Graydon, *Nat. Photonics* **2020**, *14*, 407.

[145] G. Blasse, B. C. Grabmaier, in *Luminescent Materials*, Springer Berlin Heidelberg, Berlin, Heidelberg **1994**, pp. 1–9.

[146] J. Li, K. Pu, *Chem. Soc. Rev.* **2019**, *48*, 38.

[147] D. Kong, K. Zhang, J. Tian, L. Yin, X. Sheng, *Adv. Mater. Technol.* **2021**, 2100006, https://doi.org/10.1002/admt.202100006.

[148] R. Tong, G. Chen, J. Tian, M. He, *Carbohydr. Polym.* **2020**, *227*, 115366.

[149] F. Mo, Z. Chen, G. Liang, D. Wang, Y. Zhao, H. Li, B. Dong, C. Zhi, *Adv. Energy Mater.* **2020**, *10*, 2000035.

[150] D. Ma, T. Tsuboi, Y. Qiu, L. Duan, *Adv. Mater.* **2017**, *29*, 1603253.

[151] E. Cariati, E. Lucenti, C. Botta, U. Giovanella, D. Marinotto, S. Righetto, *Coord. Chem. Rev.* **2016**, *306*, 566.

[152] X. Yang, X. Zhang, Q. Guan, X. Zhang, *J. Mater. Chem. C* **2021**, *9*, 2815.

[153] Kenry, C. C. , B. Liu, *Nat. Commun.* **2019**, *10*, 2111.

[154] X. Zhu, J. Zhang, J. Liu, Y. Zhang, *Adv. Sci.* **2019**, *6*, 1901358.

[155] Z. Song, Z. Zhao, Q. Liu, *Inorg. Chem. Front.* **2019**, *6*, 2969.

[156] G. Yang, S. Z. F. Phua, A. K. Bindra, Y. Zhao, *Adv. Mater.* **2019**, *31*, 1805730.

[157] Y. Li, X. Zhang, H. Huang, S. V. Kershaw, A. L. Rogach, *Mater. Today* **2020**, *32*, 204.

[158] M. S. Kwon, J. H. Jordahl, A. W. Phillips, K. Chung, S. Lee, J. Gierschner, J. Lahann, J. Kim, *Chem. Sci.* **2016**, *7*, 2359.

[159] W. P. Lustig, S. Mukherjee, N. D. Rudd, A. V. Desai, J. Li, S. K. Ghosh, *Chem. Soc. Rev.* **2017**, *46*, 3242.

[160] Y. Cui, J. Zhang, H. He, G. Qian, *Chem. Soc. Rev.* **2018**, *47*, 5740.

[161] K. J. McHugh, L. Jing, A. M. Behrens, S. Jayawardena, W. Tang, M. Gao, R. Langer, A. Jaklenec, *Adv. Mater.* **2018**, *30*, 1706356.

[162] L. Zhang, S. Lyu, Q. Zhang, S. C. Chmely, Y. Wu, C. Melcher, K. Rajan, D. P. Harper, S. Wang, Z. Chen, *Ind. Crops Prod.* **2020**, *145*, 112066.

[163] B. Xue, Z. Zhang, Y. Sun, J. Wang, H. Jiang, M. Du, C. Chi, X. Li, *Carbohydr. Polym.* **2018**, *186*, 176.

[164] Y. Wu, L. Wang, Y. Qing, N. Yan, C. Tian, Y. Huang, *Sci. Rep.* **2017**, *7*, 4380.

[165] X. Guo, D. Xu, H. Yuan, Q. Luo, S. Tang, L. Liu, Y. Wu, *J. Mater. Chem. A* **2019**, *7*, 27081.

[166] J. He, K. Bian, N. Li, G. Piao, *J. Mater. Chem. C* **2019**, *7*, 9278.

[167] M. Chekini, E. Prince, L. Zhao, H. Mundoor, I. I. Smalyukh, E. Kumacheva, *Adv. Opt. Mater.* **2020**, *8*, 1901911.

[168] N. O'Donnell, I. A. Okkelman, P. Timashev, T. I. Gromovykh, D. B. Papkovsky, R. I. Dmitriev, *Acta Biomater.* **2018**, *80*, 85.

[169] Y. Wei, V.-T. Tran, C. Zhao, H. Liu, J. Kong, H. Du, *ACS Appl. Mater. Interfaces* **2019**, *11*, 21445.

[170] H. Hu, F. Wang, L. Yu, K. Sugimura, J. Zhou, Y. Nishio, *ACS Sustainable Chem. Eng.* **2018**, *6*, 1436.

[171] B. Lee, J.-Y. Oh, H. Cho, C. W. Joo, H. Yoon, S. Jeong, E. Oh, J. Byun, H. Kim, S. Lee, J. Seo, C. W. Park, S. Choi, N.-M. Park, S.-Y. Kang, C.-S. Hwang, S.-D. Ahn, J.-I. Lee, Y. Hong, *Nat. Commun.* **2020**, *11*, 663.

[172] W. Li, Z. Chen, H. Yu, J. Li, S. Liu, *Adv. Mater.* **2021**, *33*, 2000596.

[173] F. Temerov, A. Belyaev, B. Ankudze, T. T. Pakkanen, *J. Lumin.* **2019**, *206*, 403.

[174] S. Rai, B. K. Singh, P. Bhartiya, A. Singh, H. Kumar, P. K. Dutta, G. K. Mehrotra, *J. Lumin.* **2017**, *190*, 492.

[175] B. Xue, Y. Yang, Y. Sun, J. Fan, X. Li, Z. Zhang, *Int. J. Biol. Macromol.* **2019**, *122*, 954.

[176] L. D. Carlos, R. A. S. Ferreira, V. Z. de Bermudez, S. J. L. Ribeiro, *Adv. Mater.* **2009**, *21*, 509.

ADVANCED
SCIENCE NEWS

www.advancedsciencenews.com

ADVANCED
MATERIALS

www.advmat.de

[177] L. D. Carlos, R. A. S. Ferreira, V. de Zea Bermudez, B. Julián-López, P. Escribano, *Chem. Soc. Rev.* **2011**, *40*, 536.

[178] H. Li, X. Wang, T. Y. Ohulchanskyy, G. Chen, *Adv. Mater.* **2021**, *33*, 2000678.

[179] K. Zheng, K. Y. Loh, Y. Wang, Q. Chen, J. Fan, T. Jung, S. H. Nam, Y. D. Suh, X. Liu, *Nano Today* **2019**, *29*, 100797.

[180] L. Zong, Z. Wang, R. Yu, *Small* **2019**, *15*, 1804510.

[181] D. E. Barry, D. F. Caffrey, T. Gunnlaugsson, *Chem. Soc. Rev.* **2016**, *45*, 3244.

[182] Y. Fan, F. Zhang, *Adv. Opt. Mater.* **2019**, *7*, 1801417.

[183] Q. Wang, D. Xie, J. Chen, G. Liu, M. Yu, *ACS Sustainable Chem. Eng.* **2020**, *8*, 13176.

[184] S. Zhang, G. Liu, H. Chang, X. Li, Z. Zhang, *ACS Sustainable Chem. Eng.* **2019**, *7*, 9966.

[185] W. Gan, S. Xiao, L. Gao, R. Gao, J. Li, X. Zhan, *ACS Sustainable Chem. Eng.* **2017**, *5*, 3855.

[186] W. Li, M. Xu, C. Ma, Y. Liu, J. Zhou, Z. Chen, Y. Wang, H. Yu, J. Li, S. Liu, *ACS Appl. Mater. Interfaces* **2019**, *11*, 23512.

[187] A. Tymiński, E. Śmiechowicz, I. R. Martín, T. Grzyb, *ACS Appl. Nano Mater.* **2020**, *3*, 6541.

[188] H. Yu, R. Shi, Y. Zhao, G. I. N. Waterhouse, L.-Z. Wu, C.-H. Tung, T. Zhang, *Adv. Mater.* **2016**, *28*, 9454.

[189] A. Cayuela, M. L. Soriano, C. Carrillo-Carrión, M. Valcárcel, *Chem. Commun.* **2016**, *52*, 1311.

[190] J. B. Essner, G. A. Baker, *Environ. Sci. Nano* **2017**, *4*, 1216.

[191] J. B. Essner, C. H. Laber, S. Ravula, L. Polo-Parada, G. A. Baker, *Green Chem.* **2016**, *18*, 243.

[192] M. Lu, Y. Duan, Y. Song, J. Tan, L. Zhou, *J. Mol. Liq.* **2018**, *269*, 766.

[193] H. Xu, L. Xie, J. Li, M. Hakkarainen, *ACS Appl. Mater. Interfaces* **2017**, *9*, 27972.

[194] C. Cheng, Y. Shi, M. Li, M. Xing, Q. Wu, *Mater. Sci. Eng., C* **2017**, *79*, 473.

[195] Y.-Y. Yao, G. Gedda, W. M. Girma, C.-L. Yen, Y.-C. Ling, J.-Y. Chang, *ACS Appl. Mater. Interfaces* **2017**, *9*, 13887.

[196] B. K. Walther, C. Z. Dinu, D. M. Guldi, V. G. Sergeyev, S. E. Creager, J. P. Cooke, A. Guiseppi-Elie, *Mater. Today* **2020**, *39*, 23.

[197] L. Yan, L. Chen, X. Zhao, X. Yan, *Adv. Funct. Mater.* **2020**, *30*, 1909042.

[198] F. Yuan, S. Li, Z. Fan, X. Meng, L. Fan, S. Yang, *Nano Today* **2016**, *11*, 565.

[199] S. Anwar, H. Ding, M. Xu, X. Hu, Z. Li, J. Wang, L. Liu, L. Jiang, D. Wang, C. Dong, M. Yan, Q. Wang, H. Bi, *ACS Appl. Bio Mater.* **2019**, *2*, 2317.

[200] M. Xu, X. Wu, Y. Yang, C. Ma, W. Li, H. Yu, Z. Chen, J. Li, K. Zhang, S. Liu, *ACS Nano* **2020**, *14*, 11130.

[201] Z. Bi, T. Li, H. Su, Y. Ni, L. Yan, *ACS Sustainable Chem. Eng.* **2018**, *6*, 9314.

[202] Z. Wang, F. Yuan, X. Li, Y. Li, H. Zhong, L. Fan, S. Yang, *Adv. Mater.* **2017**, *29*, 1702910.

[203] F. Zu, F. Yan, Z. Bai, J. Xu, Y. Wang, Y. Huang, X. Zhou, *Microchim. Acta* **2017**, *184*, 1899.

[204] K. Jin, J. Zhang, W. Tian, X. Ji, J. Yu, J. Zhang, *ACS Sustainable Chem. Eng.* **2020**, *8*, 5937.

[205] R. Xiong, S. Yu, M. J. Smith, J. Zhou, M. Krecker, L. Zhang, D. Nepal, T. J. Bunning, V. V. Tsukruk, *ACS Nano* **2019**, *13*, 9074.

[206] K. A. S. Fernando, S. Sahu, Y. Liu, W. K. Lewis, E. A. Guliants, A. Jafariyan, P. Wang, C. E. Bunker, Y.-P. Sun, *ACS Appl. Mater. Interfaces* **2015**, *7*, 8363.

[207] H. Su, Z. Bi, Y. Ni, L. Yan, *Green Energy Environ.* **2019**, *4*, 391.

[208] Z. Liu, M. Chen, Y. Guo, J. Zhou, Q. Shi, R. Sun, *Chem. Eng. J.* **2020**, *384*, 123260.

[209] J. Zhou, H. Zhou, J. Tang, S. Deng, F. Yan, W. Li, M. Qu, *Microchim. Acta* **2017**, *184*, 343.

[210] G. Yang, X. Wan, Y. Su, X. Zeng, J. Tang, *J. Mater. Chem. A* **2016**, *4*, 12841.

[211] B. Zhang, Y. Liu, M. Ren, W. Li, X. Zhang, R. Vajtai, P. M. Ajayan, J. M. Tour, L. Wang, *ChemSusChem* **2019**, *12*, 4202.

[212] Y. Liu, H. Yang, C. Ma, S. Luo, M. Xu, Z. Wu, W. Li, S. Liu, *ACS Appl. Mater. Interfaces* **2020**, *12*, 36628.

[213] S. Zhao, X. Song, X. Chai, P. Zhao, H. He, Z. Liu, *J. Cleaner Prod.* **2020**, *263*, 121561.

[214] S. A. Veldhuis, P. P. Boix, N. Yantara, M. Li, T. C. Sum, N. Mathews, S. G. Mhaisalkar, *Adv. Mater.* **2016**, *28*, 6804.

[215] Q. Van Le, H. W. Jang, S. Y. Kim, *Small Methods* **2018**, *2*, 1700419.

[216] C. Kang, C. Lin, C. Lin, T. Li, S. Huang Chen, C. Tsai, C. Sher, T. Wu, P. Lee, X. Xu, M. Zhang, C. Ho, J. He, H. Kuo, *Adv. Sci.* **2019**, *6*, 1902230.

[217] T. Li, X. Xu, C. Lin, X. Guan, W. Hsu, M. Tsai, X. Fang, T. Wu, J. He, *Adv. Sci.* **2020**, *7*, 1902439.

[218] S. Filali, F. Pirot, P. Miossec, *Trends Biotechnol.* **2020**, *38*, 163.

[219] D. Wang, F. Yin, Z. Du, D. Han, J. Tang, *J. Mater. Chem. A* **2019**, *7*, 26205.

[220] S. V. Kershaw, A. S. Susha, A. L. Rogach, *Chem. Soc. Rev.* **2013**, *42*, 3033.

[221] X.-B. Li, C.-H. Tung, L.-Z. Wu, *Nat. Rev. Chem.* **2018**, *2*, 160.

[222] X. Li, Y. Hu, *Carbohydr. Polym.* **2019**, *203*, 167.

[223] Q. Fu, M. Yan, E. Jungstedt, X. Yang, Y. Li, L. A. Berglund, *Compos. Sci. Technol.* **2018**, *164*, 296.

[224] Y. Li, S. Yu, J. G. C. Veinot, J. Linnros, L. Berglund, I. Sychugov, *Adv. Opt. Mater.* **2017**, *5*, 1600834.

[225] Y. Wei, H. Dong, C. Wei, W. Zhang, Y. Yan, Y. S. Zhao, *Adv. Mater.* **2016**, *28*, 7424.

[226] H. Huang, M. Liu, S. Luo, K. Wang, Q. Wan, F. Deng, D. Xu, X. Zhang, Y. Wei, *Chem. Eng. J.* **2016**, *304*, 149.

[227] J. Luo, Z. Xie, J. W. Y. Lam, L. Cheng, B. Z. Tang, H. Chen, C. Qiu, H. S. Kwok, X. Zhan, Y. Liu, D. Zhu, *Chem. Commun.* **2001**, *18*, 1740.

[228] U. Resch-Genger, M. Grabolle, S. Cavaliere-Jaricot, R. Nitschke, T. Nann, *Nat. Methods* **2008**, *5*, 763.

[229] Y. Cui, H. Huang, M. Liu, J. Chen, F. Deng, N. Zhou, X. Zhang, Y. Wei, *Carbohydr. Polym.* **2019**, *223*, 115102.

[230] E. Vasileva, Y. Li, I. Sychugov, M. Mensi, L. Berglund, S. Popov, *Adv. Opt. Mater.* **2017**, *5*, 1700057.

[231] A. Szczeszak, M. Skwierczyńska, D. Przybylska, M. Runowski, E. Śmiechowicz, A. Erdman, O. Ivashchenko, T. Grzyb, S. Lis, P. Kulpiński, K. Olejnik, *J. Mater. Chem. C* **2020**, *8*, 11922.

[232] R. Xiong, X. Zhang, M. Krecker, S. Kang, M. J. Smith, V. V. Tsukruk, *Angew. Chem., Int. Ed.* **2020**, *59*, 20167.

[233] J. Guo, D. Liu, I. Filpponen, L.-S. Johansson, J.-M. Malho, S. Quraishi, F. Liebner, H. A. Santos, O. J. Rojas, *Biomacromolecules* **2017**, *18*, 2045.

[234] M. Li, X. Li, M. Jiang, X. Liu, Z. Chen, S. Wang, T. D. James, L. Wang, H. Xiao, *Chem. Eng. J.* **2020**, *399*, 125741.

[235] S. Yu, W. Li, Y. Fujii, T. Omura, H. Minami, *ACS Sustainable Chem. Eng.* **2019**, *7*, 19157.

[236] H. Zheng, B. Ju, X. Wang, W. Wang, M. Li, Z. Tang, S. X.-A. Zhang, Y. Xu, *Adv. Opt. Mater.* **2018**, *6*, 1801246.

[237] H. Yang, Y. Liu, J. Li, C. Wang, Y. Li, *Chem. Eng. J.* **2021**, *403*, 126406.

[238] Y. H. Song, S. H. Choi, J. S. Yoo, B. K. Kang, E. K. Ji, H. S. Jung, D. H. Yoon, *Chem. Eng. J.* **2017**, *313*, 461.

[239] Y. H. Song, J. S. Yoo, B. K. Kang, S. H. Choi, E. K. Ji, H. S. Jung, D. H. Yoon, *Nanoscale* **2016**, *8*, 19523.

[240] L. Chen, C. Lai, R. Marchewka, R. M. Berry, K. C. Tam, *Nanoscale* **2016**, *8*, 13288.

[241] B. Peng, M. Almeqdadi, F. Laroche, S. Palantavida, M. Dokukin, J. Roper, O. H. Yilmaz, H. Feng, I. Sokolov, *Mater. Today* **2019**, *23*, 16.

[242] G. Iasilli, R. Francischello, P. Lova, S. Silvano, A. Surace, G. Pesce, M. Alloisio, M. Patrini, M. Shimizu, D. Comoretto, A. Pucci, *Mater. Chem. Front.* **2019**, *3*, 429.

**ADVANCED
SCIENCE NEWS**

www.advancedsciencenews.com

**ADVANCED
MATERIALS**

www.advmat.de

[243] H. Assender, *Science* **2002**, *297*, 973.

[244] S. Kasani, K. Curtin, N. Wu, *Nanophotonics* **2019**, *8*, 2065.

[245] T. M. Tran Khanh, D. Nguyen Thanh, *J. Sci.: Adv. Mater. Devices* **2017**, *2*, 1.

[246] N. Kooy, K. Mohamed, L. Pin, O. Guan, *Nanoscale Res. Lett.* **2014**, *9*, 320.

[247] A. Peter Amalathas, M. Alkaisi, *Micromachines* **2019**, *10*, 619.

[248] M. C. Traub, W. Longsine, V. N. Truskett, *Annu. Rev. Chem. Biomol. Eng.* **2016**, *7*, 583.

[249] Y. Li, Q. Yan, N. Koshizaki, *Nanotechnology* **2017**, *28*, 500201.

[250] S. Takei, *Macromol. Mater. Eng.* **2020**, *305*, 1900853.

[251] B. Kamali, S. Asiaei, B. Beigzadeh, A. A. Ebadi, *Colloids Surf., A* **2018**, *555*, 389.

[252] W. Zhang, Y. Lei, F. Ming, Q. Jiang, P. M. F. J. Costa, H. N. Alshareef, *Adv. Energy Mater.* **2018**, *8*, 1801840.

[253] S. Lochmann, J. Grothe, K. Eckhardt, D. Leistenschneider, L. Borchardt, S. Kaskel, *Nanoscale* **2018**, *10*, 10109.

[254] A. Wolfberger, A. Petritz, A. Fian, J. Herka, V. Schmidt, B. Stadlober, R. Kargl, S. Spirk, T. Griesser, *Cellulose* **2015**, *22*, 717.

[255] Z. Wang, X. Zhuang, Y. Chen, B. Wang, J. Yu, W. Huang, T. J. Marks, A. Facchetti, *Chem. Mater.* **2019**, *31*, 7608.

[256] S. Takei, A. Oshima, T. Wakabayashi, T. Kozawa, S. Tagawa, *Appl. Phys. Lett.* **2012**, *101*, 033106.

[257] H. Zeng, R. Lajos, V. Metlushko, E. Elzy, S. Y. An, J. Sautner, *Lab Chip* **2009**, *9*, 699.

[258] A. Espinha, C. Dore, C. Matricardi, M. I. Alonso, A. R. Goñi, A. Mihi, *Nat. Photonics* **2018**, *12*, 343.

[259] G. Chu, A. Camposeo, R. Vilensky, G. Vasilyev, P. Martin, D. Pisignano, E. Zussman, *Matter* **2019**, *1*, 988.

[260] G. Chu, D. Qu, A. Camposeo, D. Pisignano, E. Zussman, *Mater. Horiz.* **2020**, *7*, 511.

[261] D. Yun, M. Kim, *Electronics* **2020**, *9*, 948.

[262] D. Nedelcu, C. Ciofu, N. M. Lohan, *Composites, Part B* **2013**, *55*, 11.

[263] M. Worgull, M. Schneider, M. Röhrig, T. Meier, M. Heilig, A. Kolew, K. Feit, H. Hölscher, J. Leuthold, *RSC Adv.* **2013**, *3*, 20060.

[264] N. Jürgensen, B. Fritz, A. Mertens, J. Tisserant, M. Kolle, G. Gomard, G. Hernandez-Sosa, *Adv. Mater. Technol.* **2021**, *6*, 1900933.

[265] T. Mäkelä, T. Haatainen, J. Ahopelto, *Microelectron. Eng.* **2011**, *88*, 2045.

[266] T. Mäkelä, M. Kainlauri, P. Willberg-Keyriläinen, T. Tammelin, U. Forsström, *Microelectron. Eng.* **2016**, *163*, 1.

[267] T. Mäkelä, A. Hokkanen, A. Sneck, T. Ruotsalainen, A. Khakalo, T. Tammelin, *Microelectron. Eng.* **2020**, *225*, 111258.

[268] A. Khakalo, T. Mäkelä, L.-S. Johansson, H. Orelma, T. Tammelin, *ACS Appl. Bio Mater.* **2020**, *3*, 7428.

[269] S. Zhu, Y. Tang, C. Lin, X. Y. Liu, Y. Lin, *Small Methods* **2021**, *5*, 2001060.

[270] J.-F. Revol, H. Bradford, J. Giasson, R. H. Marchessault, D. G. Gray, *Int. J. Biol. Macromol.* **1992**, *14*, 170.

[271] J.-F. Revol, L. Godbout, D. G. Gray, *J. Pulp Pap. Sci.* **1998**, *24*, 146.

[272] W. Hong, Z. Yuan, X. Chen, *Small* **2020**, *16*, 1907626.

[273] C. Schütz, J. R. Bruckner, C. Honorato-Rios, Z. Tosheva, M. Anyfantakis, J. P. F. Lagerwall, *Crystals* **2020**, *10*, 199.

[274] S. N. Fernandes, L. F. Lopes, M. H. Godinho, *Curr. Opin. Solid State Mater. Sci.* **2019**, *23*, 63.

[275] G. R. Meseck, A. S. Terpstra, M. J. MacLachlan, *Curr. Opin. Colloid Interface Sci.* **2017**, *29*, 9.

[276] M. Giese, L. K. Blusch, M. K. Khan, M. J. MacLachlan, *Angew. Chem., Int. Ed.* **2015**, *54*, 2888.

[277] M. Giese, M. Spengler, *Mol. Syst. Des. Eng.* **2019**, *4*, 29.

[278] J. Xue, F. Song, X. W. Yin, Z. L. Zhang, Y. Liu, X. L. Wang, Y. Z. Wang, *ACS Sustainable Chem. Eng.* **2017**, *5*, 3721.

[279] T. Hiratani, W. Y. Hamad, M. J. MacLachlan, *Adv. Mater.* **2017**, *29*, 1606083.

[280] J. Tao, C. Zou, H. Jiang, M. Li, D. Lu, S. Mann, Y. Xu, *CCS Chem.* **2020**, *2020*, 932.

[281] Y. Cao, W. Y. Hamad, M. J. MacLachlan, *Adv. Opt. Mater.* **2018**, *6*, 1800412.

[282] J. A. De La Cruz, Q. Liu, B. Senyuk, A. W. Frazier, K. Peddireddy, I. I. Smalyukh, *ACS Photonics* **2018**, *5*, 2468.

[283] J. P. F. Lagerwall, C. Schütz, M. Salajkova, J. Noh, J. H. Park, G. Scalia, L. Bergström, *NPG Asia Mater.* **2014**, *6*, 80.

[284] H. Zheng, W. Li, W. Li, X. Wang, Z. Tang, S. X. Zhang, Y. Xu, *Adv. Mater.* **2018**, *30*, 1705948.

[285] J. Majoinen, E. Kontturi, O. Ikkala, D. G. Gray, *Cellulose* **2012**, *19*, 1599.

[286] A. G. Dumanli, H. M. Van Der Kooij, G. Kamita, E. Reisner, J. J. Baumberg, U. Steiner, S. Vignolini, *ACS Appl. Mater. Interfaces* **2014**, *6*, 12302.

[287] H. Coles, S. Morris, *Nat. Photonics* **2010**, *4*, 676.

[288] R. Balamurugan, J. H. Liu, *React. Funct. Polym.* **2016**, *105*, 9.

[289] S. Beck, J. Bouchard, R. Berry, *Biomacromolecules* **2011**, *12*, 167.

[290] T. Abitbol, D. Kam, Y. Levi-Kalisman, D. G. Gray, O. Shoseyov, *Langmuir* **2018**, *34*, 3925.

[291] X. M. Dong, T. Kimura, J.-F. Revol, D. G. Gray, *Langmuir* **1996**, *12*, 2076.

[292] J. Pan, W. Hamad, S. K. Straus, *Macromolecules* **2010**, *43*, 3851.

[293] G. Guidetti, S. Atifi, S. Vignolini, W. Y. Hamad, *Adv. Mater.* **2016**, *28*, 10042.

[294] M. Xu, W. Li, C. Ma, H. Yu, Y. Wu, Y. Wang, Z. Chen, J. Li, S. Liu, *J. Mater. Chem. C* **2018**, *6*, 5391.

[295] I. Hoeger, O. J. Rojas, K. Efimenko, O. D. Velev, S. S. Kelley, *Soft Matter* **2011**, *7*, 1957.

[296] Y. Habibi, T. Heim, R. Douillard, *J. Polym. Sci., Part B: Polym. Phys.* **2008**, *46*, 1430.

[297] E. D. Cranston, D. G. Gray, *Sci. Technol. Adv. Mater.* **2006**, *7*, 319.

[298] J. Sugiyama, H. Chanzy, G. Maret, *Macromolecules* **1992**, *25*, 4232.

[299] K. J. De France, K. G. Yager, T. Hoare, E. D. Cranston, *Langmuir* **2016**, *32*, 7564.

[300] F. Kimura, T. Kimura, M. Tamura, A. Hirai, M. Ikuno, F. Horii, *Langmuir* **2005**, *21*, 2034.

[301] B. Frka-Petesic, G. Guidetti, G. Kamita, S. Vignolini, *Adv. Mater.* **2017**, *29*, 1701469.

[302] S. N. Fernandes, P. L. Almeida, N. Monge, L. E. Aguirre, D. Reis, C. L. P. de Oliveira, A. M. F. Neto, P. Pieranski, M. H. Godinho, *Adv. Mater.* **2017**, *29*, 1603560.

[303] S. Caveney, *Proc. R. Soc. London, Ser. B* **1971**, *178*, 205.

[304] S. Kang, Y. Li, D. Bukharina, M. Kim, H. Lee, M. L. Buxton, M. J. Han, D. Nepal, T. J. Bunning, V. V. Tsukruk, *Adv. Mater.* **2021**, *33*, 2103329.

[305] P. R. Anusuyadevi, R. Shanker, Y. Cui, A. V. Riazanova, M. Järn, M. P. Jonsson, A. J. Svagan, *Adv. Mater.* **2021**, *33*, 2101519.

[306] X. Yang, K. Shi, I. Zhitomirsky, E. D. Cranston, *Adv. Mater.* **2015**, *27*, 6104.

[307] X. Mu, D. G. Gray, *Cellulose* **2015**, *22*, 1103.

[308] K. W. Klockars, N. E. Yau, B. L. Tardy, J. Majoinen, T. Kämäräinen, K. Miettunen, E. Boutonnet, M. Borghei, J. Beidler, O. J. Rojas, *Cellulose* **2019**, *26*, 491.

[309] A. Gençer, C. Schütz, W. Thielemans, *Langmuir* **2017**, *33*, 228.

[310] M. A. C. Stuart, W. T. S. Huck, J. Genzer, M. Müller, C. Ober, M. Stamm, G. B. Sukhorukov, I. Szleifer, V. V. Tsukruk, M. Urban, F. Winnik, S. Zauscher, I. Luzinov, S. Minko, *Nat. Mater.* **2010**, *9*, 101.

[311] Z. Li, X. Yang, W. Li, H. Liu, *Carbohydr. Polym.* **2019**, *210*, 350.

[312] M. Wei, Y. Gao, X. Li, M. J. Serpe, *Polym. Chem.* **2017**, *8*, 127.

[313] A. Moreno, M. H. Sipponen, *Mater. Horiz.* **2020**, *7*, 2237.

[314] X. Cao, X. Peng, L. Zhong, R. Sun, *J. Agric. Food Chem.* **2014**, *62*, 10000.

[315] Q. Zhu, S. Liu, J. Sun, J. Liu, C. J. Kirubaharan, H. Chen, W. Xu, Q. Wang, *Carbohydr. Polym.* **2020**, *235*, 115933.

[316] Z. Peng, Q. Lin, Y.-A. A. Tai, Y. Wang, *J. Agric. Food Chem.* **2020**, *68*, 12940.

[317] C. Xu, C. Huang, H. Huang, *Appl. Mater. Today* **2021**, *22*, 100912.

[318] Y. Huang, H. Kang, G. Li, C. Wang, Y. Huang, R. Liu, *RSC Adv.* **2013**, *3*, 15909.

[319] I. Filpponen, H. Sadeghifar, D. S. Argyropoulos, *Nanomater. Nano-technol.* **2011**, *1*, 7.

[320] K. Upadhyay, S. Thomas, R. K. Tamrakar, N. Kalarikkal, in *Advanced Functional Polymers for Biomedical Applications*, Elsevier, New York **2019**, pp. 211–233.

[321] W. Yuan, C. Wang, S. Lei, J. Chen, S. Lei, Z. Li, *Polym. Chem.* **2018**, *9*, 3098.

[322] I. Otsuka, C. J. Barrett, *Cellulose* **2019**, *26*, 6903.

[323] Y. Kim, D. Jeong, V. V. Shinde, Y. Hu, C. Kim, S. Jung, *Int. J. Biol. Macromol.* **2020**, *163*, 824.

[324] B. Bao, S. Bai, J. Fan, J. Su, W. Wang, D. Yu, *Dyes Pigm.* **2019**, *171*, 107778.

[325] J. Keyvan Rad, A. R. Mahdavian, *J. Phys. Chem. C* **2016**, *120*, 9985.

[326] W. Tian, J. Zhang, J. Yu, J. Wu, J. Zhang, J. He, F. Wang, *Adv. Funct. Mater.* **2018**, *28*, 1703548.

[327] B.-B. Sun, B.-H. Yao, Y.-Q. He, B. Yang, *Coatings* **2020**, *10*, 569.

[328] K. Jin, X. Ji, T. Yang, J. Zhang, W. Tian, J. Yu, X. Zhang, Z. Chen, J. Zhang, *Chem. Eng. J.* **2021**, *406*, 126794.

[329] Z. Abousalman-Rezvani, P. Eskandari, H. Roghani-Mamaqani, H. Mardani, M. Salami-Kalajahi, *Polymer (Guildf)* **2019**, *182*, 121830.

[330] M. Mrlik, P. Sobolciak, I. Krupa, P. Kasak, *Emergent Mater.* **2018**, *1*, 35.

[331] H. Orelma, M. Vuoriluoto, L.-S. Johansson, J. M. Campbell, I. Filpponen, M. Biesalski, O. J. Rojas, *RSC Adv.* **2016**, *6*, 85100.

[332] R. Nasseri, C. P. Deutschman, L. Han, M. A. Pope, K. C. Tam, *Mater. Today Adv.* **2020**, *5*, 100055.

[333] G. Zhao, Y. Zhang, S. Zhai, J. Sugiyama, M. Pan, J. Shi, H. Lu, *ACS Appl. Mater. Interfaces* **2020**, *12*, 17833.

[334] Y. Zhao, G. Gao, D. Liu, D. Tian, Y. Zhu, Y. Chang, *Carbohydr. Polym.* **2017**, *174*, 39.

[335] Y. Zhang, Z. Tian, Y. Fu, Z. Wang, M. Qin, Z. Yuan, *Carbohydr. Polym.* **2020**, *228*, 115387.

[336] D. Qu, H. Zheng, H. Jiang, Y. Xu, Z. Tang, *Adv. Opt. Mater.* **2019**, *7*, 1801395.

[337] T. H. Zhao, R. M. Parker, C. A. Williams, K. T. P. Lim, B. Frka-Petesic, S. Vignolini, *Adv. Funct. Mater.* **2019**, *29*, 1804531.

[338] H. Wan, X. Li, L. Zhang, X. Li, P. Liu, Z. Jiang, Z.-Z. Yu, *ACS Appl. Mater. Interfaces* **2018**, *10*, 5918.

[339] W. Song, J.-K. Lee, M. S. Gong, K. Heo, W.-J. Chung, B. Y. Lee, *ACS Appl. Mater. Interfaces* **2018**, *10*, 10353.

[340] T. Lu, H. Pan, J. Ma, Y. Li, S. W. Bokhari, X. Jiang, S. Zhu, D. Zhang, *ACS Appl. Mater. Interfaces* **2017**, *9*, 18231.

[341] K. Yao, Q. Meng, V. Bulone, Q. Zhou, *Adv. Mater.* **2017**, *29*, 1701323.

[342] C. Sun, D. Zhu, H. Jia, K. Lei, Z. Zheng, X. Wang, *ACS Appl. Mater. Interfaces* **2019**, *11*, 39192.

[343] Y. Gao, Z. Jin, *ACS Sustainable Chem. Eng.* **2018**, *6*, 6192.

[344] C. Chen, Y. Kuang, S. Zhu, I. Burgert, T. Keplinger, A. Gong, T. Li, L. Berglund, S. J. Eichhorn, L. Hu, *Nat. Rev. Mater.* **2020**, *5*, 642.

[345] X. Sun, Q. Wu, X. Zhang, S. Ren, T. Lei, W. Li, G. Xu, Q. Zhang, *Cellulose* **2018**, *25*, 1103.

[346] D. O. Klemm, T. Lindström, D. Abitbol, D. Kralisch, in *Nanocellulose Based Composite Electronics*, Elsevier, New York **2021**, pp. 1–14.

[347] M. Morales-Masis, S. De Wolf, R. Woods-Robinson, J. W. Ager, C. Ballif, *Adv. Electron. Mater.* **2017**, *3*, 1600529.

[348] W. Wu, N. G. Tassi, H. Zhu, Z. Fang, L. Hu, *ACS Appl. Mater. Interfaces* **2015**, *7*, 26860.

[349] K. Miettunen, J. Vapaavuori, A. Poskela, A. Tiihonen, P. D. Lund, *WIREs Energy Environ.* **2018**, *7*, e302.

[350] S. Yook, H. Park, H. Park, S.-Y. Lee, J. Kwon, H. J. Youn, *Cellulose* **2020**, *27*, 4509.

[351] C. Cordt, A. Geissler, M. Biesalski, *Adv. Mater. Interfaces* **2021**, *8*, 2001265.

[352] R. Koppolu, J. Lahti, T. Abitbol, A. Swerin, J. Kuusipalo, M. Toivakka, *ACS Appl. Mater. Interfaces* **2019**, *11*, 11920.

[353] S. Chandrasekaran, M. Sotenko, A. Cruz-Izquierdo, Z. Rymansaib, P. Iravani, K. Kirwan, J. L. Scott, *J. Polym. Environ.* **2020**, *29*, 17.

[354] J.-S. Kang, J.-G. Kang, Y. Sohn, K. T. Leung, *ACS Appl. Mater. Interfaces* **2018**, *10*, 44768.

[355] D. Kim, Y. Ko, G. Kwon, U.-J. Kim, J. You, *ACS Appl. Mater. Interfaces* **2018**, *10*, 38517.

[356] C. Zhang, R. Cha, R. Li, L. Tang, K. Long, Z. Zhang, L. Zhang, X. Jiang, *ACS Sustainable Chem. Eng.* **2020**, *8*, 7774.

[357] L. Chen, H. Yu, M. Dirican, D. Fang, Y. Tian, C. Yan, J. Xie, D. Jia, H. Liu, J. Wang, F. Tang, X. Zhang, J. Tao, *Adv. Mater. Interfaces* **2020**, *7*, 2000928.

[358] J. Tao, R. Wang, H. Yu, L. Chen, D. Fang, Y. Tian, J. Xie, D. Jia, H. Liu, J. Wang, F. Tang, L. Song, H. Li, *ACS Appl. Mater. Interfaces* **2020**, *12*, 9701.

[359] M. Shibano, H. Ochiai, K. Suzuki, H. Kamitakahara, H. Kaji, T. Takano, *Macromolecules* **2020**, *53*, 2864.

[360] J. Zimmermann, L. Porcarelli, T. Rödlmeier, A. Sanchez-Sanchez, D. Mecerreyes, G. Hernandez-Sosa, *Adv. Funct. Mater.* **2018**, *28*, 1705795.

[361] H. Zhang, J. Li, D. Liu, S. Min, T.-H. Chang, K. Xiong, S. H. Park, J. Kim, Y. H. Jung, J. Park, J. Lee, J. Han, L. Katehi, Z. Cai, S. Gong, Z. Ma, *Nat. Commun.* **2020**, *11*, 3118.

[362] J. Rao, H. Gao, Y. Guan, W. Li, Q. Liu, *Carbohydr. Polym.* **2019**, *208*, 513.

[363] P. Ezati, J.-W. Rhim, M. Moradi, H. Tajik, R. Molaei, *Carbohydr. Polym.* **2020**, *246*, 116614.

[364] A. Rahmawati, C.-F. Shih, T. Imae, *Polym. J.* **2020**, *52*, 1235.

[365] K. Solin, M. Borghei, O. Sel, H. Orelma, L.-S. Johansson, H. Perrot, O. J. Rojas, *ACS Appl. Mater. Interfaces* **2020**, *12*, 36437.

[366] X. Yun, Q. Zhang, B. Luo, H. Jiang, C. Chen, S. Wang, D. Min, *Electroanalysis* **2020**, *32*, 2282.

[367] T. Stockinger, B. Liedl, M. Steiner, R. Schwödiauer, F. Padinger, S. Bauer, M. Kaltenbrunner, U. Müller, *Sens. Actuators, B* **2020**, *324*, 128750.

[368] H. Guan, J. Meng, Z. Cheng, X. Wang, *ACS Appl. Mater. Interfaces* **2020**, *12*, 46357.

[369] M. Alle, S. C. Park, R. Bandi, S.-H. Lee, J.-C. Kim, *Carbohydr. Polym.* **2021**, *253*, 117239.

[370] A. Petropoulou, S. Kralj, X. Karagiorgis, I. Savva, E. Loizides, M. Panagi, T. Krasia-Christoforou, C. Riziotis, *Sci. Rep.* **2020**, *10*, 367.

[371] X. Zhang, N. Xiao, M. Chen, Y. Wei, C. Liu, *Carbohydr. Polym.* **2020**, *229*, 115336.

[372] C. T. Tracey, M. A. Torlopov, I. S. Martakov, E. A. Vdovichenko, M. Zhukov, P. V. Krivoshapkin, V. I. Mikhaylov, E. F. Krivoshapkina, *Carbohydr. Polym.* **2020**, *247*, 116704.

[373] J. Sonia, G. K. M. Zanhal, K. S. Prasad, *Microchem. J.* **2020**, *158*, 105164.

[374] H. Ning, Y. Zeng, Y. Kuang, Z. Zheng, P. Zhou, R. Yao, H. Zhang, W. Bao, G. Chen, Z. Fang, J. Peng, *ACS Appl. Mater. Interfaces* **2017**, *9*, 27792.

[375] F. Shao, P. Feng, C. Wan, X. Wan, Y. Yang, Y. Shi, Q. Wan, *Adv. Electron. Mater.* **2017**, *3*, 1600509.

[376] P. Grey, S. N. Fernandes, D. Gaspar, E. Fortunato, R. Martins, M. H. Godinho, L. Pereira, *Adv. Funct. Mater.* **2019**, *29*, 1805279.

[377] X.-S. Zhang, M. Su, J. Brugger, B. Kim, *Nano Energy* **2017**, *33*, 393.

[378] S. Parandeh, M. Khaziha, F. Karimzadeh, *Nano Energy* **2019**, *59*, 412.

[379] I. Kim, H. Jeon, D. Kim, J. You, D. Kim, *Nano Energy* **2018**, *53*, 975.

[380] R. O. J. Otoni, C. G. , H. M. C. Azeredo, B. D. Mattos, M. Beaumont, D. S. Correa, unpublished.

[381] B. L. Tardy, B. D. Mattos, C. G. Otoni, M. Beaumont, J. Majoinen, T. Kämäräinen, O. J. Rojas, *Chem. Rev.* **2021**.

Joice Jaqueline Kaschuk is a chemist (2012, FAFIUV, Brazil) and holds a Ph.D. in Physical Chemistry (2019, IQSC-USP, Brazil). Currently, she is a Postdoctoral Researcher at the Department of Bioproducts and Biosystems – Aalto University (Finland, since 2019). She has been working with cellulosic materials for multifunctional optoelectronics substrates.

Yazan Al Haj received his B.Sc. degree (2016) in Sustainable and Renewable Energy from the University of Sharjah (UOS). In 2019, he joined Prof. Jaana Vapaavuori's research group at Aalto University as a Ph.D. candidate. His research interests focus on the synthesis and development of cellulose-based nanocomposites and their application in luminescence, energy conversion, and energy storage fields.

Orlando J. Rojas is a Canada Excellence Research Chair at the University of British Columbia. He is the Director of the BioProducts Institute sharing affiliation in the Departments of Chemical and Biological Engineering, Wood Science and Chemistry, and he is also Adjunct professor in Aalto University, Finland. He is the recipient of the 2018 Anselme Payen Award, the highest recognition in the field of cellulose and Renewable Materials. He is elected as Fellow of the American Chemical Society (2013), the recipient of the Tappi Nanotechnology Award (2015), and the Finnish Academy of Science and Letters (2017). His most recent research grants include the prestigious European Research Commission Advanced Grant (ERC-Advanced). He is a PI of the Finnish Materials Bioeconomy Flagship (FinnCERES) and leads several projects in Canada and Finland, under the Boreal Alliance initiative.

Kati Miettunen leads Solar Energy Materials and Systems group (established in 2020) at Department of Mechanical and Materials Engineering, University of Turku. She graduated as D.Sc. (tech) in Applied Physics in 2009 and did a post doc at Imperial College London (2011) after which she had a post-doctoral project and academy fellowship at Aalto University funded by Academy of Finland. She currently leads several national and international projects which investigate for instance developing stable emerging photovoltaics and light responsive materials based renewable and abundant materials such as wood derivatives.

ADVANCED
SCIENCE NEWS
www.advancedsciencenews.com

ADVANCED
MATERIALS
www.advmat.de

Tiffany Abitbol is a senior researcher at RISE Research Institutes of Sweden (since 2017). Tiffany obtained her Ph.D. in Chemistry from McGill University in 2011 and has post-doctoral experience from McMaster University (2012–2014) and the Hebrew University of Jerusalem (2014–2016). Tiffany's research interests focus on the application of biobased materials to address diverse contemporary material challenges.

Jaana Vapaavuori (Department of Chemistry and Materials Science, Aalto University) received her Ph.D. in Applied Physics in 2013. She leads Multifunctional Materials Design Group, established in 2019. She has received multiple recognitions, such as Banting Postdoctoral Fellowship (Canada), the Young Researcher of the Year 2020 award of Finnish Foundation of Technology Promotion, ERC Starting grant of European Research Council, and she is also leader of a Nordic Network beyond e-Textiles. Her research interests involve developing new designed materials for light-controllable nanostructures, liquid crystals, multifunctional porous materials, biomaterial-based light management layers for photovoltaics and sustainable material solutions for electrochemical devices.